

# **The role of chemotactic gradients in dendritic cell migration**

A dissertation submitted in partial fulfillment of the requirements for  
the degree of

**Doctor of Philosophy**

at the Institute of Science and Technology Austria, Klosterneuburg

**Kathrin Schumann**

München, March 2011

## **Erklärung**

Diese Dissertation wurde im Sinne der Prüfungsordnung der Graduate School des Institute of Science and Technology, Klosterneuburg, vom 30. November 2009 von Herrn Prof. Dr. Michael Sixt betreut.

## **Ehrenwörtliche Versicherung**

Ich erkläre hiermit an Eides statt, dass ich die vorliegende Arbeit ohne unzulässige Hilfe Dritter und ohne Benutzung anderer als der angegebenen Quellen und Hilfsmittel angefertigt habe. Wörtlich oder sinngemäß übernommenes Gedankengut habe ich als solches kenntlich gemacht.



---

Kathrin Schumann

1. Gutachter: Prof. Dr. Michael Sixt, IST Austria
2. Gutachter: Prof. Dr. Sanjiv Luther, UNIL
3. Gutachter: Prof. Dr. Tobias Bollenbach, IST Austria

## Abnahme der Dissertation

Hiermit bestätige ich, dass die gewünschten Verbesserungen an der Dissertation vorgenommen wurden.



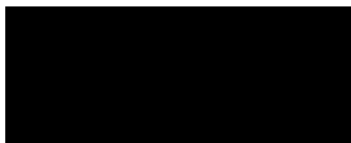
---

1. Gutachter: Prof. Dr. Michael Sixt, IST Austria



---

2. Gutachter: Prof. Dr. Sanjiv Luther, UNIL



---

3. Gutachter: Prof. Dr. Tobias Bollenbach, IST Austria

## Summary

Chemokines organize immune cell trafficking by inducing either directed (tactic) or random (kinetic) migration and by activating integrins in order to support surface adhesion (haptic). Beyond that the same chemokines can establish clearly defined functional areas in secondary lymphoid organs. Until now it is unclear how chemokines can fulfill such diverse functions. One decisive prerequisite to explain these capacities is to know how chemokines are presented in tissue. In theory chemokines could occur either soluble or immobilized, and could be distributed either homogeneously or as a concentration gradient. To dissect if and how the presenting mode of chemokines influences immune cells, I tested the response of dendritic cells (DCs) to differentially displayed chemokines. DCs are antigen presenting cells that reside in the periphery and migrate into draining lymph nodes (LNs) once exposed to inflammatory stimuli to activate naïve T cells. DCs are guided to and within the LN by the chemokine receptor CCR7, which has two ligands, the chemokines CCL19 and CCL21. Both CCR7 ligands are expressed by fibroblastic reticular cells in the LN, but differ in their ability to bind to heparan sulfate residues. CCL21 has a highly charged C-terminal extension, which mediates binding to anionic surfaces, whereas CCL19 is lacking such residues and likely distributes as a soluble molecule. This study shows that surface-bound CCL21 causes random, haptokinetic DC motility, which is confined to the chemokine coated area by inside-out activation of  $\beta 2$  integrins that mediate cell binding to the surface. CCL19 on the other hand forms concentration gradients which trigger directional, chemotactic movement, but no surface adhesion. In addition DCs can actively manipulate this system by recruiting and activating serine proteases on their surfaces, which create - by proteolytically removing the adhesive C-terminus - a solubilized variant of CCL21 that functionally resembles CCL19. By generating a CCL21 concentration gradient DCs establish a positive feedback loop to recruit further DCs from the periphery to the CCL21 coated region. In addition DCs can sense chemotactic gradients as well as immobilized haptokinetic fields at the same time and integrate these signals. The result is chemotactically biased haptokinesis - directional migration confined to a chemokine coated track or area - which could explain the dynamic but spatially tightly controlled swarming leukocyte locomotion patterns that have been observed in lymphatic organs by intravital microscopists.

The finding that DCs can approach soluble cues in a non-adhesive manner while they attach to surfaces coated with immobilized cues raises the question how these cells transmit intracellular forces to the environment, especially in the non-adherent migration mode. In order to migrate, cells have to generate and transmit force to the extracellular substrate. Force transmission is the prerequisite to procure an expansion of the leading edge and a forward motion of the whole cell body. In the current conceptions actin polymerization at the leading edge is coupled to extracellular ligands via the integrin family of transmembrane receptors, which allows the transmission of intracellular force. Against the paradigm of force

## Summary

---

transmission during migration, leukocytes, like DCs, are able to migrate in three-dimensional environments without using integrin transmembrane receptors (Lämmermann et al., 2008). This reflects the biological function of leukocytes, as they can invade almost all tissues, whereby their migration has to be independent from the extracellular environment. How the cells can achieve this is unclear. For this study I examined DC migration in a defined three-dimensional environment and highlighted actin-dynamics with the probe Lifeact-GFP. The result was that chemotactic DCs can switch between integrin-dependent and integrin-independent locomotion and can thereby adapt to the adhesive properties of their environment. If the cells are able to couple their actin cytoskeleton to the substrate, actin polymerization is entirely converted into protrusion. Without coupling the actin cortex undergoes slippage and retrograde actin flow can be observed. But retrograde actin flow can be completely compensated by higher actin polymerization rate keeping the migration velocity and the shape of the cells unaltered. Mesenchymal cells like fibroblast cannot balance the loss of adhesive interaction, cannot protrude into open space and, therefore, strictly depend on integrin-mediated force coupling. This leukocyte specific phenomenon of “adaptive force transmission” endows these cells with the unique ability to transit and invade almost every type of tissue.

## Table of contents

<b>Erklärung .....</b>	<b>2</b>
<b>Abnahme der Dissertation.....</b>	<b>3</b>
<b>Summary.....</b>	<b>4</b>
<b>Table of contents.....</b>	<b>6</b>
<b>Abbreviations .....</b>	<b>10</b>
<b>1 Introduction.....</b>	<b>15</b>
1.1 Dendritic cells (DCs).....	15
1.1.1 Functions of DCs .....	15
1.1.2 DC maturation.....	16
1.2 Secondary lymphoid organs (SLOs).....	17
1.2.1 Spleen: Structure and Function.....	17
1.2.2 Lymph node: Structure and function .....	18
1.2.3 Stroma cell networks in SLOs .....	20
1.3 Chemokines .....	22
1.3.1 Chemokine classifications.....	22
1.3.2 Inflammatory chemokines .....	24
1.3.3 Homeostatic chemokines.....	24
1.3.3.1 CXCL12 : Precursor retention in the bone marrow and localization of plasma cells in SLOs .....	24
1.3.3.2 CXCL13: Organization of B cell areas in SLOs .....	25
1.3.3.3 CCL19 and CCL21: Organization of T cell areas in SLOs.....	25
1.3.4 Chemokine immobilization on proteoglycans .....	28
1.3.5 Chemokine receptors.....	30
1.3.6 CCR7: Guidance of mature DCs .....	31
1.4 Chemokine guided migration in the immune system.....	32
1.4.1 Leukocyte trafficking .....	32
1.4.2 Cell migration modes .....	33
1.4.3 Evidence for kinesis.....	34
1.4.4 Evidence for taxis .....	34
1.4.5 Leukocytes as chemotactic organizers.....	35
1.5 Cytoskeleton of migrating leukocytes .....	36
1.5.1 Basal mechanisms of leukocyte migration .....	36
1.5.2 Force generation: Actin-myosin interactions .....	37
1.5.3 Force transduction: Integrins.....	39

## Table of contents

---

1.5.4	Actin dynamics in the lamellipodium: Retrograde actin flow .....	42
<b>2</b>	<b>Aims of this thesis .....</b>	<b>43</b>
<b>3</b>	<b>Material and Methods .....</b>	<b>44</b>
3.1	Mice .....	44
3.2	Chemicals .....	44
3.3	Cell culture .....	44
3.3.1	General.....	44
3.3.2	Cell passaging .....	45
3.3.3	GM-CSF and M-CSF production .....	45
3.3.4	Generation of bone marrow derived DCs .....	45
3.3.5	Maturation of DCs.....	46
3.3.6	Cryo-preservation and thawing of DCs.....	46
3.3.7	Transfection of DCs .....	46
3.3.8	Generation of <i>Itg</i> <sup>-/-</sup> DCs .....	47
3.3.9	Generation of bone marrow derived macrophages .....	47
3.3.10	Isolation of CD4 <sup>+</sup> T cells from the spleen .....	48
3.3.11	Isolation of B cells from the spleen.....	48
3.4	Molecular biology techniques .....	49
3.4.1	DNA agarose gel electrophoresis.....	49
3.4.2	PCR.....	49
3.4.3	Plasmid preparation .....	51
3.4.4	DNA restriction digest .....	51
3.4.5	Plasmid de-phosphorylation.....	51
3.4.6	DNA ligation.....	52
3.4.7	Preparation of heat-competent <i>Escherichia coli</i> ( <i>E.coli</i> ) XL1 blue .....	52
3.4.8	Transformation of heat-competent <i>Escherichia coli</i> .....	52
3.4.9	DNA sequencing.....	53
3.5	Production and purification of recombinant chemokine.....	54
3.5.1	Production of recombinant CCL21 in the yeast <i>Pichia pastoris</i> .....	54
3.5.1.1	Preparation of electro-competent <i>Pichia pastoris</i> .....	54
3.5.1.2	Electroporation of <i>Pichia pastoris</i> .....	55
3.5.1.3	CCL21 test expression in <i>Pichia pastoris</i> .....	55
3.5.1.4	CCL21 large scale expression in <i>Pichia pastoris</i> .....	55
3.5.1.5	CCL21 purification with MagneHis™ Ni beads .....	56
3.5.1.6	CCL21 purification with Ni-NTA agarose.....	56
3.5.2	Expression and purification of full-length and C-terminal truncated CCL21 in <i>Escherichia coli</i> B834(DE3)pLysS .....	57
3.6	Biochemical methods .....	58
3.6.1	<i>In vitro</i> CCL21 cleavage.....	58

## Table of contents

---

3.6.2	CCL21 pull-down from LN-lysate .....	58
3.6.3	SDS-polyacrylamide gel electrophoresis (SDS-PAGE) .....	59
3.6.4	Western-Blot.....	60
3.7	Immunostainings .....	61
3.7.1	Immunostaining of LN cryosections .....	61
3.7.2	Quantification of immobilized CCL21 and CCL19 by immunofluorescence ...	62
3.8	Cell migration and spreading assays .....	62
3.8.1	Time lapse video microscopy.....	62
3.8.2	<i>In vitro</i> migration on LN-cryosections .....	63
3.8.3	<i>In vivo</i> migration of DCs.....	63
3.8.4	Chemokine spot migration assay .....	63
3.8.5	DC spreading on with polysialic acid (polySia)-coated surfaces .....	63
3.8.6	DC adherence on CCL21-coated fibroblasts .....	64
3.8.7	Under-agarose migration assay (UAA).....	64
3.8.8	Modified UAA for TIRF microscopy .....	65
3.8.9	Carbon fiber migration assay .....	66
3.9	Statistical analysis .....	67
<b>4</b>	<b>Results .....</b>	<b>68</b>
4.1	Chemotactically biased haptokinesis .....	68
4.1.1	A reductionist <i>in vitro</i> system to study chemokine-driven DC migration.....	68
4.1.2	Soluble chemotactic gradient guides DCs on cryosection .....	70
4.1.3	Response patterns to CCL21 .....	71
4.1.4	DCs turn immobilized CCL21 into soluble CCL21 that resembles CCL19 .....	73
4.1.5	Plasmin cleavage of CCL21.....	76
4.1.6	Immobilized but not soluble chemokine triggers integrin activation on DCs...	80
4.1.7	Directional steering of haptokinetic movement.....	84
4.2	Adaptive force transmission in amoeboid cell migration.....	88
4.2.1	Retrograde actin flow in WT and <i>Itg<sup>-/-</sup></i> DCs .....	88
4.2.2	Flexible actin polymerization in the molecular clutch system.....	91
4.2.3	Adhesive interaction with CCL21/ICAM-1 .....	92
4.2.4	Macrophages also adapt their actin polymerization rate.....	94
4.2.5	Substrate-independent chemotactic DC migration .....	95
<b>5</b>	<b>Discussion .....</b>	<b>98</b>
5.1	Chemotactically biased haptokinesis .....	98
5.1.1	CCL19 and CCL21 are functionally not redundant .....	99
5.1.2	CCL21 is cleaved by serine proteases .....	102
5.1.3	Plasmin cleaves CCL21 <i>in vitro</i> .....	103
5.1.4	Haptokinetic migration scaffold .....	104
5.1.5	Chemotactic bias .....	105



## Table of contents

---

5.1.6	Competition between immobilized and soluble CCR7 ligands .....	106
5.1.7	Cell biological implications .....	107
5.1.8	Concluding remarks to chemotactically biased haptokinesis .....	108
5.2	Adaptive force transmission in amoeboid cell migration.....	110
5.2.1	Amoeboid cells can adapt to different degrees of force coupling via actin polymerization.....	110
5.2.2	Surface anchoring cells cannot protrude into open space .....	112
5.2.3	Immobilized chemokine influences adaptive force transmission.....	113
5.2.4	Concluding remarks to 'adaptive force transmission' .....	114
<b>6</b>	<b>References .....</b>	<b>116</b>
<b>7</b>	<b>Supplementary movie legends .....</b>	<b>134</b>
<b>8</b>	<b>Supplementary statistical analyses.....</b>	<b>138</b>
<b>9</b>	<b>Publications .....</b>	<b>139</b>
	<b>Curriculum vitae .....</b>	<b>140</b>
	<b>Acknowledgement.....</b>	<b>141</b>

### Abbreviations

-/-	knockout
3D	three-dimensional
3T3	fibroblast cell line "3-day transfer, inoculum $3 \times 10^5$ cells"
ACK	ammonium-chloride-potassium
ADP	adenosine-5'-diphosphate
ANOVA	analysis of variance
AOX1	alcohol oxidase promoter
Apr	aprotinin
Arp2/3	actin related protein 2/3
ATP	adenosine-5'-triphosphate
ATPase	adenosine-5'-triphosphatase
BMGY	buffer glycerol-complex medium
BMMY	buffer methanol-complex medium
Bp/kbp	base pair(s), kilo base pairs
BSA	bovine serum albumin
C	cysteine
C57BL/6	inbred mouse strain "C57 black 6"
CAP	cyclase associated protein
CCL	CC- or $\beta$ -chemokine
CCX-CKR	CC-X-chemokine receptor
CCR	CC- or $\beta$ -chemokine receptor
CD	cluster of differentiation
cDC	conventional dendritic cells
C-terminus, C-terminal	carboxy-terminus, carboxy-terminal
ctrl	control
CX3CL	CXXXC- or $\gamma$ -chemokine
CX3CR	CXXXC- or $\gamma$ -chemokine receptor
CXCL	CXC- or $\alpha$ -chemokine
CXCR	CXC- or $\alpha$ -chemokine receptor

## Abbreviations

---

CFSE	carboxyfluorescein succinimidyl ester
CRAC	Ca <sup>2+</sup> -release activated Ca <sup>2+</sup>
Cy	cyanine
D10	DMEM supplemented with glutamine and 10% FCS
DAG	diacylglycerol
DC	dendritic cell
ddH <sub>2</sub> O	double distilled water
ddNTP	dideoxynucleotide -5'-triphosphate
DMEM	Dulbecco's Modified Eagle Medium
DMSO	dimethyl sulfoxide
DNA	deoxyribonucleic acid
dNTP	deoxynucleotide -5'-triphosphate
DRY-motive	aspartic acid-arginine-tyrosine motive
ECM	extracellular matrix
<i>E.coli</i>	<i>bacteria: Escherichia coli</i>
EDTA	ethylenediaminetetraacetic acid
ELR-motive	glutamate-leucine-arginine motive
ER	endoplasmatic reticulum
FACS	fluorescence-activated cell sorting
FCS	fetal calf serum
FDC	follicular dendritic cell
FITC	fluorescein isothiocyanate
FRC	fibroblastic reticular cell
GAG	glycosaminoglycan
GDP	guanosine-5'-diphosphate
GEF	guanine nucleotide exchange factor
GFP	green fluorescent protein
GM-CSF	granulocyte-macrophage colony-stimulating factor
gp38	glycoprotein 38
GPCR	G protein-coupled receptor
GTP	guanosine-5'-triphosphate
GTPase	guanosine-5'-triphosphatase
HBSS	Hank's buffered salt solution

## Abbreviations

---

HEPES	N-(2-hydroxyethyl)-piperazine-N'-2-ethanesulfonic acid
HEV	high endothelial venule
HRP	horseradish peroxidase
HS	heparan sulfate
HSG	half-synthetic, glycerol-based
ICAM-1	intercellular adhesion molecule 1
IFN	interferon
Ig	immunoglobulin
IL	interleukine
InsP3	inositol-1,4,5-trisphosphate
IPTG	isopropyl $\beta$ -D-1-thiogalactopyranoside
<i>Itg</i>	<i>gene: integrin</i>
kDa	kilodaltons
KO	knockout
LB	Lysogeny broth, mediium for bacteria
LFA1	lymphocyte function-associated antigen 1
LN	lymph node
LoxP	locus of X-over P1; site on the bacteriophage P1 genome consisting of an asymmetric 8 bp sequence in between with two sets of palindromic sequences
LPS	lipopolysaccharide
MACS	magnetic-activated cell sorting
M-CSF	macrophage colony-stimulating factor
MEF	mouse embryonic fibroblast
MEM	minimum essential medium
MHC	major histocompatibility complex
MOPS	3-(N-morpholino)propanesulfonic acid
MP	mouse plasma
MRC	marginal reticular cells
Mx	promoter: myxovirus resistance
ns	not significant
NTA	nitrilotriacetic acid
N-terminus, N-terminal	amino-terminus, amino-terminal

## Abbreviations

---

OD	optical density
p19 <sup>ARF</sup>	ADP ribosylation factor, 19 kDa protein
PAMP	pathogen-associated molecular pattern
PALP	periarteriolar lymphoid sheath
PBS	phosphate buffered saline
PCR	polymerase chain reaction
pDC	plasmacytoid dendritic cell
PDCA-1	plasmacytoid dendritic cell antigen 1
PE	phycoerythrin
PEG	polyethylene glycol
PIP3	phosphatidylinositol-3,4,5-trisphosphate
PLC	phospholipase C
<i>Plg</i>	<i>gene: plasminogen</i>
<i>plt</i>	<i>gene mutations: paucity of lymph node T cells</i>
PLT	primary lymphoid organs
PMSF	phenylmethylsulfonyl fluoride, serine protease inhibitor
Poly(I)·Poly(C)	polyinosinic-polycytidylic acid
polySia	polysialic acid
<i>P.pastoris</i>	<i>yeast: Pichia pastoris</i>
PSGL-1	P-selectin glycoprotein ligand 1
PtdIns(4,5)P2	phosphatidylinositol-4,5-bisphosphate
Ptx	pertussis toxin
PVDF	polyvinylidene fluoride
R10/20	RPMI supplemented with glutamine, penicillin/streptomycin and 10% or 20% FCS, respectively
Rac	ras-related C3 botulinum toxin substrate
rpm	repeats per minute
RPMI	Roswell Park Memorial Institute medium
RT	room temperature
SAP	shrimp alkaline phosphatase
SCS	subcapsular sinus
SDS	sodium dodecyl sulfate
SDS-PAGE	sodium dodecyl sulfate polyacrylamide gel electrophoresis

## Abbreviations

---

SEM	standard error of the mean
SLO	secondary lymphoid organ
SUMO	small ubiquitin-like modifier
Sup	supernatant
TAE	Tris-acetate-EDTA
TBS	Tris buffered saline
TD	thoracic duct
TEMED	N,N,N',N'-tetramethylethylenediamine
TFB	transformation buffer
Th cell	T helper cell
TIRF	total internal reflection fluorescence
TNF	tumor necrosis factor
T <sub>reg</sub>	regulatory T cell
trunc.	truncated
TSM	Tris-sucrose-magnesium buffer
UAA	under-agarose migration assay
VCAM-1	vascular cell adhesion molecule 1
VLA4	very late antigen 4
WT	wild-type
XCL	C- or $\delta$ -chemokine
XCR	C- or $\delta$ -chemokine receptor
YPDS	yeast extract peptone dextrose medium with sorbitol

# 1 Introduction

In higher eukaryotes the immune system can be subdivided into the innate and the adaptive immune response. Innate immunity defends the host by non-specific mechanisms, whereas the adaptive response is specific to an antigen. During adaptive immune response antigens must be captured, transported and displayed to specific leukocytes, which leads finally to the generation of effector cells and high-affinity antibodies. The initiation of adaptive immunity depends on:

- Dendritic cells (DCs) as the most important antigen-presenting cells
- Secondary lymphatic organs (SLOs) and their micro-architecture facilitating successful DC-T cell encounters – a crucial step during adaptive immune response
- Chemokines as leukocyte guidance and positioning cues

I will focus here on the characteristics and tasks of DCs, their maturation process and how the infrastructure of lymph node (LN) and spleen can influence the immune response. Beyond that, I will give insights into the cytoskeletal organization during leukocyte migration and will summarize the current knowledge how chemokines influence leukocyte positioning and migration in SLOs.

## 1.1 Dendritic cells (DCs)

### 1.1.1 Functions of DCs

DCs are specialized antigen-presenting cells that play a dual role in initiating the adaptive immune response to foreign antigens and maintaining self-tolerance. Most DCs are strategically positioned to sense and respond to invading pathogens. They can be found in all organs, which are exposed to the environment, like the skin or the gut, and SLOs. But differentiated DCs and their precursors also circulate in the blood from where they can be recruited to sites of infection (Alvarez, Vollmann & von Andrian, 2008).

In mice all DCs express CD11c and major histocompatibility complex class II (MHCII) and can be further classified by the expression of CD11b, CD8 $\alpha$ , CD4, PDCA-1, Langerin and a growing list of other markers. But the most fundamental distinction can be made between CD11c<sup>high</sup> MHCII<sup>+</sup> DCs (conventional DCs, cDCs) and interferon (IFN) producing CD11c<sup>low</sup> MHCII<sup>+/low</sup> DCs (plasmacytoid DCs, pDCs; Alvarez, Vollmann & von Andrian, 2008). Immature cDCs sample the peripheral tissue to collect antigenic material, which leads to cell maturation and migration to SLOs where they interact with naïve T cells. Naïve T cells scan

these migratory cDCs until they find one which presents MHCII-antigen complexes that matches to their individual T cell receptor. Successful encounter induces activation and proliferation of the cognate T cell, as well as differentiation into the adequate effector type (O'Shea & Paul, 2010). Another subtype of cDCs are lymphoid tissue resident DCs, which do not migrate in the lymph. Instead their function is restricted during their whole lifetime to one lymphoid organ, where they collect and present foreign as well as self-antigens (Shortman & Naik, 2007). pDCs mostly circulate in the blood and also access LNs via high endothelial venules (HEVs). These cells are responsible for sensing viruses and the release of high amounts of type 1 interferons. pDC-derived interferons modulate strength and quality of natural killer cell, T and B cell responses during viral infection (Ito, Wang & Liu, 2005).

I will focus here on migratory cDCs and in the following text the terms `DC` and `migratory cDC` are used synonymously.

### 1.1.2 DC maturation

DCs express different cell surface receptors like Toll-like-, C-type-lectins, chemokine and cytokine receptors, which allow them to sense pathogen associated molecular patterns (PAMPs) and pro-inflammatory cytokines in their environment (Randolph, Angeli & Swartz 2005). These signals initiate phenotypic changes: The maturing cells transport more antigen-MHCII complexes to the cell surfaces, become motile, develop dendrites, small cell extensions, and start to migrate into the next draining LN (Bancherau & Steinman, 1998). During migration the cells engage ligands, mainly chemokines expressed on the afferent lymphatics, which complete the maturation process (Figure 1; Marsland et al., 2005). These fully matured cDCs express T cell co-stimulatory molecules like CD80 and CD86 and secrete interleukins and type I interferons, which lead to generation of T helper cells (Th; Bancherau & Steinman, 1998). When DCs only sense cytokines without microbial signals, the cells collect and present self-antigens and remain in a semi-mature stage which leads to the induction of regulatory T cells ( $T_{reg}$ ; Randolph, Angeli & Swartz, 2005).

Immature DCs express the chemokine receptors CCR1, CCR2, CCR5, CCR6, CXCR1 and CXCR2. Their ligands, inflammatory chemokines, guide the cells to pathogens or inflamed tissue. During the maturation process these chemokine receptors are down-regulated and instead CCR7 is induced. This process is also called `chemokine receptor switch` (Rot & von Andrian, 2004). CCR7 and its ligands CCL19 and CCL21 are the central guidance cues which direct mature DCs to the draining LN (Figure 1; Randolph, Angeli & Swartz, 2005).



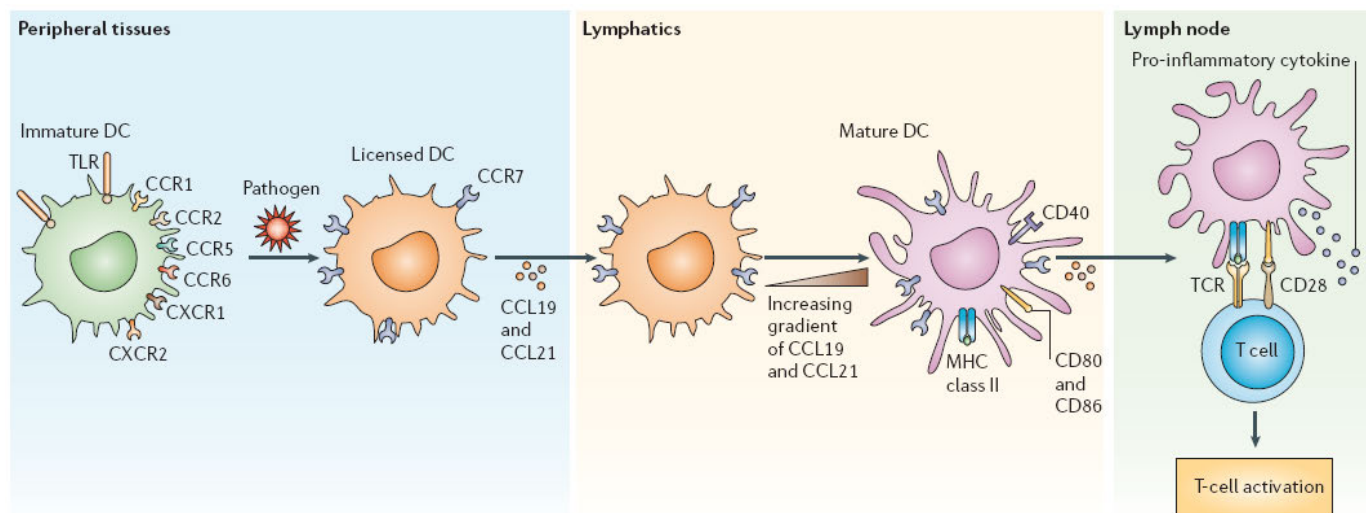


**Figure 1: 'Chemokine receptor switch'.** Immature DCs reside in peripheral tissues and express several chemokine receptors, which guide the cells to pathogens or inflamed tissue. After contact with pathogen associated molecular patterns (PAMPs) DCs undergo a maturation program. During this process these chemokine receptors are down-regulated and instead CCR7 is expressed on high levels. The CCR7 ligands CCL19 and CCL21 guide the DCs to draining LNs, where they can drive naïve T cell activation. CCL19, CCL21 and other ligands expressed on afferent lymphatics provide further DC maturation signals, which lead to the expression of co-stimulatory molecules and the secretion of cytokines and interferons (taken from: Bachmann, Kopf & Marsland, 2006).

## 1.2 Secondary lymphoid organs (SLOs)

SLOs provide a specialized micro-environment to enable efficient encounters between different leukocyte subsets. I will focus here on the organization of LNs and the lymphoid tissue in the spleen, because here chemokine-dependent cell positioning is best investigated.

### 1.2.1 Spleen: Structure and Function

The spleen is the body's main blood filter and is situated in a prime position to capture blood-borne antigens and initiate an adaptive immune response against them. The spleen consists mainly of CXCL12 rich red pulp responsible for red blood disposal and discrete areas of lymphoid tissue surrounding the central arterioles, the white pulp. The white pulp is subdivided into CCL21 expressing T cell areas around central arterioles, also called periarteriolar lymphoid sheaths (PALs), and globular CXCL13 expressing B cell follicles at the periphery of the T cell zones. The white pulp is surrounded by the marginal zone, where branches of central arterioles terminate. Therefore, the marginal zone forms an interface between the white pulp, the red pulp and the blood circulation. For that reason the marginal zone is an important site of antigen capture, where marginal zone macrophages and tissue resident splenic DCs encounter blood-borne antigens, apoptotic cells and microorganisms

(Figure 2; Mebius & Kraal 2005). Also incoming B and T cells enter the spleen at the marginal zone from where they migrate along bridging channels formed by stromal cells into the white pulp. Activated lymphocytes leave the spleen by entering the blood circulation again in the marginal zone (Villadangos & Schnorrer, 2007; Turley, Fletcher & Elpek, 2010).

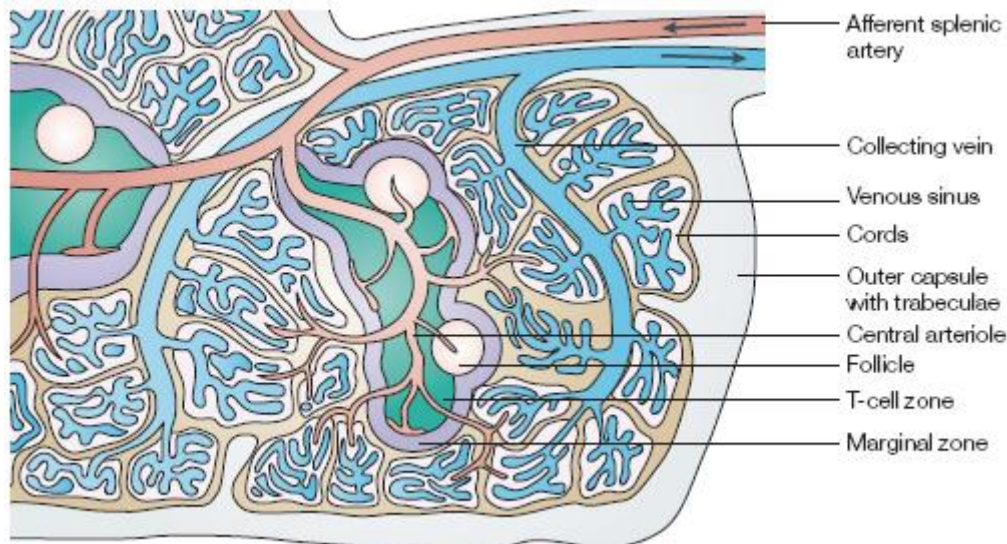


**Figure 2: Structure of the spleen.** The afferent splenic artery splits into several central arterioles. Each arteriole is surrounded by white pulp, which consists of a T cell zone (also called periarteriolar lymphoid sheath; PALS) and B cell follicles. The white pulp is surrounded by the so-called marginal zone, the interface between blood coagulation, red and white pulp, where tissue resident macrophages and DCs encounter blood-derived microorganisms and antigens. The arterioles end in the red pulp cords, which transport the blood to the venous sinus and subsequently into the collecting vein (adapted from: Mebius & Kraal, 2003).

### 1.2.2 Lymph node: Structure and function

To initiate the adaptive immune response an antigen-loaded DC must physically interact with a matching naïve T cell. The success rate of such interactions is extremely low, because the frequency of a naïve T cell recognizing a specific antigen is  $1: 10^5 - 10^6$  (Moon et al., 2007; Lämmermann & Sixt, 2008). SLOs, especially LNs, enhance the feasibility of this rare stochastic event. In LNs cell associated and soluble antigens from the periphery encounter circulating lymphocytes. Thus, LNs are a compact projection of the peripheral patch of tissue they drain. Besides that, LNs function as fluid filters inhibiting the systemic spread of pathogens and acting as the central regulators of fluid equilibration between interstitium and blood.

Two main zones can be distinguished histologically in the LN: The cortex and the medulla. The medullary sinus consists of a labyrinth of lymph drainage vessels, which collect lymph and drain it into the efferent lymph vessel. Besides that, lymphocytes exit LNs through the medullary sinus. The surrounding medullary cords contains plasma cells, memory T cells

and to a smaller amount macrophages. The cortex can be further divided into the CCL21 expressing paracortex or T cell area as well as the CXCL13 rich B cell zone, which consists of primary B cell follicles and after successful antigen engagement of germinal centers (Figure 3). The B cell areas are the centre of the humoral immune response, whereas in the T cell area DC-T cell-encounters take place (von Andrian & Mempel, 2003). DCs enter the LN via the afferent lymphatics and migrate around the B cell follicles into the deep T cell zone, where they position near high endothelial venules (HEVs) (Lämmermann et al., 2008; Miyasaka & Tanaka, 2004). The entry side of the afferent lymphatics in the LN is called subcapsular sinus (SCS) and is populated by resident cells, for example SCS macrophages (Lämmermann & Sixt, 2008). Via the afferent lymphatics not only cells, but the whole interstitial fluid including soluble antigens, intact microbes, particles of pathogens and extracellular signaling molecules like chemokines and cytokines enter the LN. In the blood stream circulating naïve T and B cells enter the paracortex via HEVs. The areas in proximity to HEVs therefore facilitate quick and efficient encounters between incoming T cells and waiting mature DCs (Miyasaka & Tanaka, 2004). HEVs are specialized postcapillary venules lined by high endothelial cells and are mostly located in the T cell area near the B cell follicles, an area also called cortical ridge (Figure 3; Katakai et al., 2004). The entry of DCs as well as of T cells is CCR7-dependent (Debes et al., 2005, Bromley et al., 2005).

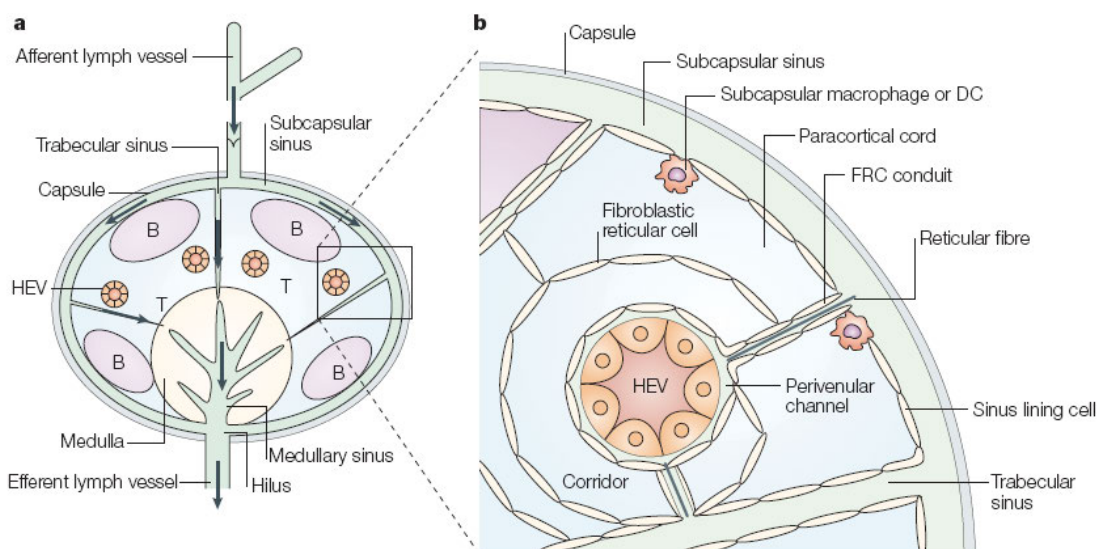


**Figure 3: Lymph node (LN) organization. (A):** LNs can be divided into the medulla (yellow) and the cortex, which consists of the T cell area (blue) and B cell follicles (purple). The blind-ending afferent lymph vessels collect the interstitial fluid and transport it to the subcapsular sinus (SCS) from where it can circulate directly to the efferent lymph vessel or enter the conduit system. The lymph flow is indicated with black arrows. **(B)** Magnified picture detail of the T cell area: T and B cells enter LNs via high endothelial venules (HEVs), specialized blood vessels. HEVs are surrounded by a layer of fibroblastic reticular cells (FRCs). Besides that, FRCs form a network of reticular fibers and conduits, which channel lymph from the sinus into the HEVs (taken from: von Andrian & Mempel, 2003).

### 1.2.3 Stroma cell networks in SLOs

Stroma cells in SLOs contribute to the immune response by providing chemokines, presenting antigen as well as adhesion molecules and acting as scaffold for leukocyte trafficking.

The T cell zone of LNs consists to 95% of densely packed T cells. The residual space is captured by resident DCs and stroma cells. The stroma, the only non-hematopoietic, immobile component of this area, is formed by fibroblastic reticular cells (FRCs). The T cell stroma constitutes a filigree three-dimensional network that is reminiscent of the skeleton of a sponge. The FRCs secrete extracellular matrix (ECM) which associates to so-called conduits. These structures, varying in diameter from 200 nm and 3  $\mu\text{m}$ , channel small molecules (<70 kDa, 20-200 nm in diameter (Manolova et al., 2008)) from the sinus through the T cell area into HEVs. Conduits persist of a loosely packed bundle of collagen (I, III) fibrils stabilized by molecules like fibromodulin and decarin which provide spaces between the fibrils to allow the passage of fluid and small soluble molecules. The collagen bundle is sheathed by various layers of microfibrills consisting of fibrillin and fibronectin. Finally, the fibrillar core is enwrapped by a basal membrane. FRCs produce these structures and at the same time sit on the basal membrane to seal 95% of it by close cell-cell-contacts (Figure 3 B; Figure 4; Lämmermann & Sixt, 2008). On the remaining 5% resident DCs are closely associated with the FRC network scanning the fluid in the conduits for antigens thereby rapidly informed about the periphery (Figure 4; Hayakawa, Kobayashi & Hoshino, 1988).

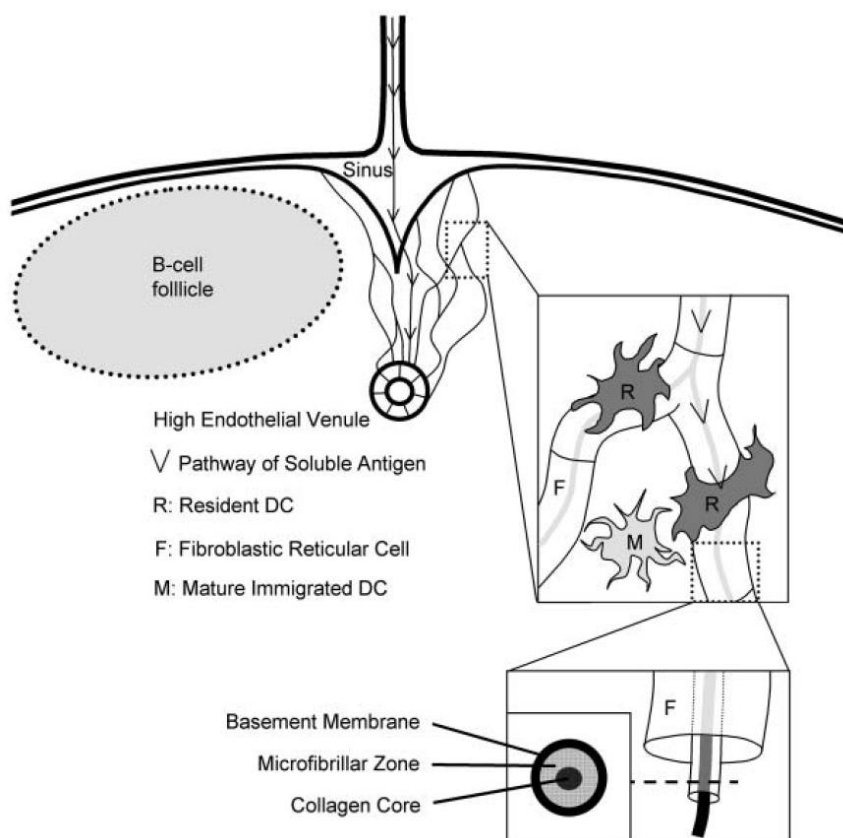


**Figure 4: Composition and function of conduits in the LN. Lymph enters the LN via the afferent lymphatics and is transported via the sinus and conduits to HEVs. The conduits form a network and are partly decorated by resident DCs. The conduits consist of a loosely packed collagen core exhibiting space for lymph flow. The core is surrounded by a microfibrillar zone and a basement membrane. This structure is enlaced by FRCs, which also secrete the ECM components to build the inner conduit (taken from: Sixt et al., 2005).**

FRCs are the main producers of the chemokines CCL19 and CCL21, which bind to the chemokine receptor CCR7 (Luther et al., 2001; Carlsen et al., 2005; Link et al., 2007). CCL21 also seems to be associated with the surfaces of FRCs (Katakai et al., 2004). One potential CCL21 binding partner on FRCs is the proteoglycan podoplanin (Bekiaris et al., 2007). Both FRC organization and CCL21 secretion are induced by interstitial lymph flow in the LN (Tomei et al., 2009). Additionally FRCs express the integrin ligands intercellular adhesion molecule 1 (ICAM1) and vascular cell adhesion molecule 1 (VCAM1) (Ma et al., 1994, Xu et al., 2001). But the corresponding ligands lymphocyte function-associated antigen 1 (LFA1,  $\alpha\text{L}\beta\text{2}$  integrin) and very late antigen 1 (VLA4,  $\alpha\text{4}\beta\text{1}$  integrin) on DCs or T cells, respectively, are not essential for their movement within the LN (Woolf et al., 2007; Lämmermann et al., 2008). Nevertheless, CCL21 influences the migration speed of T cells in the LN (Worbs et al., 2007; Okada & Cyster 2007; 1.3.3.3, p.25).

Current data emphasize further immunological functions of FRCs: These stroma cells can also directly present antigens to naïve T cells and induce proliferation (Fletcher et al., 2010). Moreover, the FRCs regulate naive  $\text{CD4}^+$  and  $\text{CD8}^+$  T cell homeostasis by secreting interleukine (IL)-7 and CCL19 (Link et al., 2007; Turley, Fletcher & Elpek, 2010). Beyond that FRCs act as guidance structures for T cell migration, thus organizing random T cell swarming within the T cell zone (Bajenoff et al., 2006). DCs are also closely associated with FRCs network and might also use the stromal network for movement (Hayakawa, Kobayashi & Hoshino, 1988).

The composition and organization of the FRC network in the splenic PALSs resembles the LN T cell area stroma very closely. Splenic conduits connect the central arteriole with the marginal zone. The splenic conduit system seems to distribute blood-borne and locally produced molecules to the PALSs. In contrast to LN conduits, the splenic conduits can channel larger molecules. Beyond that the homeostatic chemokines CCL21 and CXCL13 can be found within the tubular system as well as on the fiber network (Nolte et al., 2003).

In B cell follicles CXCL13 expressing follicular dendritic cells (FDCs) form a network in the center of the follicles in LNs, spleen and other lymphoid organs. FDCs appear morphologically similar to DCs due to numerous, thin dendrites, but are of non-hematopoietic, mesenchymal origin (Mueller & Germain, 2009). FDCs can directly capture antigens and present them to naïve B cells (Allen & Cyster, 2008). Beyond that, B cell migration was observed to be FDC guided, but also freely moving B cells without stromal association could be detected (Bajenoff et al., 2006; Suzuki et al., 2009). There is also a conduit system described in B cell follicles, which is less dense and shows reduced branching compared to T cell area conduits. These B cell follicle conduits channel antigens directly to naïve B cells (Pape et al., 2007; Roozendaal et al., 2009; Bajenoff & Germain, 2009). The origin of these conduits, if they are formed by FDCs or by remaining FRCs in the B cell areas, is not clarified yet (Roozendaal et al., 2009; Bajenoff & Germain, 2009).

Beyond that, similar stromal cell networks are described in the splenic PALSs, the marginal zones in the spleen and underneath the SCS in LNs especially at the edges of B cell follicles (Nolte et al., 2003; Bajenoff et al., 2008). These stromal networks are formed by another

mesenchymal cell subset called marginal reticular cells (MRCs). MRCs express like FDCs CXCR13 and are able to form conduits delivering antigens directly from the SCS to B cells and FDCs (Katakai et al., 2008; Balogh et al., 2004; Roozendaal et al., 2009).

### 1.3 Chemokines

Chemokines (from „chemotactic cytokines“) are secreted proteins, 8 to 17 kDa in size, that function as the most important communication system of immune cells. Their main task is the regulation of leukocyte migration and positioning. But chemokines are also participating in processes like cell adhesion, cell differentiation as well as apoptosis and influence the proliferation and maturation of immune cells. Currently 43 chemokines are known in humans and mice.

#### 1.3.1 Chemokine classifications

The protein family of chemokines is not defined by a common function, but by structural similarities. Nearly all chemokines exhibit four invariant cysteine residues, that form two cysteine bridges, one in between the first and the third residue, the second bridge in between the second and the fourth cysteine. The classification of chemokines in different subgroups depends on the relative position of the first two cysteines.

Chemokines with a non-conserved amino acid in between the first two cysteines are known as CXC- or  $\alpha$ -chemokines. This subgroup comprises 16 chemokines (systematic nomenclature: CXCL1 to CXCL16). The second big subgroup are the CC- or  $\beta$ -chemokines, where the first two cysteine residues succeed directly (CCL1 to CCL28, CCL9 and CCL10 are identical). CC-chemokines partly possess six cysteines, which can form three cysteine bridges (C6-CC: CCL1, 15, 21, 23, 28). The third subgroup consists of only one member, which is known as CX3C- or  $\gamma$ -chemokine, because it exhibits three amino acids between the first two cysteines (CX3CL1). The trivial name of this chemokine is fractalkine and in the chemokine family it is the only surface receptor with a transmembrane domain. There are two exceptions of the '4-cysteine paradigm', XCL1 and XCL2, which have only two cysteines and belong to the fourth subgroup of C- or  $\delta$ -chemokines (Figure 5; Rot & von Andrian, 2004).

For chemokines a special folding structure was described, consisting of three anti-parallel  $\beta$ -sheets and a carboxy (C)-terminal  $\alpha$ -helix. A further structural similarity is the very flexible amino (N)-terminus, which lacks a fixed structure and is responsible for the receptor binding and activation (Figure 5; Figure 7; Frederick & Clayman, 2001).

Chemokines can be further classified according to their expression pattern. Homeostatic chemokines are constitutively secreted and among other tasks guide leukocytes to



## Introduction

lymphatic organs. Moreover, homeostatic chemokines segregate lymphoid organ compartments through spatially restricted expression. The expression of inflammatory chemokines on the other hand is limited to infections or pro-inflammatory situations, where they direct leukocytes to inflamed or injured tissue (Rot & von Andrian, 2004).

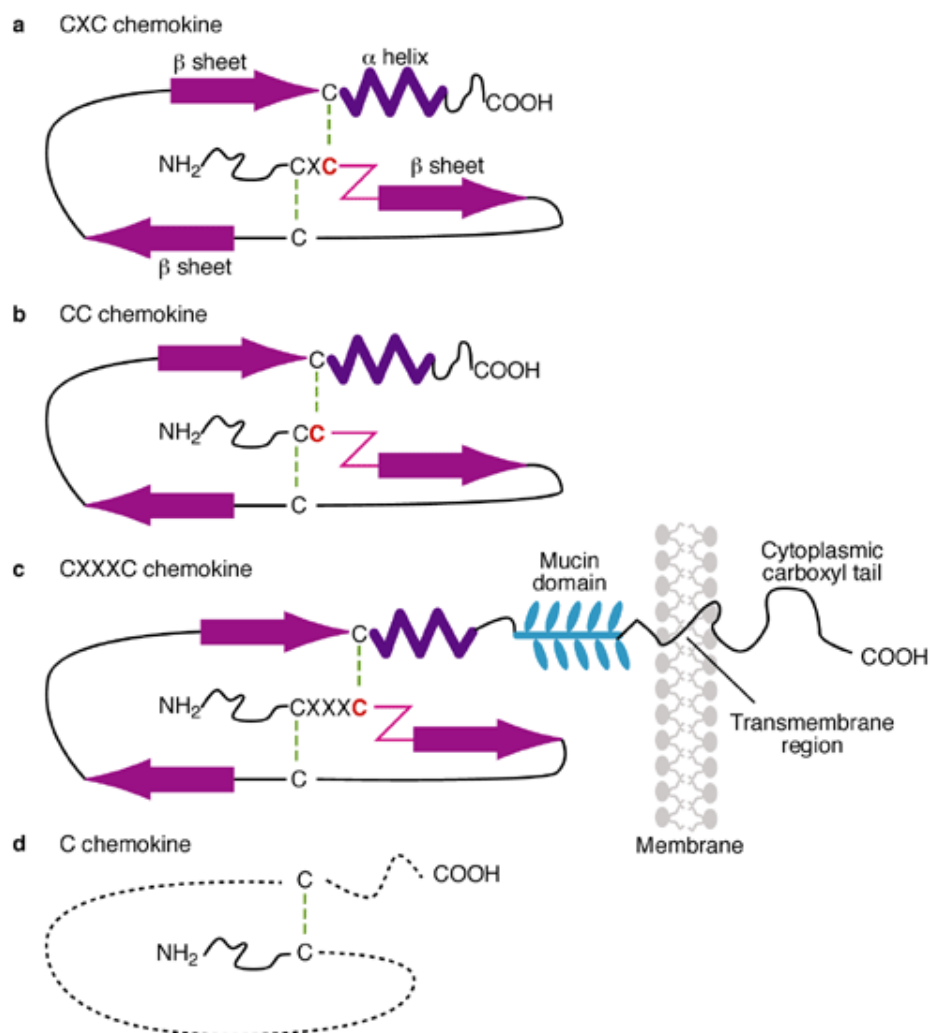


**Figure 5: Schematic depiction of the four chemokine subtypes.** The flexible N- and C-termini are illustrated in irregular lines. The first three chemokine groups have an α-helix (purple jagged line) followed by three β-sheets (pink arrows), which are connected by loops. Green dashed lines indicate cysteine bridges. The CX3C-chemokine fractalkine is the only one with a mucin and a transmembrane domain. The structure of the C-chemokines is widely unknown and is therefore only indicated with a pointed line (taken from: Frederick & Clayman, 2001).

### 1.3.2 Inflammatory chemokines

Inflammatory chemokines can be secreted by a great diversity of cells as a response to viruses, bacteria and physically damaging agents like silica or urate crystals. The secretion of inflammatory chemokines can be triggered by PAMPs, as well as endogenous molecules that are associated with infection and injuries, like elastase, defensins and fibrinogen. The expression of these chemokines can further be stimulated by inflammatory or immunomodulatory cytokines like IL-1, tumor necrosis factor (TNF)- $\alpha$ , INF- $\gamma$ , IL-4, IL-5, IL-6, IL-13 and IL-17. Inflammatory chemokines are typically ligands of the chemokine receptors CCR1, CCR2, CCR3, CCR5, CXCR2 and CXCR3. Besides the recruitment of DCs residing in the tissue, inflammatory chemokines also recruit monocytes, neutrophils and other effector cells from the blood to sites of infections (Rot & von Andrian, 2004).

### 1.3.3 Homeostatic chemokines

Homeostatic chemokines are constitutively produced in the healthy individual by specialized stroma cells and control homing, retention and motility of lymphocytes and DCs. During immune response lymphatic tissues transiently down-regulate the transcription of homeostatic chemokines to regulate overall cellularity in SLOs (Mueller et al., 2007). Moreover, homeostatic chemokines, like CXCL12, CXCL13 and CCL21, are indispensable for SLO formation and organization.

#### 1.3.3.1 CXCL12 : Precursor retention in the bone marrow and localization of plasma cells in SLOs

CXCL12 (also: stromal cell derived factor 1, SDF-1) is broadly expressed by stroma cells within bone marrow and many epithelial tissues. Six different isoforms of CXCL12 are described in humans, three in mice, which differ in their affinity towards proteoglycans. The exact organ specific expression patterns of the different CXCL12 splice variants are unclear (Rueda et al., 2008; Lortat-Jacob, 2009; Torres & Ramirez, 2009). Generally high CXCL12 concentrations can be observed in splenic red pulp, LN medullary cords and the subepithelial region of tonsils, but also in non-lymphatic tissues like gut, heart and brain (Hargreaves et al., 2001; Casamayor-Palleja et al., 2001; Egawa et al., 2001). Deficiency in either receptor or ligand causes perinatal lethality because of severe defects in bone marrow homeostasis, gut vasculogenesis, heart and brain development (Egawa et al., 2001). CXCL12 serves as a chemoattractant and cell positioning guidance cue for naive B cells and T cells, special DC subsets, like Langerhans cells, and plasma cells, which all express the corresponding chemokine receptor CXCR4 (Hargreaves et al., 2001, Egawa et al., 2001, Kabashima et al., 2007). *CXCR4*<sup>-/-</sup> plasma cells transferred to wild-type (WT) recipients



accumulate adjacent to the white pulp or within the marginal zone (Hargreaves et al., 2001). In the LN *CXCR4*<sup>-/-</sup> plasma cells localize adjacent to follicles, at the perimeter of the medulla (Cyster, 2003). Furthermore, CXCL12-dependent cell sorting is responsible for the establishment of the dark zone of germinal centers, where maturing B cells and antibody-producing plasma cells accumulate. In the bone marrow CXCL12 seems to function as a retention signal for precursor cells to avoid too early cell egress and thereby regulate hematopoietic cell homeostasis (Nagasawa et al., 1996). Besides that, CXCL12 is expressed on HEVs and promotes together with CCR7 ligands B cell attachment to HEVs (Okada et al., 2002).

### 1.3.3.2 CXCL13: Organization of B cell areas in SLOs

The main task of the homeostatic chemokine CXCL13 (also: B cell chemoattractant, BLC) is the guidance of naïve B cells into the B cell follicles of SLOs as convincingly shown with B cells deficient in the corresponding chemokine receptor CXCR5 transferred to WT recipients. These *CXCR5*<sup>-/-</sup> B cells are detained in homing to B cell follicles in spleen and peyer's patches and instead they are trapped in T cell zones (Okada et al., 2002; Förster et al., 1996). CXCR5 is also expressed on mature re-circulating B cells, subsets of CD4<sup>+</sup> and CD8<sup>+</sup> T cells and skin derived migratory DCs (Förster et al., 1994; Saeki et al., 2000).

CXCL13 is produced by MRCs in the subcapsular region of the follicle and in the centre of the follicle by FDCs (Cyster et al., 2000; Katakai et al., 2008). In addition to that, the formation of the germinal center light zone, where activated B cells undergo affinity-maturation, depends on CXCL13 expression by FDCs (Cozine, Wolniak & Waldschmidt, 2005). The motility of GC B cells is significantly reduced in *CXCR13*<sup>-/-</sup> mice (Allen et al., 2007). CXCL13 can bind to heparin sulfates and collagen and is therefore found to be concentrated on collagen fibers and stromal cells like FDCs (de Paz et al., 2007; Yang et al., 2007; Nolte et al., 2003). In *CXCR5*<sup>-/-</sup> and *CXCL13*<sup>-/-</sup> mice up to 95% of all peripheral LNs and peyer's patches are lacking. In the residual SLOs the characteristic highly organized B cell follicles are missing. The resulting rudimentary B cell enriched areas exhibit only poorly demarked borders between B cell rich areas and T cell zone and lack the typical FDC network. Therefore, in these organs B cells are located in the outer regions of lymphoid tissue forming a ring around the T cell areas (Förster et al., 1996; Ansel et al., 2000).

### 1.3.3.3 CCL19 and CCL21: Organization of T cell areas in SLOs

CCL19 (also: ELC, MIP-3 $\beta$ , CK $\beta$ 11, Exodus3) and CCL21 (also: SLC, 6CKine, Exodus 2, TCA-4) are both ligands of the chemokine receptor CCR7. They are likely of similar structure and have comparable binding constants towards CCR7 (Frederick & Clayman, 2001; Yoshida et al., 1998; Pilkington et al., 2004). The two CCR7 ligands also bind to CC-X-chemokine receptor (CCX-CKR), a so-called interceptor (Gosling et al., 2000). Interceptors

show no chemokine receptor signaling, but instead scavenge chemokines from extracellular spaces (Comerford et al., 2006; Heinzel, Benz & Bleul, 2007). Both chemokines stimulate endocytosis and antigen presentation by DCs and induce a pro-inflammatory differentiation program in semi-mature DCs on their way to draining LNs (Yanagawa & Onoe, 2003; Marsland et al., 2005; 1.1.2, p.16). However, these two homeostatic chemokines also exhibit considerable differences.

CCL21 is produced by FRCs and in mice also by HEVs (Link et al., 2007; Carlsen et al., 2005). Additionally FRCs express CCL19, but at a 100-fold lower level (Luther et al., 2001; Link et al., 2007). Beyond that, monocytes, macrophages as well as several matured DC subsets are an accessory source of CCL19 (Figure 6 A; Sallusto et al., 1999; Cyster, 1999; Luther et al., 2000). In mice the gene locus encoding the two CCR7 ligands was duplicated during evolution. By point mutation two functional CCL21 variants developed out of two CCL21 genes, which only differ in amino acid 65, where one CCL21 exhibit a serine (CCL21-Ser), the other one a leucine (CCL21-Leu). CCL21-Ser is expressed in lymphoid organs, CCL21-Leu in lymphatic vessels and also in non-lymphatic organs like lung, colon, stomach, heart and skin (Gunn et al., 1998). In contrast to that, only one CCL21 variant persists in humans (Vassileva et al., 1999). Even though the whole gene locus encoding both CCR7 ligands was duplicated, only one functional CCL19 gene exists. The duplicated CCL19 gene exhibits a mutated stop codon which prevents protein expression (Nakano & Gunn, 2001).

In a naturally occurring strain of mutant mice the locus coding for CCL21-Ser and the active copy of CCL19 is deleted. The mutation called '*paucity of lymph node T cell*' (*plt*) results in a loss of CCL21 and CCL19 expression in SLOs (Vassileva et al., 1999; Mori et al., 2001; Nakano & Gunn 2001; Figure 6 B). In *plt/plt* mice the homing of DCs as well as naïve T cells to SLOs and thymus is impaired. Only a few matured DCs accumulate in the SCS of LNs without reaching the T cell area (Gunn et al., 1999; Marsland et al., 2005). Therefore, T and B cell priming occurs in *plt/plt* mice mainly in superficial cortical areas of LNs (Junt et al., 2002). Due to impaired T cell homing to the thymus as well as to all SLOs T cell numbers are impaired and no clear T cell zones are detectable (Misslitz et al., 2004; Nakano et al., 1997; Nakano et al., 1998). Due to these defects T cell development is disturbed, especially the establishment of self-tolerance is impaired. *Plt/plt* mice have therefore a delayed adaptive immune response and develop multi-organ autoimmunity (Kurobe et al., 2006; Nitta et al., 2009; Förster, Davalos-Misslitz & Rot, 2008).

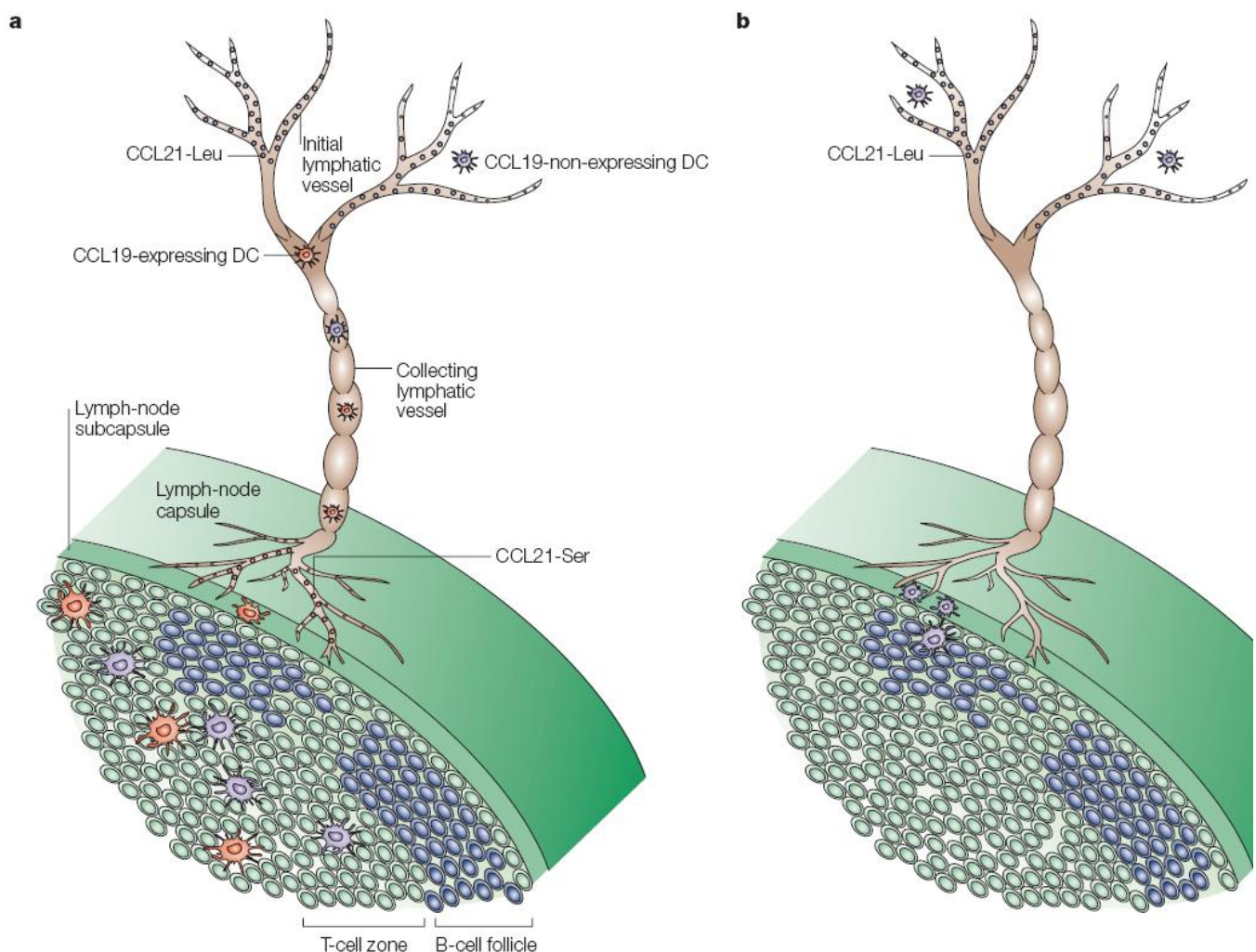


**Figure 6: Expression pattern of CCR7 ligands in LNs. (A)** CCL21-Leu is expressed in the initial lymphatics. Whereas the second CCL21 variant CCL21-Ser can be found in the terminal subcapsular sinus (SCS) lymphatics as well as in the LN T cell area. The CCL21 variant expressed in collecting vessels is not identified yet. CCL19 is like CCL21-Ser secreted by the stromal cells in the T cell zone but in much lower amounts. In addition to that, many hematopoietic cells like mature DCs produce CCL19. **(B)** In *plt/plt* mice only CCL21-Leu is expressed in the initial lymphatics. Mature DCs are not able anymore to enter the T cell area, instead the cells accumulate in the SCS (taken from: Randolph, Angeli & Swartz, 2006).

A unique feature of CCL21 is its elongated C-terminus consisting of 32 amino acids 12 of which are basic. The CCL21 C-terminus facilitates binding to negatively charged proteins, like glycosaminoglycans (GAGs) of the heparan and chondroitin sulfate subgroups (Hirose et al., 2001; Hirose et al., 2002; Ueno et al., 2002; Uchimura et al., 2006). In contrast to that, CCL19 interacts only weakly with GAGs and remains therefore predominantly soluble (de Paz et al., 2007). CCL21 immobilization might be required for efficient chemokine presentation on endothelial cells and potentially FRCs to DCs and T cells (Yoshida et al., 1998; Gunn et al., 1998; Stein et al., 2000; Ueno et al., 2002; Bao et al., 2010; 1.3.4, p. 28). CCL21

expressed by FRCs influences the migration speed of T cells in the LN. In *plt/plt* mice a 30% reduction in velocity could be measured (Worbs et al., 2007; Okada & Cyster 2007). By intravenous application of CCL21 the migration velocity can be restored. CCL19 was not tested in this experimental setup (Worbs et al., 2007). Thus, continuous CCL21-signaling seems to drive T cell motility. It is still under discussion if immobilized CCL21 covers the T cell area homogeneously or exhibits a higher concentration in the center of the T cell zone. Okada et al. (2005) observed a CCL21 gradient extending from the T cell zone into the B cell follicle.

Beyond that CCL21 is very efficient in the induction of tertiary lymphoid organs. When CCL21 is artificially introduced into tumor tissue or pancreatic islets, the chemokine entails large, highly organized infiltrates including HEVs and a complex stromal cell network. The infiltrates recapitulate the architecture of SLOs. CCL19 is less capable in recruiting cells in these experimental setups; the infiltrates are less organized and DCs, T and B cells are frequently interspersed (Nomura et al., 2001; Luther et al., 2001). Apart from these features CCL21 also increases T cell interactions with DCs and promotes immune responses by co-stimulating T cell activation and proliferation (Friedmann, Jacobelli & Krummel, 2006; Flanagan et al., 2004).

Surprisingly *CCL19*<sup>-/-</sup> mice have no gross abnormalities in T cell migration and positioning (Link et al., 2007). Furthermore, DC migration, maturation and function occur normally in the absence of CCL19. CCL21 alone is sufficient to fulfill these functions (Britschgi et al., 2010). After CCR7 binding both chemokines induce signaling, but only CCL19 also effectively stimulates CCR7 phosphorylation and internalization subsequently leading to receptor desensitization and degradation. Following receptor binding almost 4 times more CCL19 than CCL21 is internalized. When the endocytosis of CCL19 is blocked, DCs cannot migrate towards a CCL19 source anymore (Otero, Groettrup & Legler, 2006; Byers et al., 2008). Beyond that also the interceptor CCX-CKR, which scavenges the CCR7 ligands from extracellular spaces, internalizes CCL19 much more efficiently than CCL21 (Comerford et al., 2006, Heinzl et al., 2007). Another unique feature of CCL19 is that it transforms the morphology of mature DCs. The chemokine evokes extension and probing of dendrites of DCs thereby potentially leading to a more efficient interaction of DCs with naïve T cells (Yanagawa & Onoe, 2002). Moreover, CCL19 promotes much more efficient T cell emigration from explanted thymus slices compared to CCL21. But by removing the C-terminal tail of CCL21 the chemokine gains this function of CCL19 and T cell egress could be restored (Ueno et al., 2002).

### 1.3.4 Chemokine immobilization on proteoglycans

The structure of chemokines influences their mode of presentation and distribution within tissues or extracellular matrix. Chemokines are secreted proteins, but many of them can

bind to proteoglycans (also: glycoproteins). Proteoglycans consist of a core protein with one or more covalently attached GAG chains. GAGs are long unbranched polysaccharides consisting of a repeating disaccharide unit and can be divided into six subgroups: Chondroitin sulfates, dermatan sulfates, keratan sulfates, heparan sulfates, heparin and hyaluronan. A common feature of GAGs is their negative charge due to the high amount of sulfate- and carboxyl-groups, so they can interact with basic proteins, as for example chemokines. But chemokine-GAG interactions do not exclusively depend on overall electrostatic interactions; chemokines selectively bind specifically functional domains of GAGs (Kuschert et al., 1999; Witt et al., 1994; Patel et al., 2001). Most chemokines exhibit heparan sulfate (HS) binding sites (Amara et al., 1999; Santiago et al., 2006). HS comprise 95% of the proteoglycans and are composed of alternating  $\alpha$ -linked N-acetyl- or N-sulfo-glucosamine and  $\alpha/\beta$ -linked hexuronic acid. The predominant heparan sulfate proteoglycans on cell membranes are transmembrane syndecans and GPI-anchored glypicans (Handel et al., 2005). Many homeostatic chemokines interact with GAGs: CCL21 immobilize with its C-terminus on heparan and chondroitin sulfates (Hirose et al., 2001; Hirose et al., 2002; Uchimura et al., 2006; Rot und von Andrian, 2004; Miyasaka und Tanaka, 2004). Binding to these GAGs mediate for example the CCL21 immobilization on the proteoglycans P-selectin glycoprotein ligand-1 (PSGL-1), which is expressed on white blood cells and endothelial cells (Veerman et al., 2007). Beyond that CCL21 immobilizes to podoplanin (also: gp38), which is expressed on lymphatic endothelial cells as well as on FRCs and potentially presents CCL21 to DCs (Breiteneder-Geleff et al., 1999; Kriehuber et al., 2001; Pegu et al., 2007; Bekiaris et al., 2007). CCL21 binds furthermore to ECM proteins like collagen IV, MAC25 and to basement membranes of HEVs (Miyasaka und Tanaka, 2004). CXCL13 binds to heparin sulfates as well as to collagen fibers. Potentially these interactions facilitate the immobilization of CXCL13 on FDCs in B cell follicles *in vivo* (Cyster et al., 2000, Nolte et al., 2003). For the germinal center chemokine CXCL12 three different isoforms with widely divergent HS binding capacities are published. CXCL12 $\gamma$  for example can form one of the most stable GAG-chemokine complexes (Rueda et al., 2008; Lortat-Jacob, 2009). *In vitro* many chemokines can also be immobilized on artificial substrates like polycarbonate membranes (Kohrgruber et al., 2004).

The immobilization of chemokines on GAGs has several functions: Through binding GAGs can store, protect from degradation or limit the distribution of chemokines. GAGs enhance for example the local chemokine concentration on endothelial cells that line the interior of blood and lymph vessels; without such a mechanism chemokine accumulation would be disrupted by the shear forces of blood or lymph flow (Ali et al., 2000). Immobilized chemokines on endothelial cells are a prerequisite for leukocyte extravasation, the movement from blood capillaries into the surrounding tissue. Before the cells can squeeze through the endothelial cell layer, integrins on the leukocyte's surface must be activated by surface-bound chemokines to allow tight adhesion to capillaries' walls (Ley et al., 2007; Shamri et al., 2005). Immobilized CCL21 on vascular and lymphatic endothelia is for example a prerequisite for efficient B and T cell recruitment to SLOs (Bao et al., 2010; Shamri et al.,

2005). Hirose et al. (2002) showed that immobilization of CCL21 on heparan sulfates supports integrin activation, whereas CCL21 binding to chondroitin sulfates prevents integrin activation and signaling. Proudfoot et al. (2003) further sustained the *in vivo* relevance of chemokine immobilization followed by chemokine oligomerization with an elegant *in vivo* peritoneal recruitment assay. Non-GAG binding chemokine mutants were unable to induce cell recruitment. The same result was observed with mutants that were not able to form higher-order oligomers. It is unclear if GAG-bound chemokines can signal through G protein-coupled receptors (GPCRs) or if they first have to dissociate from the receptor (Proudfoot et al., 2003). *In vitro* chemokine function is independent of chemokine binding to or oligomerization on GAGs (Paavola et al., 1998, Proudfoot et al., 2003).

Therefore, chemokine immobilization in particular microenvironments can be influenced by the expression pattern of GAGs. In interstitial spaces GAG binding may create immobilized chemokine gradients. But evidence for the existence of continuous chemokine gradients *in vivo* is scarce, due to difficulties of visualizing chemokines *in vivo* (McDonald et al., 2010). Another possibility is that GAG-binding supports the establishment of immobilized chemokines shape fields (Pelletier et al., 2000). Also the release of GAG-bound chemokines for example by proteolytic shedding is possible. But the system is even more complex because also GAGs can be soluble, surface bound or be degraded to soluble ectodomains (Handel et al., 2005). Thus, chemokines can also be immobilized on soluble GAGs. The binding of chemokines to GAGs is maybe another level of regulation and may result in fine-tuning migration, localization and activation of leukocytes (Hoogewerf et al., 1997; Rot, 1993; Middleton et al., 1997).

### 1.3.5 Chemokine receptors

Chemokines bind to G-protein coupled receptors (GPCRs) with seven transmembrane domains, which transmit the signal into the cell. Chemokine receptors consist of a single polypeptide chain with three extra and three intracellular domains, an acidic N-terminal, extracellular domain as well as a serine/threonine-rich intracellular C-terminus. Together the extracellular protein domains specify the ligand recognition. The cytoplasmic protein loops and the C-terminal domain are responsible for signaling and receptor internalization (Figure 7). Ligand binding induces allosteric changes in the tertiary structure of the chemokine receptor, which then allows binding and activation of heterotrimeric G-Proteins, consisting of an  $\alpha$ -  $\beta$ - and  $\gamma$ -subunit, on the intracellular domains. Activated G-proteins exchange guanosine-5'-diphosphate (GDP) for guanosine-5'-triphosphate (GTP) followed by the dissociation into an  $\alpha$ - and a  $\beta\gamma$ -subunit. The  $\beta\gamma$ -subunit activates phosphoinositide-3 kinase (PI3K) which in turn produces phosphatidylinositol-3,4,5-trisphosphate (PIP3). PIP3 induces the activation of the small GTPase Rac that subsequently leads to the activation of the actin nucleating and elongating factor actin related protein 2/3 (Arp2/3) thereby enhancing actin polymerization (Rot & von Andrian, 2004; Thelen & Stein, 2008). Chemokine receptors can

couple to different G $\alpha$  subunits, but the most significant are pertussis toxin sensitive G $\alpha_i$  subunits (Rot & von Andrian, 2004). G $\alpha_i$  subunits inhibit adenylylase, activate a variety of phospholipases and phosphodiesterases, and promote the opening of several ion channels (Birnbaumer, 2007). Pertussis toxin keeps G $\alpha_i$  in a GDP-bound, inactive state, prevents binding to the chemokine receptor and thereby inhibits GPCR-dependent signaling (Smrcka, 2008).

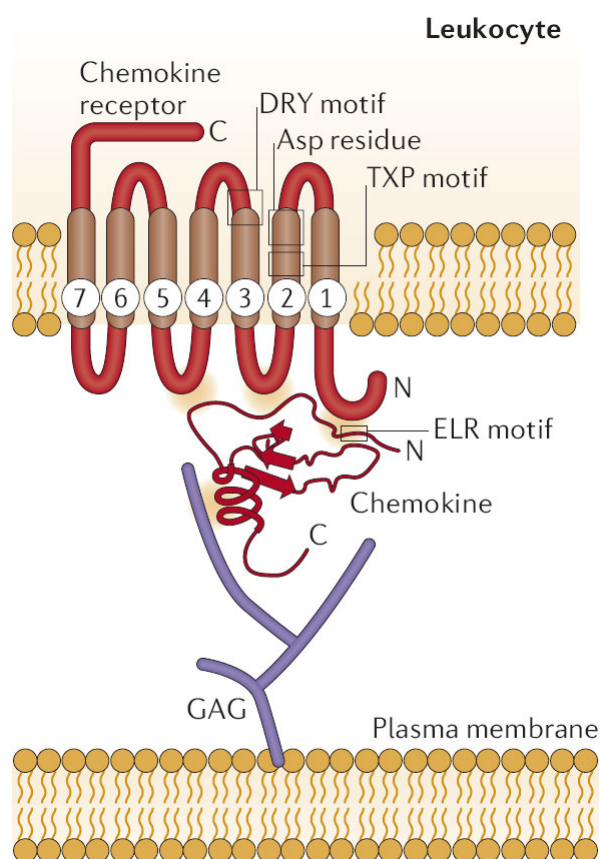


**Figure 7: Chemokine-chemokine receptor interaction.** Chemokines can bind as soluble molecules to the chemokine receptor or be presented by glycosaminoglycans (GAGs) to the receptor as shown here. Chemokines possess a glutamate-leucine-arginine motif (ELR) in their flexible N-terminus, which interacts with the N-terminus of the receptor. Chemokine receptors exhibit seven transmembrane domains and three conserved sequence motifs that are important for signal transmission: An aspartate-residue followed by a threonine-X-proline-motif (TXP, X: any amino acid) in the second transmembrane domain and between the second intracellular loop and the third transmembrane domain a aspartic acid-arginine-tyrosine motif (DRY; taken from: Mantovani, Bonecchi & Locati 2006).

Currently 19 chemokine receptors are known: 11 CC-chemokine receptors (CCR1 to CCR11), 6 CXC-chemokine receptors (CXCR1 to CXCR6), one C-chemokine receptor (XCR1) and finally one CXC3-chemokine receptor (CX3CR1).

### 1.3.6 CCR7: Guidance of mature DCs

The chemokine receptor CCR7 is expressed in semi-mature and mature DCs, thymocytes during defined development stages, naïve B and T cells, T<sub>reg</sub> cells, central memory T cells (T<sub>CM</sub>) and also in non-lymphoid cell types for example in various malignancies (Ohl et al., 2004; Misslitz et al., 2004; Reif et al., 2002; Sallusto et al., 1999; Szanya et al., 2002; Schneider et al., 2007; Shields et al., 2007).

The *CCR7*<sup>-/-</sup> mice exhibit only a weak and delayed adaptive immune response due to alterations in the micro-architecture of the thymus as well as of SLOs: In the paracortical areas of LNs, Peyer's patches and the white pulp of the spleen T and B cell areas are not clearly separated. The medullary areas of the thymus are smaller, but more numerous and located to the outer rim of the organ. Instead the mice develop ecotopic lymphoid aggregates in mucosal sites like lungs, stomach and intestine with well segregated B and T cell zones as well as HEVs. These morphological changes are due to impaired cell homing and positioning in SLOs. *CCR7*<sup>-/-</sup> mice show impaired migration of DCs from the skin, lung and the intestine to draining LNs. LN homing and positioning of naïve T cells, T<sub>CM</sub> and T<sub>reg</sub> cells is also strongly impaired, which results in LNs and Peyer's patches that are largely devoid of T cells, which accumulate instead in the red pulp of the spleen. Due to the disturbed thymic architecture T cell development and maturation is hindered which leads on one hand to a delayed adaptive immune response and on the other hand to impaired central and peripheral tolerance. Ineffective tolerance to self antigens causes the development of multi-organ autoimmunity in *CCR7*<sup>-/-</sup> mice (Förster et al., 1999; Förster, Davalos-Misslitz & Rot, 2008).

## 1.4 Chemokine guided migration in the immune system

Leukocyte trafficking is indispensable for innate and especially adaptive immunity. Chemokines are the main guidance cues in the immune system and responsible for leukocyte migration and positioning. Here, I will discuss how the presentation mode of chemokines influences cells and the current knowledge about chemokine-dependent directional and non-directional migration *in vivo*.

### 1.4.1 Leukocyte trafficking

A number of discrete migration processes can be described for leukocytes: The exit of progenitors, committed and differentiated cells from the primary lymphoid organs, thymus and bone marrow, into the blood circulation; the extravasation from the blood vasculature into target tissues or SLOs; crawling within interstitial tissues to scan for antigens; the entry into lymph vessels after antigen encounter to reach draining LNs and the exit from SLO by entering the blood circulation again (Figure 8; Alvarez, Vollmann & von Andrian, 2008).

All these processes depend to certain extends on chemokines. Some of these migration events like the directional migration towards LNs implicate the existence of chemokine concentration gradients (Lämmermann et al., 2008; Pflücke et al., 2009). Whether these gradients are soluble or immobilized is indistinct till now. The extravasation of leukocytes on the other hand is controlled by immobilized chemokines, as mentioned before. But in most of



the cases the presenting mode is unclear, although it massively influences leukocyte cell behavior.

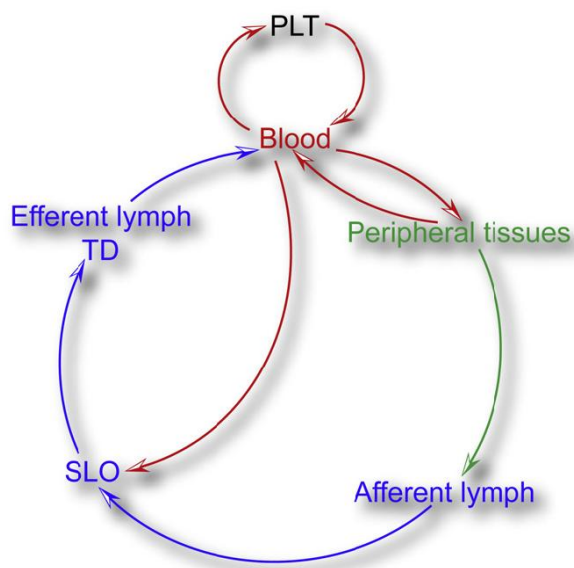


**Figure 8: Trafficking routes of leukocytes.** Leukocytes originate from precursors in primary lymphoid tissues (PLTs) like the bone marrow or the thymus. Precursor or committed cells enter the blood circulation to migrate to peripheral tissues and SLOs. After antigen encounter in the periphery DCs migrate via afferent lymphatics to draining LNs. B and T cells enter SLOs directly from the blood stream. Leukocytes leave SLOs via efferent lymphatics followed by entering the blood circulation again via the thoracic duct (TD; taken from: Alvarez, Vollmann & von Andrian, 2008).

### 1.4.2 Cell migration modes

How cells migrate, random or directed, adhesive or non-adhesive, depends on the activation state of its integrins and in which form chemokines are presented to the cell. Activated integrins on cell surfaces define the cells' capability to position and migrate in specific environments. This migration mode has been termed *haptic*. Haptic movement is strictly confined to a preformed path because the immobilized integrin-ligands act as mechanical anchor. The best characterized stimuli for integrin activation on leukocytes are GAG-bound chemokines (Ley et al., 2007; Shamri et al., 2005; Bao et al., 2010). If chemokine immobilization is always a prerequisite for integrin activation on leukocytes is unclear. Random adhesive migration in a homogenous chemokine field is termed *haptokinesis*. *Haptotaxis* describes the migration along concentration gradients of extracellular ligands. Leukocytes have the unique capability to migrate within confined three-dimensional environments like the interstitium of mesenchymal tissues without using transmembrane force coupling via integrins. Such integrin-independent movement can be triggered *in vitro* by soluble chemokines. In a homogenous, soluble chemokine field the cells show *chemokinesis*, random migration, whereas the cells perform *chemotaxis*, directional migration, in a soluble chemokine concentration gradient (Lämmermann et al., 2008).

Available experimental data from SLOs only allow the distinction between random, kinetic and directional, tactic motility. If haptic interactions with other cells or the ECM take place, cannot be distinguished in these experiments due to technical limitations like microscopically

resolution or experimental design, which often does not visualize the surrounding cells or ECM.

### 1.4.3 Evidence for kinesis

A homogenous chemokine distribution results in a random locomotion pattern. The corresponding *in vivo* cell migration pattern is also often described as cell “swarming”, because the cells scan their environment, especially other immune cells, in a non-directional way (“stochastic model”) (Asperti-Boursin et al., 2007; Okada and Cyster, 2007; Worbs et al., 2007). Chemokine dependent, kinetic swarming behavior is described for many leukocytes. Dermal DCs for example continuously crawl through interstitial spaces in the skin in a Gai dependent manner, the responsible chemokines are not determined yet (Ng et al., 2005). Another example are double-negative as well as double-positive CXCR4 expressing thymocytes, which are confined to thymic cortex where they move slowly without directional bias (Witt et al., 2005; Ehrlich et al., 2009). Furthermore, after entry into lymphoid organs T and B cells localize to their distinct areas and show a random migration pattern within their specific zone (Miller et al., 2002; Miller et al., 2003; Wei et al., 2005). But the random migration is still organized. The three-dimensional scaffolds of T cell area FRCs and the B cell area FDCs represent tracks along which T and B cells migrate, a phenomenon that has been described as “guided randomness” (Bajenoff et al., 2006; Mempel et al., 2006). Mechanistically, it was suggested that CCL21 and CXCL13 immobilized on the stroma surface might form a kinetic scaffold that keeps the cells motile (Bajenoff et al., 2006; Bajenoff et al., 2008; Roozendaal et al., 2009).

### 1.4.4 Evidence for taxis

During adaptive immune response leukocyte subsets accumulate in distinct regions within B or T cell areas or perform directed migration to converge and interact with each other. These observations can only be explained with the assumption of graded guidance cues which direct the cells. It is possible to correlate chemokine receptor levels with accurate cell positioning in lymphoid organs. Here, the cells show responsiveness to two chemokines and distinct thresholds of chemokine receptors which guide the cells to positions where the attraction to both chemokines is balanced. These experiments were mainly carried out either in static tissue sections or in engineered two-dimensional microenvironments (Randolph et al., 1999; Ansel et al., 1999; Hardtke et al., 2005; Ricart et al., 2010). Until now it was not possible to visualize chemokine gradients in lymphatic tissue. Thus, it remains speculative if long range chemotactic gradients *in vivo* exist, but it would be a plausible explanation for the experimental data I will discuss here. I focus here on data derived from spleen and LNs, because they have been most extensively studied, harbor similar cell subsets and feature matching basic structures.

Activated T cells differentiate into cytokine secreting effector cells for example into diverse Th cell subtypes. Th1 cells maximize the killing efficiency of macrophages and the proliferation of cytotoxic CD8<sup>+</sup> T cells, whereas Th2 cells mainly stimulate B cell class switching and antibody maturation (Zhu & Paul 2010; Paul & Zhu, 2010). In the spleen CCR7 expressing naïve T cells and Th1 cells localize to the deep T cell areas, whereas Th2 cells which lack CCR7 home in close proximity to B cell follicles, where they can get into contact with naïve B cells (Randolph et al., 1999). To finally enter CXCL13 producing B cell follicles activated T cells further upregulate CXCR5 (Ansel et al., 1999; Hardtke et al., 2005). Simultaneously, after antigen-binding B cells upregulate CCR7 followed by migration to the B cell-T cell area edge to gain T cell help (Reif et al., 2002). After successful B cell stimulation germinal centers are established within the B cell follicle. Germinal center organization is based upon sorting CXCL12 sensitive maturing B cells and antibody-producing plasma cells into the so-called dark zone and B cells, which carry already their specific antibody on their surface, into the CXCL13 expressing light zone to undergo affinity maturation (Allen et al., 2004; Hargreaves et al., 2001). Moreover, it was demonstrated that also DC subsets are spatially separated by graded chemokine receptor expression in the LN: Dermis derived DCs express CXCR5 and localize in proximity to B cell follicles. On the other hand only CCR7 expressing epidermal DCs settle strictly in the deep T cell area (Kissenpfennig et al., 2005; Saeki et al., 2000; Wu & Hwang, 2002).

With the help of confocal or two-photon intravital microscopy directional cell migration could be observed in unfixed tissue slices and living animals. For example during maturation DCs migrate directionally towards efferent lymphatics followed by directed movement towards the T cell area (Pflücke and Sixt, 2009; Sen et al., 2010). Furthermore, activated B cells start to upregulate CCR7 and move then directionally towards the boundary between T and B cell area (Okada et al., 2005). Leukocytes also perform directional migration *in vivo* when they are exposed to artificially applied soluble gradients (Worbs et al., 2007; Khandoga et al., 2009). T cells for example can glide into the SCS when exposed to artificial CCL19 gradients (Worbs et al., 2007). Besides that, microinjection of chemoattractants into the murine cremaster muscle induces polarization and directional interstitial migration of neutrophils and monocytes towards the locally administered stimuli (Khandoga et al., 2009).

### 1.4.5 Leukocytes as chemotactic organizers

Leukocytes are not only guided by chemotactic gradients; recent studies have provided evidence that they can actively manipulate or generate chemotactic gradients during inflammatory conditions. For instance skin-derived DCs secrete CCL22 and can thereby attract recently activated CD4<sup>+</sup> T cells to promote further stimulation (Tang and Cyster 1999). Furthermore, neutrophil-derived CCL3 is essential for the rapid recruitment of immature DCs to the site of *Leishmania major* inoculation to induce adaptive immunity (Charmoy et al., 2010). Such a behavior could also be monitored *in vivo* via two photon

microscopy. In with *Toxoplasma gondii* infected LNs neutrophil swarms could be observed initiated by cooperative action of neutrophils. The correlation between size and persistence of the swarms suggests that the neutrophils themselves generate a gradient for swarm formation, which is likely mediated by CXCL8 and CXCL1 (Chtanova et al., 2008). Moreover, the chemokines CCL3 and CCL4 are released following productive interactions between CD4<sup>+</sup> T cells and DCs in the reactive LN to recruit CD8<sup>+</sup> naïve T cells and rapidly induce cytotoxic immune response (Castellino et al., 2006).

## 1.5 Cytoskeleton of migrating leukocytes

The migratory properties of leukocytes are indispensable for innate and adaptive immune responses. The migration speed of leukocytes lies in the range of 10 - 40 µm per minute which is for example more than ten times faster as the migration of fibroblasts (Friedl, Borgmann & Bröcker, 2001; Friedl & Weiglin, 2008). On their way leukocytes encounter a multitude of different environments as they can invade almost all tissues. These features imply unique properties of the cytoskeleton in rapid migrating leukocytes in comparison to slowly migrating cells of epithelial or mesenchymal origin which are restricted to distinct tissues. In these slow cell types the force of the actomyosin system has to be mechanically transduced to the extracellular environment via transmembrane receptors of the integrin family. Thus migration always relies on cell adhesions. But a number of recent studies demonstrated that in leukocytes, adhesion and migration can occur independently (Lämmermann et al., 2008).

### 1.5.1 Basal mechanisms of leukocyte migration

The course of events during mesenchymal and epithelial cell migration is normally described as followed: First, the leading edge of the cell expands generating a protrusion. The front side of this protrusion attaches to the extracellular substrate subsequently followed by contraction of the actin-myosin network resulting in the movement of the whole cell body. Finally adhesion sites in the rear of the cell are weakened leading together with the actin-myosin contraction to the detachment of the cell back. The transmission of intracellular forces to the environment, also called traction, by adhesive interaction is a prerequisite for locomotion in these cell types.

Leukocytes, as amoeboid cells, are independent of adhesive interactions in three-dimensional environments, potentially because they can convey traction by inserting protrusion into the fibrillar ECM network, which provides physical foothold (Lämmermann et al., 2008). This migration mode is also called 'chimneying' (Figure 11). Amoeboid cells (termed after the protozoon *Amoeba proteus*: *amoibe* after the Greek word for 'change' and *Proteus* after the Greek 'god of change') have in common that they undergo rapid shape

changes during migration at which cell deformation is generated by the actin-myosin cytoskeleton. The proportion of myosin and actin can widely diverge during amoeboid motility. This morphological term integrates different biophysical migration modes from contraction-dependent blebbing motility to complete actin polymerization-based gliding (Lämmermann & Sixt, 2009).

### 1.5.2 Force generation: Actin-myosin interactions

The movement of the actin cortex as well as the intracellular force generation strictly depends on actin polymerization and the action of myosin II.

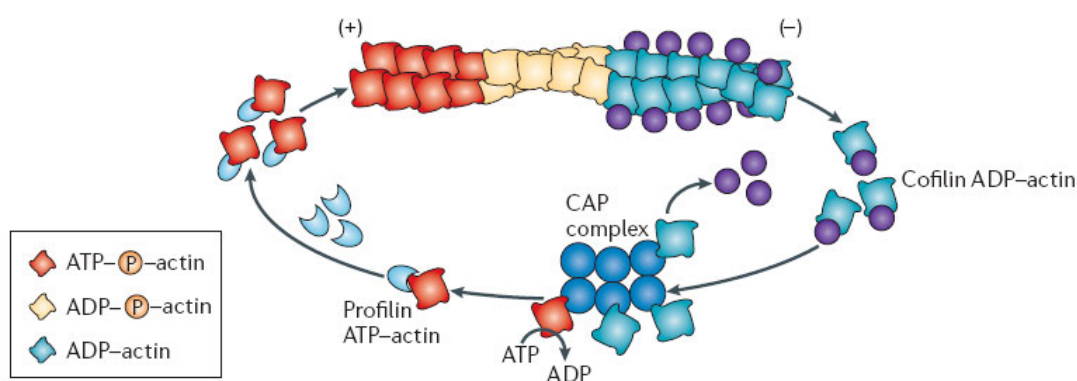


**Figure 9: Actin treadmilling.** Actin monomers assemble into polar filaments with a (+) and a (-) end which consists of two parallel protofilaments twisted in a right-handed helix. ATP-actin binds to the barbed (+) end and subsequently hydrolyzes by its ATPase function the bound ATP and releases phosphate. The remaining ADP-actin has a lower affinity to the filament and is subsequently released from the slower growing pointed (-) end. ADP is substituted against ATP supported by the cyclase associated protein (CAP) complex to generate again ATP-actin monomers. The transport of ATP-actin to the (+) end and the release of ADP-actin from the (-) end is assisted by profilin and cofilin, respectively (taken from: Baum et al., 2006).

The 43 kDa protein actin is one of the most abundant proteins in eukaryotic non-muscle cells. Actin can assemble to filaments, also called microfilaments, and operates besides microtubuli and intermediate filaments as the main cytoskeletal structure. Actin monomers always assemble head-to-tail resulting in a polar filament with a (+) and a (-) end which consists of two parallel protofilaments twisted in a right-handed helix. The subsequent addition of actin monomers is feasible on both ends of the filament, but in most cases the binding of adenosine-5'-triphosphate (ATP)-actin monomers at the (+) end is favored. The ATPase function of actin subsequently hydrolyzes ATP and releases the phosphate-group. Hydrolysis does not occur directly, but rather with a lag of time after integration of the monomer into the filament. The generated adenosine-5'-diphosphate (ADP)-actin monomers disassemble from the slower growing 'pointed' (-) end of the microfilament. Afterwards ADP is replaced by ATP preparing the monomers for another round of polymerization. These

## Introduction

features together with the lower affinity of ADP-actin to filament ends than ATP-actin result in the so-called 'actin treadmilling'. Treadmilling is the balanced process of actin assembly at the (+) and disassembly at the (-) end (Figure 9; Baum et al., 2006). Actin filaments are polarized in lamellipodia with their (+) oriented towards the plasma membrane (Small, Isenberg & Celis, 1978). Therefore, elongating actin filaments push against the leading cell membrane thereby extending the lamellipodium (Renkawitz & Sixt, 2010).

Myosins are actin-dependent motors which convert chemical energy stored in ATP into mechanical force. 24 different myosin classes are described, but myosin II class proteins are the mayor motor proteins that regulate actomyosin contractility in both muscle and non-muscle cells. Myosins II function as actin cross-linkers and contractile motors and are mainly located at the back of the cell. Myosin II self-assembles into bipolar filaments through their C-termini (Figure 10 A). The motor domains at the N-termini associate with actin filaments. By pulling the actin filaments together myosin II generates by ATP consumption cortical tension (Figure 10 B; Clark et al., 2007).

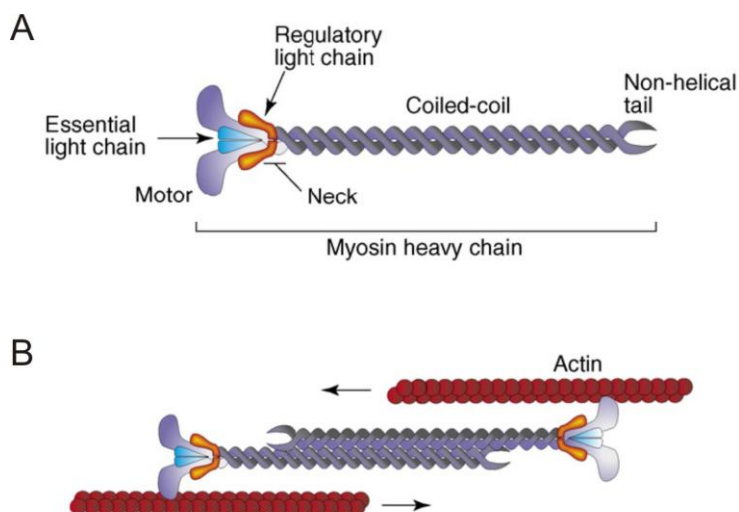


**Figure 10: Myosin II filament assembly and interaction with actin. (A) Myosin II monomers consist of two regulatory light chains, two essential light chains and two heavy chains. Two regions can be distinguished the C-terminal coiled-coil region and the N-terminal motor domain. (B) Two myosin II monomers assemble to one bipolar myosin II filament through interactions facilitated via their coiled-coil regions. The N-terminal motor regions bind to actin filaments and pull on them upon activation (adapted from: Clark et al., 2007).**

Actin-myosin contraction has several functions: It detaches the trailing edge of the cell by the inactivation and removing of integrins. Beyond that hydrostatic pressure can be created by contractility in the back to push out the membrane at the front. Contractility is not essential for leukocyte migration when the pores in the interstitium are large enough. But the passage through narrow pores depends on the actomyosin-mediated squeezing and deforming of the rigid nucleus (Figure 11; Nourshargh, Hordijk & Sixt, 2010).

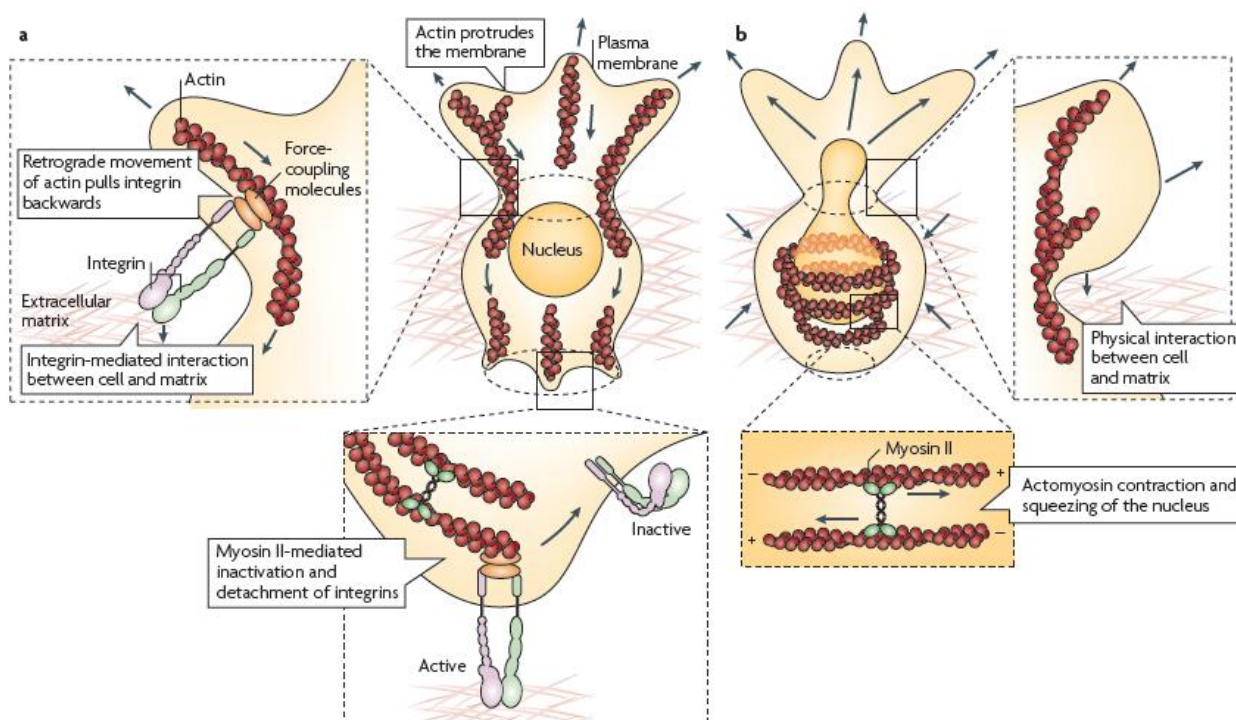


**Figure 11: Leukocyte migrating through interstitial tissue by actin-myosin interactions. (A) Polymerizing actin pushes against the membrane to generate a protrusion. Actin filaments thereby experience a counter force that leads to backwards sliding of the filaments. By successful interactions between integrins and ECM molecules this retrograde actin flow can be transformed into traction, which leads to a forward movement of the cell. Integrins in the tail of the cell are detached by actin-myosin contraction at the same time. (B) To squeeze through narrow pores the nucleus has to be deformed by actin-myosin contraction. These contractions can also generate hydrostatic pressure, which also protrudes the membrane that can intercalate into matrix pores (taken from: Nourshargh, Hordijk & Sixt, 2010).**

### 1.5.3 Force transduction: Integrins

The actin-myosin system is essential to generate forces to transform the cell shape. But in order to cause locomotion the created intracellular forces have to be transmitted to the extracellular environment. Only in this case the forces are converted into retrograde traction forces.

Integrins are transmembrane receptors that bind to ECM molecules while the cytoplasmic tail interacts with the actin-myosin cytoskeleton to provide mechanical anchorage and structural integrity in the cell. Integrins are composed of an  $\alpha$ - and a  $\beta$ -subunit. Eight different  $\beta$ - and 16  $\alpha$ -chains are known, which can form 24 different integrin dimers. Ligand specificity and affinity are defined by the composition of the dimers. Ligands are mostly ECM molecules, but also cell surface proteins or soluble proteins can interact with integrins (Figure 12). Integrins are the central component of focal adhesions. Focal adhesions are large, dynamic protein complexes that transmit mechanical force and regulatory signals at sites of integrin clustering and activation. Focal adhesions assemble in a hierarchical order:



## Introduction

First, the actin filament binding-protein  $\alpha$ -actinin is recruited, followed by proteins of the main linkage complex like vinculin and talin and finally integrins appear in the focal adhesions (Brown et al., 2006; Hu et al., 2007). Disconnection of the complex facilitated via actin-myosin contraction is assumed to occur within the linkage complex or between integrins and linkage complex (Brown et al., 2006).

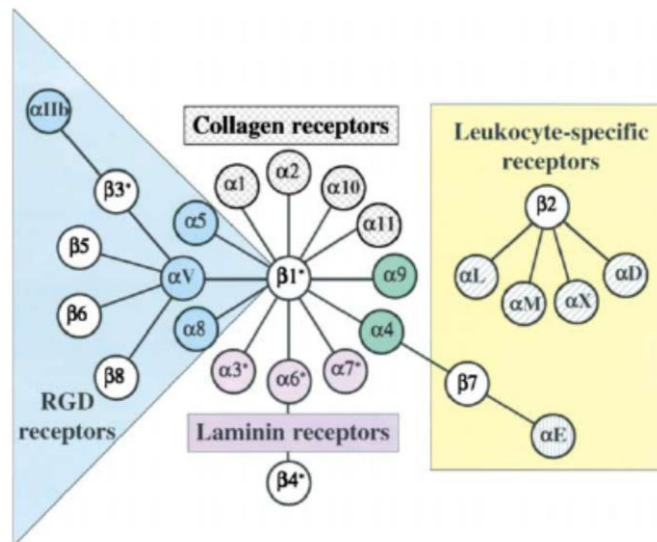


**Figure 12: The integrin family of transmembrane receptors. Integrins are heterodimers consisting of an  $\alpha$ - and a  $\beta$ - subunit. The composition of the dimers defines the ligand specificity. The expression of  $\beta 2$ - and  $\beta 7$ -subunits is restricted to leukocytes (taken from: Hynes, 2002).**

The described phenomenon of integrin-mediated force transduction is extensively described for adherent cells like fibroblasts, which carry active integrins on their surface (Hynes, 2002). Leukocytes except of macrophages and activated lymphocytes are non-adherent cells that carry mainly inactive integrins on their surfaces which can be activated for example by chemokines (Kinashi, 2005). Besides transmitting signals from the exterior to the interior of the cell after ligand binding like classical transmembrane receptors (outside-in signaling), function and activation state of integrin is also controlled from the inside of the cell (inside-out signaling) leading to bidirectional intercommunication. Inactive integrins are in a low affinity state and interact weakly with ligands. Upon stimulation a conformational change in the cytoplasmic tail is induced that propagates to the exterior part of the receptor. Thereby the integrin is transformed to a high affinity ligand binding state (Figure 13 A; Hynes, 2002). Chemokine-dependent inside-out activation of integrins is for example indispensable for tight sticking of leukocytes to the endothelium during extravasation from the bloodstream, whereupon the chemokine must be immobilized on the endothelium (Ley et al., 2007; Shamri et al., 2005; Grabovsky et al., 2000). However, activated, high-affinity integrins slow migrating leukocytes down or even immobilize them completely (Imai et al., 2008, Stanley et al., 2008). The inside-out activation of integrins allows the accurate regulation of



## Introduction

leukocyte adhesiveness and on the same time protects cells by limited activation from too extensive integrin-mediated cell adhesion.

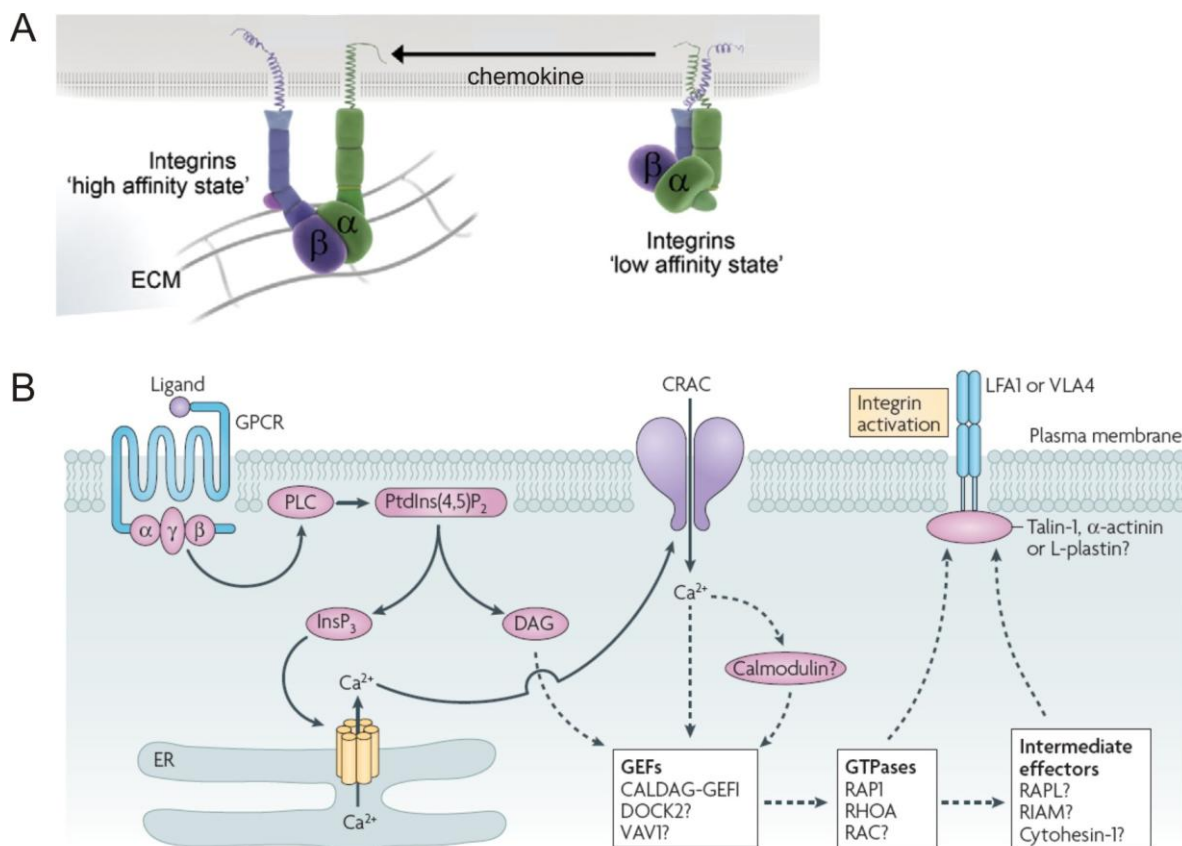


**Figure 13: Chemokine dependent integrin activation. (A)** Leukocytes carry inactive integrins on their surfaces that can be activated for example by chemokines. Once integrins are in an active state they establish adhesive interactions with the environment (adapted from: Böttcher, Lange & Fässler 2009). **(B)** G-protein coupled receptor (GPCR) signaling. After chemokine receptor activation the heterotrimeric G-proteins dissociate into an  $\alpha$ - and a  $\beta\gamma$ -subunit. The  $\beta\gamma$ -subunit activates phospholipase C (PLC), which cleaves phosphatidylinositol-4,5-bisphosphate (PtdIns(4,5)P<sub>2</sub>) into inositol-1,4,5-trisphosphate (InsP<sub>3</sub>) and diacylglycerol (DAG). InsP<sub>3</sub> triggers Ca<sup>2+</sup> release from the endoplasmic reticulum (ER), which leads to Ca<sup>2+</sup>-influx into the cell through Ca<sup>2+</sup>-release activated Ca<sup>2+</sup> (CRAC) channels. DAG, Ca<sup>2+</sup> and calmodulin trigger integrin activation by progressive activation of guanine exchange factors (GEFs), GTPases and intermediate effectors. Finally, integrin activator proteins like talin are recruited to the integrin tails and lead to integrin activation (taken from: Ley et al., 2007).

The signaling cascade which leads to integrin activation upon chemokine binding is only partly characterized. Upon chemokine receptor activation the coupled G-protein dissociates into an  $\alpha$ - and a  $\beta\gamma$ -subunit which in turn activates phospholipase C (PLC). PLC cleaves phosphatidylinositol-4,5-bisphosphate (PtdIns(4,5)P<sub>2</sub>) into inositol-1,4,5-trisphosphate (InsP<sub>3</sub>) and diacylglycerol (DAG) are generated. DAG leads to Ca<sup>2+</sup>-influx from the endoplasmic reticulum into the cytosol which in turn leads to Ca<sup>2+</sup> influx from the extracellular space. Ca<sup>2+</sup>, Ca<sup>2+</sup>-activated calmodulin and DAG subsequently lead to the activation of guanine exchange

factors (GEFs), which in turn activate GTPases like RhoA. Together with intermediate effectors, that are not well characterized yet, these GTPases lead to the recruitment of integrin activator proteins like  $\alpha$ -actinin and talin to the focal adhesion site, which finally convert the integrin heterodimers into an activated state (Figure 13 B; Ley et al., 2007).

### 1.5.4 Actin dynamics in the lamellipodium: Retrograde actin flow

For leukocyte locomotion the actin polymerization-driven deformation of the leading edge is of great relevance. As mentioned before the myosin II-dependent contractility is dispensable in three-dimensional networks with large pore sizes. In this case actin polymerization alone is sufficient for cell deformation and leukocyte locomotion.

The extending actin network directly pushes against the cell membrane thereby generating a lamellipodium. The lamellipodium includes the first 1-3  $\mu\text{m}$  of the leading edge and is a thin, sheet-like structure with a thickness of 100-150 nm. Lamellipodia are only weakly adherent and devoid of organelles. The area directly affiliated to this structure is the so-called lamella, which is thicker and more adherent. Both structures also differ in the composition of their actin network: the actin filaments of the lamellipodium are highly dynamic and orientated with the barbed ends towards the membrane. Actin dynamics in the lamella are less pronounced. At the border between lamellipodium and lamellum the first focal adhesions are located stabilizing the actin network. In three-dimensional environments the leading edge is more roundish and can intercalate into matrix pores (Figure 11 B). These cell extensions are also called 'lobopodia' (Friedl et al., 2001).

When actin filaments push against the membrane, they experience a counter force by the stiffness of the plasma membrane: The actin filaments slide backwards and retrograde actin flow can be observed. The contractility of the myosin network enhances this actin movement by pulling the cortex backwards. Retrograde flow can be coupled to the external environment via integrins thereby stopping the backwards flow and, moreover, generating parallel to the membrane traction forces (Figure 12). By force coupling the backward orientated flow can be turned into forward movement. This mechanism is called 'molecular clutch' (Cramer 1997; Giannone, Mège & Thoumine, 2007). Retrograde actin flow was observed in neural growth cones, as well as in fast moving keratocytes (Medeiros et al., 2006, Valloton et al., 2006). Besides that, it could be shown that the retrograde actin flow is inversely related to the protrusion speed in keratocytes (Jurado et al., 2005). In contrast to these observations the retrograde actin flow in stationary and migratory fibroblast with their adherent lamellipodia is not correlated with the speed of protrusion (Theriot and Mitchison 1992, Cramer et al., 1997). Until now it was not analyzed how retrograde actin flow is regulated in low-adhesive leukocytes.

## 2 Aims of this thesis

### Project 1:

Chemokines are indispensable for the establishment of functional areas with specialized assignments and sharp boundaries in lymphoid organs. At the same time these chemokines act as guidance cues for leukocytes to these organs. Furthermore, chemokines can lead to cell adhesion via integrin activation or to cytoskeletal polarization which results in directional migration. How can chemokines execute such diverse functions? And what determines whether a cell adheres, migrates or accomplishes both responses?

To answer these questions I used dendritic cells (DCs) as a model system and focused on their chemokine receptor CCR7-dependent migration to and within LN. Besides that, CCR7 is indispensable to establish T cell areas in secondary lymphatic organs. CCR7 has two ligands, the homeostatic chemokines CCL19 and CCL21. But why does CCR7 require two ligands? CCL19 and CCL21 exhibit many similarities like their affinity towards CCR7 and their expression pattern (Yoshida et al., 1998, Pilkington et al., 2004; Bachmann, Kopf & Marsland 2006). But only CCL21 carries a highly charged C-terminal extension that mediates linkage to anionic surfaces, whereas CCL19 is soluble (Ueno et al., 2002). How does the presenting mode of the CCR7 ligands influence the DC response? Chemokines can be immobilized or soluble, form a gradient or show a uniform, homogenous distribution (Miyasaka and Tanaka, 2004). Theoretically these presenting modes can be freely combined, but most likely are soluble gradients and immobilized, homogenous fields. If and how the presentation form of a chemokine affects the migratory response has not been systematically investigated. I used reductionistic *in vitro* approach to gradually dissect different chemokine response patterns of DCs.

### Project 2:

It was shown that the adhesive and migratory properties of cells are not urgently connected: DCs can use an integrin-independent amoeboid mode of migration, which is based on actin polymerization at the leading edge and myosin II controlled contraction in the rear of the cell to squeeze through narrow pores (Lämmermann et al., 2008). These results are contradictory to the paradigm of integrin-dependent transmission of traction force during mesenchymal cell migration. According to this model, cells must transmit forces generated by the actomyosin system via integrins to the environment in order to migrate. Till now it is unclear how the actin cytoskeleton in DCs adapts to the loss of adhesive interactions and supports integrin-independent migration. To answer these questions I examined the migration of DCs in a defined pseudo-three-dimensional environment. The actin flow was visualized with the probe Lifeact-green fluorescent protein (GFP). This second project was a collaboration with a master student in the lab, Jörg Renkawitz.

## 3 Material and Methods

### 3.1 Mice

*Itgb2*<sup>-/-</sup> (Wilson et al., 1993), *Ccr7*<sup>-/-</sup> (Förster et al., 1999), Lifeact-GFP (Riedl et al., 2008), *plt/plt* (Nakano et al., 1998) and *Itga<sub>v</sub>*<sup>flox/flox</sup> *Itgβ1*<sup>flox/flox</sup> *Itgβ2*<sup>-/-</sup> *Itgβ7*<sup>-/-</sup> *Mx1Cre*<sup>+/-</sup> [here called *Itg*<sup>-/-</sup>; described in Lämmermann et al., 2008; following integrins were targeted/deleted: *Itga<sub>v</sub>*<sup>flox/flox</sup> (Lämmermann et al., 2008), *Itgβ1*<sup>flox/flox</sup> (Potocnik, Brakebusch & Fässler, 2000), *Itgβ2*<sup>-/-</sup> (Wilson et al., 1993), *Itgβ7*<sup>-/-</sup> (Wagner et al., 1996), *Mx1Cre*<sup>+/-</sup> (Kühn et al., 1995)] mice were kept on a 129SV/C57BL/6 genetic mixed background. The mice were bred in a conventional animal facility at the Max Planck Institute of Biochemistry, Martinsried, according to the local regulations.

### 3.2 Chemicals

If not separately mentioned CCL21, CCL19 and ICAM-1 were purchased from R&D Systems and bovine serum albumin (BSA) from PAA.

### 3.3 Cell culture

#### 3.3.1 General

All cells were kept at 37°C, 5% CO<sub>2</sub> and a humidity of 100%. DCs, macrophages, growth factor producing hybridoma cell lines, B and T cells were cultured in R10 medium. LN derived *p19*<sup>ARF</sup><sup>-/-</sup> fibroblasts (provided by S. Luther) and mouse embryonic fibroblasts (MEFs) were cultured in D10 medium in cell culture flasks (Falcon). Cells were centrifuged at 270 g for 5 min if not separately mentioned.

*R10 medium*      *RPMI (Gibco) with 10% fetal calf serum (FCS; Gibco), 5% penicillin/streptomycin (PAA), 5 % glutamine (PAA)*

*D10 medium*      *DMEM medium with 10% FCS (Gibco), 5% penicillin/streptomycin (PAA)*

### 3.3.2 Cell passaging

Macrophages, growth factor producing hybridoma cell lines, MEFs and *p19<sup>ARF</sup>*<sup>-/-</sup> LN-fibroblasts were detached from 10 cm petri dish (Greiner) by trypsination. Therefore, adherent cells were washed with phosphate buffered saline (PBS) prior to incubation with 2 ml trypsin-ethylenediaminetetraacetic acid (EDTA) solution (Gibco; 0.25% Trypsin) for 2 min at room temperature (RT). The digestion was stopped by adding 10 ml R10 medium. Macrophages were directly used for experiments; fibroblasts were applied to experimental procedures or pelleted, resuspended and transferred to new cell culture flasks.

*PBS*                    1.4 M NaCl (Merck), 20 mM KCl (Merck), 80 mM Na<sub>2</sub>HPO<sub>4</sub> · 2 H<sub>2</sub>O (Merck),  
15 mM KH<sub>2</sub>PO<sub>4</sub> (Merck)

### 3.3.3 GM-CSF and M-CSF production

To differentiate bone marrow cells in DCs or macrophages depends on growth factors, granulocyte-macrophage colony-stimulating factor (GM-CSF; Lutz et al., 1999) and macrophage colony-stimulating factor (M-CSF; LeContel et al. 1993), respectively. Both growth factors were produced by hybridoma cell lines. The GM-CSF (provided by B. Stockinger) and M-CSF (provided by M. Lutz) producing hybridoma cells were cultivated in R10 medium in cell culture flasks (BD Falcon). When the cells reached a confluency of 90 to 100%, the cells were cultivated in the same medium for two additional days. Afterwards the cell supernatant was collected, centrifuged to remove remaining cells and finally filtered (Corning vacuum filter/storage bottle system, 0.45 µm pore size) before added to bone marrow cells. After two rounds of growth factor enrichment in the cell supernatant the cells were trypsinized, splitted and transferred to new flasks. Growth factor containing cell supernatants were stored at 4°C.

### 3.3.4 Generation of bone marrow derived DCs

DCs were generated from flushed bone marrow as described by Lutz et al. (1999). Mice were sacrificed via CO<sub>2</sub> aspiration and the femurs removed. The bones were disinfected with 70% ethanol for 30 s. Afterwards the bones were opened with sterile scissors and the bone marrow flushed with 4°C cold phosphate buffered saline (PBS). After thoroughly pipetting to separate the cells from each other, the cell suspension was centrifuged and resuspended in R10 medium supplemented with 10% GM-CSF to a final concentration of 2.5x10<sup>5</sup> cells/ml. 10 ml of this cell suspension was transferred to one 10 cm petri dish (Greiner). On day 3 of culture 10 ml of R10 medium containing 20% GM-CSF were added. On day 6 and 8 of culture 10 ml medium were removed and replaced with 10 ml R10

medium supplemented with 20% GM-CSF. DCs were cryo-preserved at day 8 to 11 of culture and used at day 9 to 12 for experiments after maturation (3.3.5, p.46).

### 3.3.5 Maturation of DCs

Immature DCs on day 9 to 11 of culture were used for overnight maturation. DCs of one petri dish were pelleted, resuspended in 10 ml R10 medium supplemented with 10% GM-CSF and transferred to a 5 cm cell culture dish (Falcon). To induce DC maturation 200 ng/ml lipopolysaccharide (LPS; Sigma-Aldrich; *E.coli*; 0127:B8) were added. On the next day the non-adherent, matured DCs were used for experiments.

### 3.3.6 Cryo-preservation and thawing of DCs

DCs of one petri dish were pelleted and resuspended in 4°C cold 1 ml freezing medium and transferred to cryo vials (Corning). The cells were stored at -80°C or for long-term storage (> 3 months) transferred into liquid nitrogen.

For recovering the cryo vials were placed in a 37°C water-bath. The thawed cell suspension was rapidly added to 20 ml R10 medium, pelleted and directly used for overnight maturation (3.3.5, p.46).

*Freezing medium FCS (Gibco) supplemented with 10% DMSO (Sigma-Aldrich)*

### 3.3.7 Transfection of DCs

For DC transfection with vinculin-GFP- (provided by S. Schmidt), CCR7-GFP- (provided by D. Legler) or Lifeact-GFP (provided by J. Riedl) plasmids the *Mouse T Cell Nucleofector® Kit* (Lonza) was used.  $5 \times 10^6$  immature DCs were pelleted (150 g, 5min) and the supernatant discarded completely. The DCs were resuspended in 100 µl room temperature *Mouse T Cell Nucleofector solution* mixed with the supplement solution. Subsequently, 4 µg deoxyribonucleic acid (DNA) were added. After exhaustively mixing the cell suspension was transferred to an electroporation cuvette (Lonza) and transfected using the *Amxa Nucleofector* with the *Nucleofector program X-001* (Lonza). Directly after transfection the DC suspension was transferred into 3 ml R10 medium supplemented with 10% GM-CSF. 4 hr after transfection 200 ng/ml LPS (Sigma-Aldrich; *E. coli* 0127:B8) were added for overnight maturation (3.3.5, p.46).

Before usage in chemotaxis assays, the cells were sorted for GFP-positive cells with a FACSAria (Beckton Dickinson; GFP: excitation 488 nm; emission 575 nm; cells sorted >  $5 \times 10^2$  fluorescence intensity).

### 3.3.8 Generation of *Itg*<sup>-/-</sup> DCs

In *Itg*<sup>-/-</sup> mice (Lämmermann et al., 2008) *Itgβ2*<sup>-/-</sup> (Wilson et al., 1993) and *Itgβ7*<sup>-/-</sup> (Wagner et al., 1996) were constitutively deleted. *Itgav*<sup>flox/flox</sup> (Lämmermann et al., 2008) and *Itgβ1*<sup>flox/flox</sup> (Potocnik, Brakebusch & Fässler, 2000) genes were flanked by LoxP sites ('flox'). The mice genomes encoded the heterogenic transgene *Mx1Cre*<sup>+/-</sup> (Kühn et al., 1995) to induce the knockout of the *Itgav* and *Itgβ1* in hematopoietic cells. In the MxCre system the Cre recombinase gene is under control of the Mx promoter, which can be activated by type I interferons. Administration of a synthetic double-stranded RNAs or synthetic homologous, like polyinosinic-polycytidylic acid (Poly(I)·Poly(C)) induces the production of interferons and subsequently leads to activation of the Mx promoter in hematopoietic precursors. For induction mice at an age between 8 and 12 weeks obtained a single intraperitoneal injection of 250 µg Poly(I)·Poly(C) (AmershamBiosciences) in 0.5 ml PBS. Mice were sacrificed via CO<sub>2</sub> aspiration 10 to 14 days after injection. The knockout efficiency of hematopoietic precursors was estimated by fluorescence-activated cell sorting (FACS) analysis of peripheral blood platelets, which corresponds with knockout efficiencies in DC precursors (T. Lämmermann, personal communication; β1 integrin staining as described below). Bone marrow of mice with at least 90% knockout efficiency was processed for DC generation (3.3.4, p. 45).

Because the knockout efficiency after Poly(I)·Poly(C) injection is always below 100%, knockout cells were isolated by FACS sorting. Therefore, after transfection with Lifeact-GFP (3.3.7, p.46) and subsequent overnight maturation (3.3.5, p.46), the mature DCs were stained with α-integrinβ1-phycoerythrin (PE) antibody (hamster IgG, Biolegends) and GFP-positive PE-negative cells isolated with a FACSAria (Beckton Dickinson; PE: excitation 488 nm; emission 518 nm; cells sorted: < 2x10<sup>2</sup> fluorescence intensity; GFP: excitation 488nm; emission 575 nm; cells sorted: > 5x10<sup>2</sup> fluorescence intensity). For the staining *Itg*<sup>-/-</sup> DCs of one transfection were resuspended in 1 ml PBS with 5 µl of the antibody for 20 min at 4°C. Because the integrin β1 knockout is always correlated with the knockout of integrin αv, the staining of *Itgβ1*<sup>-/-</sup> DCs is sufficient to identify *Itg*<sup>-/-</sup> DCs (T. Lämmermann, personal communication).

### 3.3.9 Generation of bone marrow derived macrophages

To generate bone-marrow derived macrophages a procedure analogue to the DC differentiation protocol was executed (modified after: Le Contel et al., 1993; 3.3.4, p.45). Mouse femurs were isolated and the bone marrow flushed. The cells were pelleted and resuspended in R10 medium supplemented with 10% M-CSF to a final cell concentration of 2 x10<sup>5</sup> cells/ml. 10 ml of the cell suspension was transferred to a 10 cm petri dish (Greiner).

On day 3 of culture 10 ml of R10 medium containing 20% M-CSF were added. On day 6 and 8 of culture 10 ml medium were removed and replaced with 10 ml R10 medium supplemented with 20% M-CSF. Macrophages were cryo-preserved at day 8 to 9 of culture and used at day 8 to 10 for experiments. Macrophages are already activated by attaching to the petri dish.

### 3.3.10 Isolation of CD4<sup>+</sup> T cells from the spleen

To isolate CD4<sup>+</sup> T cells from spleen cell suspension the magnetic-activated cell sorting (MACS) *CD4<sup>+</sup> T cell isolation kit* (MiltenyiBiotec) was used. The basic principle of this kit is to incubate the cell suspension first with an Biotin antibody cocktail that labels all unwanted cells ( $\alpha$ Cd8a: macrophages, mast cells,  $\alpha$ Cd11b: granulocytes, monocytes,  $\alpha$ Cd45R: B-lymphocytes,  $\alpha$ DX5: NK-cells,  $\alpha$ Ter119: erythrocytes). In a second step these selected cells are magnetically labeled via Streptavidin MicroBeads. The final cell separation is carried via a column in a strong magnetic field, where the labeled cells are retained and the unlabeled cells can be easily eluted.

Mice were sacrificed via CO<sub>2</sub> aspiration and the spleen isolated under sterile conditions. The spleen was homogenized with a 70  $\mu$ m cell strainer (BD Biosciences) in 20 ml PBS. After a centrifugation step the cell pellet was resuspended in 5 ml ammonium-chloride-potassium (ACK) lysis buffer to remove erythrocytes. The lysis reaction was stopped after 5 min at RT with 10 ml R10 medium. The cell suspension was pelleted again and the cell number determined after resuspension in 10 ml MACS buffer.

For labelling  $1 \times 10^7$  cells were resuspended in 40  $\mu$ l MACS buffer and mixed with 10  $\mu$ l *Biotin-Antibody cocktail*. After 10 min at 4°C 30  $\mu$ l MACS buffer and 20  $\mu$ l *Anti-Biotin MicroBeads* were added and incubated for additional 15 min at 4°C. The cells were washed with 20 ml MACS buffer and subsequently resuspended in 1 ml MACS buffer. The cells were transferred to *MACS LS column* (MiltenyiBiotec) equilibrated with 3 ml MACS buffer and fixed in a *MACS separator* (MiltenyiBiotec). The column was washed three times with 4 ml MACS buffer to eluate the CD4<sup>+</sup> T cells.

*ACK lysis buffer*      0.15 M NH<sub>4</sub>Cl (Merck), 1 mM KHCO<sub>3</sub> (Merck), 0.1 M Na<sub>2</sub>EDTA (Merck)

*MACS buffer*      PBS containing 0.5 % BSA (PAA), 2 mM EDTA (Merck)

### 3.3.11 Isolation of B cells from the spleen

To isolate mature B cells with CD43(Ly-48)-MicroBeads (MiltenyiBiotec) out of spleen a cell suspension was prepared as described before (3.3.10, p.48). CD43 is expressed on all



leukocytes except mature B cells.  $1 \times 10^7$  cells were resuspended in 90  $\mu$ l MACS buffer and incubated with 10  $\mu$ l CD43 MicroBead suspension at 4°C for 15 min to label the unwanted cells magnetically. The labeling reaction was stopped by adding 20 ml MACS buffer. The final separation of the non-labeled B cells with a LS MACS column (MiltenyiBiotec) was carried out as described in 3.3.10, p.48.

### 3.4 Molecular biology techniques

#### 3.4.1 DNA agarose gel electrophoresis

Agarose gels are used to separate DNA fragment of different sizes by applying an electric field. Shorter fragments move faster and farther than longer ones through an agarose meshwork.

1 to 2% agarose suspension in Tris-acetate-EDTA (TAE) buffer was boiled up in a microwave till the agarose was completely solved. After the agarose solution was cooled down to 50 °C ethidium bromide (Roth), a fluorescent DNA intercalating agent, was added to a final concentration of 1  $\mu$ g/ml. The agarose/ethidium bromide solution was filled in a custom made gel chamber. After the agarose solidified the chamber was filled with TAE buffer. To the DNA samples the appropriate amount of 6xOrangeG loading buffer (Sigma-Aldrich) was added. The size of the DNA fragments was determined with the DNA markers O'GeneRuler™ DNA Ladder Mix (Fermentas) and O'GeneRuler™ 100 bp DNA Ladder (Fermentas). The electrophoresis was carried out at a constant voltage of 80 V. DNA fragment bands were visualized by the use of UV-light of 366 nm wavelength.

TAE (50x)      2 M Tris (Sigma-Aldrich), 1 M acetic acid (Merck), 50 mM Na<sub>2</sub>EDTA (Merck), pH 8

#### 3.4.2 PCR

Polymerase chain reaction (PCR) is a method to amplify a piece of DNA by several orders of magnitude by using DNA polymerase enzymes under controlled conditions.

Recombinant CCL21 with an N-terminal Flag- and a C-terminal His-tag was produced using the *Pichia pastoris* yeast expression system (Invitrogen) and the expression vector pPICZ $\alpha$ C (Invitrogen). To the coding sequence for CCL21 (amino acids 24 - 133, without signal sequence) restriction sites for EcoRI and an XbaI were introduced.

The coding sequence of mature full-length (amino acids 24 - 133, without signal sequence) and C-terminally truncated (amino acids 24 - 98, without signal sequence) CCL21 for the *E.coli* B834(DE3)pLysS (Novagen) expression system was amplified introducing a stop codon as well as flanking restriction sites for BsaI and XhoI and subsequently cloned into the expression vector pET-6his- SUMO (small ubiquitin-like modifier; Invitrogen).

## Material and Methods

All primers were purchased from Metabion (stock: 100  $\mu$ M in ddH<sub>2</sub>O). As DNA template the plasmid pET52 (EMBL expression vector for *E.coli*) with the full CCL21 sequence was used. Each PCR reaction contained 5  $\mu$ l 10xcomplete PCR buffer (Metabion), 1  $\mu$ l 10 mM dNTPs (Fermentas), 0.5  $\mu$ l 100  $\mu$ M primer forward, 0.5  $\mu$ l 100  $\mu$ M primer reverse, 0.2  $\mu$ l Taq-Polymerase (Metabion), 2  $\mu$ l Template-DNA (pET52 + CCL21; provided by T. Lämmermann) and 38.8  $\mu$ l ddH<sub>2</sub>O. The sequences of the primers are specified in **Error! Reference source not found.**, the PCR program in **Error! Reference source not found.**

**Table 1: Primer sequences used to generate CCL21 expression plasmids for the *Pichia pastoris* yeast (Invitrogen) and the *E.coli* B834(DE3)pLysS (Novagen) expression system.**

Primer	Primer sequence
pPICZ $\alpha$ C CCL21 forward	5'- ACG TAG AAT TCC GAC TAC AAG GAC GAC GAT GAC AAG AGT GAT GGA GGG GGT CAG GAC -3'
pPICZ $\alpha$ C CCL21 reverse	5'- TAC GTA TCT AGA GG TCC TCT TGA GGG CTG TGT CTG -3'
pET-6his-SUMO-1 CCL21 forward	5'- CAA GGT CTC AGG TGG TAG TGA TGG AGG GGG TCA G -3'
pET-6his-SUMO-1 full-length CCL21 reverse	5'- CAG CTC GAG TCA TCC TCT TGA GGG CTG TGT CTG -3'
pET-6his-SUMO-1 truncated CCL21 reverse	5'-AAT CTC GAG TCA TTT CCC TGG GGC TGG AGG -3'

**Table 2: PCR program used to generate CCL21-inserts.**

t	T [°C]	repeats
10'	95	1x
30''	95	32x
1'	58	
1'	72	
15'	72	-
-	4	-

The PCR products were separated on 2% agarose gels, the DNA band of correct size cut out and eluted with the *QIAquick® Gel Extraction Kit* (Qiagen) according to the manufacturer's protocol. The CCL21 inserts were eluted with 30  $\mu$ l ddH<sub>2</sub>O.

### 3.4.3 Plasmid preparation

To isolate different amounts of plasmid DNA the Plasmid Mini or Midi Kit from Qiagen were used, respectively. The Plasmid Mini Kit was used according to the manufacturer's protocol. The protocol for the Plasmid Midi Kit was slightly modified:

50 ml LB-ampicillin medium was inoculated with a single *E.coli* colony and incubated overnight at 37°C under shaking (200 rpm). On the next day the bacteria suspension was centrifuged for 10 min at 6000 g. The resulting bacteria pellet was resuspended in 5 ml P1 buffer and 5 ml P2 buffer were added subsequently. After 2 min incubation at RT 5 ml 4°C cold neutralizing buffer P3 were added and thoroughly mixed. Next, the mixture was centrifuged for 15 min at 20,000 g and the resulting supernatant transferred on a with QBT buffer equilibrated Qiagen tip100 column, where it passed through by gravity flow. The column with bound DNA was washed extensively with QC buffer before elution with 5 ml QF buffer. For DNA precipitation 3.5 ml isopropanole were added and the DNA spun down for 30 min at 20,000 g. The DNA pellet was resolved in 200 µl ddH<sub>2</sub>O.

### 3.4.4 DNA restriction digest

Restriction enzymes recognize and cut special palindromic DNA sequences hydrolyzing a phosphodiester bond. Each vector or insert, respectively, was cut with two different restriction enzymes to generate varying 3'- and 5'- sticky ends to minimize re-ligation.

Each digest contained 20 µl PCR agarose gel eluate (3.4.2, p.49) or 5 µg plasmid DNA, 0.5 µl BSA (NEB, 10 mg/ml), 5 µl of the accordant 10xNEB buffer, 10 U of each restriction enzyme (NEB) and ddH<sub>2</sub>O to final volume of 50 µl. The digest was carried out for 3 hr at 37°C.

The plasmids were de-phosphorylated directly after the restriction digest (3.4.5, p.51). Subsequently DNA fragments were separated on an agarose gel, the fragment of the correct size cut out and the DNA eluted in 30 µl ddH<sub>2</sub>O with the QIAquick® Gel Extraction Kit (Qiagen) according to the manufacturer's recommendations.

### 3.4.5 Plasmid de-phosphorylation

Following the restriction digest the reactive 5'prime of the linearized plasmid was dephosphorylated with shrimp alkaline phosphatase (SAP) to avoid self-ligation. To the DNA restriction digest (3.4.4, p.51) the adequate amount of 10xSAP buffer and 1 U of SAP (Roche Applied Science) was added and incubated for 1 hr at 37°C. Finally the enzyme was heat-inactivated for 15 min at 65°C.

### 3.4.6 DNA ligation

The ligation reaction forms a phosphodiester bond between the 5'-phospho and the 3'-hydroxyl group of two DNA fragments which have been cut with the same restriction enzyme.

In this study the Fast-Link DNA Ligation Kit (Epicentre) was used. Each ligation sample consisted of 1.5 µl 10xFast-Link ligation buffer, 1.5 µl 10 mM ATP, 1 µl Fast-Link DNA ligase (2 U/ml) and a total of 200 ng plasmid- and insert-DNA in a molecular ratio of 1:3. ddH<sub>2</sub>O was added to a final volume of 15 µl. After 30 min incubation at RT the ligase was heat-inactivated for 15 min at 75°C. The ligation reaction was transformed into heat-competent *E.colis*.

### 3.4.7 Preparation of heat-competent *Escherichia coli* (*E.coli*) XL1 blue

5 ml of LB Tetracyclin medium were inoculated with a single *E.colis* XL1 *blue* colony and incubated overnight at 37°C under shaking (200 rpm). Next, 150 ml of 37 °C warm LB Tetracyclin medium were inoculated with 1 ml of the overnight culture and incubated at 37°C under shaking (200 rpm) till an optical density of 0.4 at 600 nm (OD600) was reached. After 10 min cool-down on ice the bacteria suspension was divided on four 50 ml conical tubes (Falcon) and centrifuged for 10 min at 4000 g. Each bacteria pellet was resuspended in 37.5 ml 4°C cold transformation buffer I (TFBI) buffer and incubated for 10 min on ice. The resulting suspensions were centrifuged again for 10 min at 4000 g before each bacteria pellet was resuspended in 3 ml 4°C cold TFBII buffer. The final suspension was snap-frozen in liquid nitrogen in 100 µl aliquots. Competent *E.coli* XL1 *blue* aliquots were stored at -80°C.

LB medium autoclaved	1% tryptone (Roth), 0.5% yeast extract (Roth), 1% NaCl (Merck), autoclaved
LB Tetracyclin medium	LB medium containing sterile filtered 5 ng/ml Tetracyclin (Sigma-Aldrich), 20 mM MgSO <sub>4</sub> (Merck), 10 mM KCl (Merck)
TFBI	25 mM potassium acetate (Merck), 50 mM MnCl <sub>2</sub> (Merck), 100 mM RbCl (Merck), 10 mM CaCl <sub>2</sub> (Merck), 15% glycerol (Merck), autoclaved
TFBII	10 mM 3-(N-morpholino)propanesulfonic acid (MOPS; Biomol), 75 mM CaCl <sub>2</sub> (Merck), 10 mM RbCl (Merck), 15% glycerol (Merck), sterile filtered

### 3.4.8 Transformation of heat-competent *Escherichia coli*

The complete ligation reaction was added to one on ice thawed 100 µl aliquot of heat-competent *E.coli* XL1 *blue* or one aliquot of *E.coli* B834(DE3)pLysS (Novagen). The mixture was intermingled carefully and incubated for 30 min on ice. Next, a heat-shock of 30 s at 42°C was performed to promote the uptake of DNA. After 2 min incubation on ice 500 µl LB

## Material and Methods

---

medium was added and the bacteria incubated for 30 min at 37°C under shaking (400 rpm). Finally, the bacteria were spun down, resuspended in 50 µl LB medium and dispensed on LB agar plates containing the respective selection antibiotic. The plates were incubated overnight at 37°C.

*LB agar plates*                      1% tryptone (Roth), 0.5 % yeast extract (Roth), 1% NaCl (Merck),  
2% agar (Roth), autoclaved, after cool down to approximately 50°C addition of 50 ng/ml ampicillin, 50 ng/ml kanamycine, respectively

### 3.4.9 DNA sequencing

Plasmids, which showed the expected results in test restriction digests, were subsequently sequenced with the Sanger method (also: chain-termination method; Sanger, Nickler & Coulson, 1977). The key principle of this method is a modified PCR reaction with dideoxynucleotide triphosphates (ddNTPs) in addition to the normally applied deoxynucleotide triphosphates (dNTPs), which function as DNA chain terminators, and subsequent sequencing of the fragments.

For each plasmid two sequencing reaction, one with a forward primer, the other one with a reverse primer, were performed. All primers were purchased from Metabion (stock: 100 µM in ddH<sub>2</sub>O). Each PCR reaction contained 200 ng plasmid DNA, 3 Big Dye 3.1 (ABI sequencing chemistry), 1 µl primer and ddH<sub>2</sub>O to a final volume of 20 µl. The PCR program is described in **Error! Reference source not found.** The DNA sequencing was carried out with an ABI 3730 sequencing machine from the sequencing core facility of the Max Planck Institute of Biochemistry, Martinsried.

**Table 3: PCR program for DNA sequencing.**

t	T [°C]	repeats
30''	95	25x
15''	50	
4'	60	
-	4	-

### **3.5 Production and purification of recombinant chemokine**

#### **3.5.1 Production of recombinant CCL21 in the yeast *Pichia pastoris***

To use *Pichia pastoris* (*P.pastoris*) as a protein expression system the desired gene has to be stable integrated into the genome by homologous recombination. The gen is placed under the control of the alcohol oxidase promoter (AOX1). Thus, by adding methanol the protein production can be started.

In this study we used the *P.pastoris* strain KM71H (Zeocin™ resistance; Invitrogen) according to the instructions of the *EasySelect™ Pichia Expression Kit* (Invitrogen). The applied plasmid pPICZαC contains α-factor-signaling sequence that induces the secretion of the recombinant protein into the cell supernatant.

After transfection with the expression vector different *P.pastoris* colonies were tested upon CCL21 expression levels. The His- and Flag-tagged protein was purified using Ni<sup>+</sup> metal affinity chromatography and subsequently tested with western-blot detection and coomassie staining (Instant Blue, Novexin) of SDS-PAGEs. Afterwards large scale expression with the most productive colony was established.

##### **3.5.1.1 Preparation of electro-competent *Pichia pastoris***

100 µl of the thawed glycerol stock of *P.pastoris* KM71H were dispensed on an YPDS plate and incubated for three days at 30°C. 5 ml YPDS medium were inoculated with a single colony and incubated overnight under shaking. 0.5 ml of the overnight pre-culture were used to inoculate 500 ml YPDS medium and incubated again overnight till an OD600 of approximately 1.3 was obtained. The cell suspension was filled into 50 ml conical tubes (Falcon) and spun down for 5 min at 1500 g and 4°C. The pellets were resuspended in 100 ml 4°C cold ddH<sub>2</sub>O and centrifuged again for 5 min at 1500 g and 4°C. This step was repeated with 50 ml 4°C cold ddH<sub>2</sub>O and 4 ml 4°C cold 1 M sorbitol (Sigma-Aldrich) for resuspension. Finally, the cell pellets were resuspended in 0.2 ml 4°C cold 1 M sorbitol.

YPDS                      2% tryptone (Roth), 1% yeast extract (Roth), 2% dextrose (Merck),  
                                 1 M sorbitol (Sigma-Aldrich), autoclaved

YPDS agar plate        2% tryptone (Roth), 1% yeast extract (Roth), 2% dextrose (Sigma-Aldrich),  
                                 2% agar (Roth), 1 M sorbitol (Sigma-Aldrich), autoclaved

### 3.5.1.2 Electroporation of *Pichia pastoris*

A mixture of 80 µl of electro-competent *P.pastoris* (3.5.1.1) and 10 µg with Scal linearized expression vector (restriction digest: 3.4.4, p.51) in 20 µl ddH<sub>2</sub>O was filled into an electroporation curette (Biorad). After 5 min reposing on ice the cells were electroporated with a Biorad gene pulsor (1.5 kV, 200 Ω, 25 µF). Directly afterwards 1 ml 4°C cold 1 M sorbitol was added and the cells transferred into a 15 ml conical tube (Falcon). For recovery the cells were incubated for 2.5 hr at 30°C without shaking. Next, 50, 100 and 700 µl of the cell suspension was dispensed on YPDS-Zeocin (Invitrogen, selection antibiotic) agar plates, respectively, and incubated for 5 days at 30°C. The grown colonies were used for CCL21 test expression.

*YPDS Zeocin agar plates* 2% tryptone (Roth), 1% yeast extract (Roth), 2% dextrose (Sigma-Aldrich), 2% agar (Roth), 1 M sorbitol (Sigma-Aldrich), autoclaved, after cooled down to approximately 50°C 100 µg/ml Zeocin<sup>TM</sup> (Invitrogen) were added

### 3.5.1.3 CCL21 test expression in *Pichia pastoris*

To test different colonies for their level of CCL21 production each 2 ml buffer glycerol-complex medium (BMGY) medium in a 24 well-plate were inoculated with a single *P.pastoris* colony. The 24 well-plate with the different test colonies was sealed with air pore tape sheet (Qiagen) and incubated overnight at 30°C under shaking (220 rpm). 20 µl of each of these pre-cultures were used to inoculate for each test colony 2 ml buffer methanol-complex medium (BMMY) medium in a new 24 well-plate sealed again with air pore tape sheet. The plate was incubated for three days under shaking (220 rpm) at 20°C. Every day 10 µl methanol were added to each test expression to induce protein expression. On day 3 the cell supernatant was isolated and the CCL21 purified using *MagneHis<sup>TM</sup> Ni beads* (3.5.1.5, p.56).

*BMGY* 1% yeast extract (Roth), 2% peptone (Roth), 1.34% YNB (BIO 101), 100 mM potassium phosphate buffer, 4x10<sup>-5</sup> % Biotin (Sigma-Aldrich), 1% glycerol (Merck)

*BMMY* 1% yeast extract (Roth), 2% peptone (Roth), 1.34% YNB (BIO 101), 100 mM potassium phosphate buffer, 4x10<sup>-5</sup> % biotin (Sigma-Aldrich), 1% glycerol (Merck)

*1M potassium phosphate buffer* 132 mM K<sub>2</sub>HPO<sub>4</sub> (Merck), 868 mM KH<sub>2</sub>PO<sub>4</sub> (Merck)

### 3.5.1.4 CCL21 large scale expression in *Pichia pastoris*

CCL21 large scale expression was performed analog to the test expression protocol (3.5.1.3, p.55). 500 ml BMMY medium inoculated with 5 ml of a BMGY overnight pre-culture were incubated for 5 days at 30°C under shaking. Each day 2.5 ml methanol were added to

induce protein expression. The protein was purified using Ni-nitrilotriacetic acid (NTA) agarose (3.5.1.6, p.56).

### 3.5.1.5 CCL21 purification with MagneHis™ Ni beads

For the protein purification the His-tag added to the N-terminus of the *P.pastoris* CCL21 construct was used. The basic principle of the enrichment is immobilized metal ion affinity chromatography with *MagneHis™ Ni beads*. Ni<sup>2+</sup> ions are bound over chelating ligands to a matrix and can interact with the side chains of histidins. Bound proteins can be eluted with buffer of high ionic strength. The whole purification was carried out at 4°C.

30 µl *MagneHis™* bead slurry (Promega, 1 mg/ml Ni<sup>2+</sup> particles) were washed three times with 200 µl washing buffer by resuspending the beads in the buffer and subsequent separation of the beads with a magnet.

To 1 ml *P.pastoris* supernatant 110 µl 10x binding buffer as well as the washed *MagneHis™* beads were added and incubated for 2 hr on a rotating wheel. Next, the beads were separated with a magnet and again washed three times with 200 µl washing buffer. To eluate the protein the beads were resuspended in 30 µl elution buffer and incubated for 1 hr under shaking (1400 rpm).

<i>binding buffer (10x)</i>	1 M N-(2-hydroxyethyl)-piperazine-N'-2-ethanesulfonic acid (HEPES; Biomol), 100 mM imidazole (Merck), 3 M NaCl (Merck), pH 7.5
<i>washing buffer</i>	100 mM HEPES (Biomol), 10 mM imidazole (Merck), 300 mM NaCl (Merck), pH 7.5
<i>elution buffer</i>	100 M HEPES (Biomol), 500 mM imidazole (Merck), 300 mM NaCl (Merck), pH 7.5

### 3.5.1.6 CCL21 purification with Ni-NTA agarose

To isolate CCL21 out of larger supernatant amounts the Ni-nitrilotriacetic acid (NTA) agarose RAQ007.2 (Qiagen, 10 mg/ml) is better suited, perhaps because of the more voluminous structure. All purification steps were performed at 4°C with the same buffers as for the *MagneHis™* purification (3.5.1.5, p.56).

50 ml *P.pastoris* supernatant were mixed with 5.5 ml 10x binding buffer and the pH adjusted to 7.8 with 6 M NaOH. 250 µl bead slurry were washed three times with 600 µl washing buffer before the beads were resuspended in the supernatant. To enable protein binding the supernatant bead mixture was incubated overnight on a rotating wheel. The beads were separated by centrifugation and washed three times with 600 µl washing buffer. Finally, 250 µl elution buffer were added and the suspension incubated for 1.5 hr under shaking (800 rpm).



**3.5.2 Expression and purification of full-length and C-terminal truncated CCL21 in *Escherichia coli* B834(DE3)pLysS**

Plasmids were transformed into *E.coli* B834(DE3)pLysS (Novagen). Bacteria were grown at 37°C in a half-synthetic, glycerol-based (HSG) medium to an OD600 of 0.5, cooled to RT for one hr prior to the addition of Isopropyl-β-d-thiogalactopyranoside (IPTG) to a final concentration of 0.5 mM. 6 hr after induction with IPTG at RT, bacteria were pelleted at 10,000 g and resuspended in 5 ml lysis buffer/g pellet. The resuspended bacteria were sonicated and subjected to a cell disruptor to open the bacteria at 2.5 kbar (Constant Systems Ltd.). Subsequently 1 mM phenylmethylsulfonyl fluoride (PMSF; Sigma-Aldrich), an irreversible serine protease inhibitor, was added and soluble chemokine-containing supernatants subsequently collected by centrifugation at 30,000 g. The supernatant was filtrated through two cellulose acetate membrane based filters, Whatman FP30/1.2 CA (GE Healthcare) and Whatman FP30/0.45 CA (GE Healthcare). The filtered supernatant was filled into a 50 ml syringe and manually loaded on a with binding buffer pre-washed HisTrap HP column (GE Healthcare), extensively washed with washing buffer and bound proteins were eluted with elution buffer using an AKTA Explorer chromatography system (Amersham Biosciences, flow rate: 1-2 ml/min). Buffer of eluted fractions with protein of interest was replaced with PBS in a with binding buffer equilibrated HighPrep Desalting column (GE Healthcare, 4 ml/ml, 0.5 Pa). The protein containing fractions were combined in a 50 ml conical tube (Falcon) and overnight digested with 4 μg C-terminal his-tagged *Ubl-specific protease 1* (ULP1)/mg protein at 4°C on a roller. The digested chemokines were first filtered through a Whatman FP30/0.45 CA (GE Healthcare) and then loaded on a Zn<sup>2+</sup> charged HiTrap IMAC FF column equilibrated with binding buffer (GE Healthcare flow rate: 1-2 ml/min). Optionally the chemokine containing fractions were applied to an additional gel-filtration step to achieve a higher purity (HiPrep Sephacryl S-200, GE Healthcare, flow rate: 1-2 ml/min).

<i>HSG medium</i>	1.49% glycerol (Merck), 0.7% yeast extract (Roth), 1.35% peptone (Roth), 43 mM NaCl (Merck), 14 mM K <sub>2</sub> HPO <sub>4</sub> (Merck), 11 mM KH <sub>2</sub> PO <sub>4</sub> (Merck), 568 nM MgSO <sub>4</sub> (Merck), pH 6.8, autoclaved
<i>lysis buffer/ binding buffer</i>	20 mM Na <sub>2</sub> HPO <sub>4</sub> (Merck), 0.5 M NaCl (Merck), 40 mM imidazole (Merck), 2 mM 2-mercaptoethanol (Sigma-Aldrich), pH 7.4
<i>washing buffer</i>	20 mM Na <sub>2</sub> HPO <sub>4</sub> (Merck), 0.7 M NaCl (Merck), 40 mM imidazole (Merck), 2 mM 2-mercaptoethanol (Sigma-Aldrich), 0.5% Triton (Merck), pH 7.4
<i>elution buffer</i>	20 mM Na <sub>2</sub> HPO <sub>4</sub> (Merck), 0.5 M NaCl (Merck), 0.5 M imidazole (Merck), 2 mM 2-mercaptoethanol (Sigma-Aldrich), pH 7.4

## 3.6 Biochemical methods

### 3.6.1 *In vitro* CCL21 cleavage

To characterize the cleavage of CCL21 DCs were incubated with the chemokine in either RPMI medium supplemented with fetal calf serum (FCS), mouse plasma (MP) or enzymes to imitate plasma. The products of CCL21 cleavage in the cell supernatants were separated by SDS/PAGE on 15 % Tris-glycine-gels and blotted on polyvinylidene fluoride (PVDF) membrane. All cleavage assays were incubated at 37 °C, 5% CO<sub>2</sub>.

- 150 ng of untagged CCL21 (R&D Systems) or 75 ng tagged CCL21 (expressed in *P.pastoris*) were incubated with 6x10<sup>5</sup> DCs in 100 µl R10 medium for 4 to 12 hr. The serine protease inhibitor aprotinin (Calbiochem) was applied at 150 mM.
- The described assay was slightly modified by replacing the 10% FCS-supplement (heat inactivated for 20 min at 57 °C) in the R10 medium by not heat inactivated FCS, complete heat inactivated FCS (for 5 min at 90°C) or not heat inactivated MP. The assays were incubated for 15 hr.
- 150 ng CCL21 were incubated with 8x10<sup>5</sup> B cells, 8x10<sup>5</sup> T cells or 4x10<sup>4</sup> MEFs in 100 µl R10 medium for 12 hr.
- 150 ng CCL21 were incubated with 6x10<sup>5</sup> DCs in 100 µl RPMI containing 5% penicillin/streptomycin and 10% not heat inactivated MP for 15 hr with different amounts of the plasmin inhibitor VFKck (Calbiochem).
- 150 ng CCL21 were incubated with 4x10<sup>4</sup> LN-derived *p19<sup>ARF</sup>*- LN-fibroblasts in 100 µl RPMI containing 5% penicillin/streptomycin and 10% not heat inactivated MP for 15 hr
- 150 ng CCL21 were incubated with 6x10<sup>5</sup> DCs in 100 µl RPMI containing 5% penicillin/streptomycin as well as different amounts of plasminogen (mouse, Biopur) for 15 hr.

Cell free cleavage assays:

- 120 ng CCL21 were incubated with 50 nM plasmin (human, Sigma-Aldrich) in PBS with 0.1% Tween-20. The reaction was stopped by heat-inactivation at 75°C for 15 min after different time points.
- Different amounts of plasmin (mouse, LOXO) were incubated with 60 ng CCL21 in PBS. The reaction was stopped after 1 hr at 37°C by heat-inactivation at 75°C for 15 min.

### 3.6.2 CCL21 pull-down from LN-lysate

Mice were sacrificed by CO<sub>2</sub> aspiration and popliteal, inguinal and axillary LNs harvested. The LNs were mechanically disrupted with the pistil of a syringe in 500 µl 4°C cold tissue

lysis-buffer. After 10 min incubation on ice the remaining tissue was completely disrupted by sonication and remaining tissue residues removed by centrifugation for 15 min at 15 g in a benchtop centrifuge. The supernatant was transferred to a new tube. 50  $\mu$ l magnetic ProteinG Dynabeads (Invitrogen) were washed three times with 200  $\mu$ l Dynabeads washing buffer by repeated resuspension followed by removal of the buffer with a magnet. The supernatant was incubated with washed Dynabeads to reduce protein background binding for 30 min under shaking (650 rpm). For antibody binding 50  $\mu$ l washed ProteinG Dynabeads were resuspended in 200  $\mu$ l washing buffer containing 10  $\mu$ g of rabbit anti-mouse Exodus2 (PeproTech) and incubated for 30 min under shaking (650 rpm). After three washing steps the beads were resuspended in the pre-treated LN-lysate and incubated for 30 min under shaking (650 rpm). Afterwards the beads were washed and resuspended in 30  $\mu$ l 6xSDS-PAGE sample buffer, heated at 95°C for 10 min and the in SDS-PAGE sample buffer eluted proteins analyzed by SDS-PAGE.

To test for *in vivo* CCL21-cleavage under inflammatory conditions  $5 \times 10^5$  mature DCs in a volume of 20  $\mu$ l PBS were injected into the hind footpads of a mouse. The popliteal LNs were harvested after 36 hr. The LN-lysate and CCL21 pull-down was carried out as described.

*tissue lysis buffer*                    50 mM Tris pH 8 (Sigma-Aldrich), 150 mM NaCl (Merck), 10 mM Na<sub>2</sub>EDTA (Merck), 0.05% desoxycholate, 1% Triton (Merck) + protease inhibitor cocktail (complete Mini EDTA-free, Roche, one tablet diluted in 10 ml buffer)

*Dynabeads washing buffer*        PBS containing 1% Triton (Merck), pH 7.4

### 3.6.3 SDS-polyacrylamide gel electrophoresis (SDS-PAGE)

SDS-PAGE is the most commonly used method to separate proteins under denaturing conditions. The negatively charged detergent sodium dodecyl sulfate (SDS) becomes associated with the proteins and promotes their solubilisation. Thus, the proteins become negatively charged and can be electrophoretically separated in the meshwork of a polyacrylamide-gel according to their individual molecular size and shape. All SDS-PAGE protein separations in this study were performed with the so-called discontinuous method, where a stacking gel is poured on top of a resolving gel, combined with a BisTris buffer system.

The stacking gels had an acrylamide concentration of 5% and the resolving gels of 15%. The gels were prepared in a *Biorad Mini gel casting device*. The polymerized gels were fixed in a *BioRad Mini Protean III electrophoresis module* that was subsequently filled with running buffer.

The protein samples were mixed with the appropriate amount of 6xSDS sample buffer and boiled for 5 min at 95°C and subsequently cooled down to RT before loading on the stacking

## Material and Methods

---

gel. As a protein standard the *Precision Plus Protein<sup>TM</sup> Standards Kaleidoscope* (Biorad) was applied.

The electrophoresis was carried out at 80 V (stacking gel) to 120 V (resolving gel), respectively.

5% SDS-stacking gel (10 ml):	6.8 ml ddH <sub>2</sub> O, 1.7 ml acrylamide mix (Serva), 1.25 ml 1 M Tris pH 6.8 (Sigma-Aldrich), 100 µl 10% SDS (Merck), 100 µl 10% APS (Sigma-Aldrich), 10 µl N,N,N',N'- tetramethylethylenediamine (TEMED; Serva)
15% SDS-resolving gel (20 ml)	4.6 ml ddH <sub>2</sub> O, 10 ml acrylamide mix (Serva), 5 ml 1,5 M Tris pH 8.8 (Sigma-Aldrich), 200 µl 10% SDS (Merck), 200 µl 10% APS (Sigma-Aldrich), 8 µl TEMED (Serva)
SDS-running buffer (10x)	250 mM Tris (Sigma-Aldrich), 2 M glycine (Riedel-de Haen), 35 mM SDS (Roth)
SDS-loading buffer (6x)	300 mM Tris (Sigma-Aldrich), pH 6.8, 0.2% bromphenol blue (Sigma-Aldrich), 50% glycerol (Merck), 5% 2-mercaptoethanol (Sigma-Aldrich)

### 3.6.4 Western-Blot

Western blotting is a very sensitive method to detect and quantify specific proteins by means of antibodies. The proteins are firstly separated on a SDS-PAGE and subsequently electrophoretically transferred on a membrane. Here, a tank-blotting system was used for the electrophoretic transfer. On the membrane the proteins can be visualized by horseradish peroxidase (HRP)-coupled antibodies in combination with chemiluminescence immunodetection reagents. The enzyme HRP catalyzes the release of light by oxidizing the chemiluminescent substrate with hydrogen peroxides.

The polyvinylidene fluoride (PVDF) membrane (Immobilon, 0.2 µm, Millipore) was first incubated for 1 min in methanol and ddH<sub>2</sub>O, respectively, and finally for 10 min in blotting buffer. The blotting sandwich was composed of a sponge, one layer of Whatman paper, the SDS-PAGE, the pre-incubated PVDF-membrane, a second layer of Whatman paper and another sponge. All components were soaked with blotting buffer and layered bubble-free in the described order. The blot-sandwich was employed in a Mini Trans-Blot Cell (Biorad) with the membrane side of the blot-sandwich orientated toward the anode. The Trans-Blot Cell was filled with 4°C cold blotting-buffer. Blotting took place overnight at 4°C with a constant voltage of 25 V.

For the immune detection the membranes were blocked with Tris buffered saline (TBS) + 0.1% Tween20 (Sigma--Aldrich) containing 5% BSA for 1 hr at RT and incubated with the respective first antibody diluted in TBS + 0.1% Tween20 containing 5% BSA for 1.5 hr at RT. After washing the membrane three times for 15 min with TBS + 0.1% Tween20, the

## Material and Methods

membrane was incubated with HRP-conjugated secondary antibody diluted in TBS + 0.1% Tween20 containing 5% BSA for 1.5 hr at RT. The membrane was washed as described before followed by the antibody detection using *Western Lightning™ Chemiluminescence Reagent Plus* (PerkinElmer). For chemiluminescence detection the PVDF membrane was incubated for 1 min with a mixture of 1 ml Solution A and 1 ml Solution B. All incubation steps were carried out under continuous shaking. The chemiluminescent signal was detected with an Image Reader LAS-4000 (Fuji Film).

**Table 4: Antibodies used for western-blot detection.**

Protein/tag	First antibody	Dilution	Secondary antibody	Dilution
CCL21	Exodus 2 (PeproTech, 200 ng/μl)	1:1500	α-rabbit-HRP (Bio-rad)	1:10.000
His-Tag	α-His-Tag (monoclonal, Novagen, 50 μg/ml)	1:1500	α-mouse-HRP (Bio-rad)	1:10.000
Flag-Tag	α-Flag M2-Peroxidase HRP (Sigma-Aldrich)	1:15.000	-	-

*blotting buffer (10x)*      250 mM Tris (Sigma-Aldrich) 2 M glycine (Riedel-de Haen)

*blotting buffer (1x)*      200 ml methanol (Fisher Scientific), 100 ml 10x blotting buffer,  
700 ml ddH<sub>2</sub>O

*TBS (10x)*                      200 mM Tris (Sigma-Aldrich), 1.4 M NaCl (Merck), pH 7.5

## 3.7 Immunostainings

### 3.7.1 Immunostaining of LN cryosections

Mice were sacrificed via CO<sub>2</sub> aspiration, LNs isolated and the surrounding fat tissue carefully removed. Afterwards the LNs were embedded in tissue freezing medium (Thermo). With a cryostat 8 μm thick sections were cut and collected on glass slides. The sections were encircled with PapPen (Kisker) and subsequently fixed in pre-cooled methanol at -20° for 10 min. After the slides completely dried the tissue was blocked with 1% BSA for 30 min at RT. Thenceforward the tissue sections were kept constantly wet with the help of a humidifying chamber. Primary antibodies were diluted in 1% BSA in PBS and incubated on the slides for 45 min at RT followed by three PBS washing steps each 10 min at RT. Next, the sections were incubated with secondary antibody diluted in 1% BSA in PBS for additional 45 min at RT. Finally, the sections were washed as described before three times with PBS and mounted with Elvanol. Stained sections were examined using either a Zeiss Axiophot

fluorescence microscope and documented with the Openlab software version 3.1.2 (Improvision) or an inverted confocal microscope (Leica, SP2).

The following antibodies were used for immunofluorescence: Rabbit anti-mouse pan-laminin 1 (rabbit anti-mouse, Sigma), ICAM-1 (hamster anti-mouse, BD Biosciences), anti-mouse Exodus2 (rabbit anti-mouse, PeproTech). Primary antibodies were detected using fluorescein isothiocyanate (FITC)- or cyanine3 (Cy3)-conjugated goat anti-hamster or goat anti-rabbit IgG secondary antibodies (Dianova), respectively.

*Elvanol*                      12 g Mowiol 4 – 88 (Roth) dissolved in 30 ml 87% glycerol (Merck),  
60 ml Tris-HCl pH 8.5 (Sigma-Aldrich) and 30 ml H<sub>2</sub>O

### **3.7.2                      Quantification of immobilized CCL21 and CCL19 by immunofluorescence**

Microscope slides were incubated for 1 min in a plasma cleaner (Harrick) to enhance protein loading capacity by charging the surface. Compartments were demarcated with PapPen (Kisker). Within the compartments drops of either 22.5 µg/ml CCL21 or 22.5 µg/ml CCL19 mixed with 10 µg/ml ICAM-1 were applied, the contour of the drops marked and incubated for 30 min. All incubation steps were carried out in a humidifying chamber at RT. Spots were washed with PBS and subsequently incubated with either 1 µg/ml anti-CCL21 (Exodus2; rabbit; Peprtech) or 1 µg/ml anti-CCL19 (goat; R&D Systems) in PBS with 1% BSA for 30 min. After washing the coated areas were incubated with 7.5 µg/ml anti-rabbit Cy3 (donkey; Jackson ImmunoResearch) or anti-goat Cy3 (donkey; Jackson ImmunoResearch) in PBS with 1% BSA. After thoroughly rinsing with PBS the slides were embedded in Elvanol. The stainings were evaluated with a Zeiss Imager Z1 (40x objective) operated via AxioVision Rel.4.6.3 software. Fluorescence intensities were quantified using Image J software (<http://rsbweb.nih.gov/ij/>).

## **3.8                      Cell migration and spreading assays**

### **3.8.1                      Time lapse video microscopy**

Experiments were performed at 37°C and 5% CO<sub>2</sub> in a humidified and climatized chamber using a Zeiss Axiovert 40 CFL microscope operated via FireWire Recorder software (custom made, SVS-Vistek).

### 3.8.2 *In vitro* migration on LN-cryosections

For migration on cryosections mouse inguinal LNs were snap-frozen in liquid nitrogen. 8-10  $\mu\text{m}$  thick sections were collected on glass slides. The slides with the section were then immobilized on the bottom of a custom-built migration chamber, covered with  $1 \times 10^6$  DC/ml DCs in R10 medium and observed by time-lapse video microscopy.

Colour-coded composites were generated by superimposing background-subtracted binary layers using Openlab software version 3.1.2 (Improvision; Figure 16 C, Figure 17 C). Automated cell counting was done by creating background subtracted binary layers and subsequent automated pixel density measurements in the marked areas using Openlab software (Figure 16 B, Figure 17 A).

### 3.8.3 *In vivo* migration of DCs

Mature DCs were fluorescently labelled with 5  $\mu\text{M}$  5-, 6-carboxyfluorescein diacetate succinimidyl ester (CFSE, Molecular Probes). The DCs were washed with PBS and resuspended to a final cell concentration of  $1 \times 10^8$  in PBS. 4  $\mu\text{M}$  CFSE was added to the cell suspension. After 10 min incubation at RT the labelling reaction was stopped by adding the tenfold amount of R10 medium.

After labelling and extensive washing in PBS,  $5 \times 10^5$  DC in a volume of 20  $\mu\text{l}$  PBS were injected into mouse hind footpads. Draining popliteal LNs were harvested after 24 hr and snap-frozen in liquid nitrogen.

### 3.8.4 Chemokine spot migration assay

Custom-made glass bottom cell culture dishes were applied for this assay and partially incubated for 1 min in a plasma cleaner (Harrick) before use. Afterwards a solution of 22.5  $\mu\text{g/ml}$  CCL21 or 22.5  $\mu\text{g/ml}$  CCL19 mixed with 5  $\mu\text{g/ml}$  ICAM-1 were dropped onto the cover slip and the contour of the drops marked. The drop had in average a diameter of 1 mm. After 30 min at 37 °C the drop was washed three times with PBS and covered with  $1 \times 10^6$  DC/ml. The cell behavior was followed by time-lapse video microscopy. 2D projected cell surface areas were determined with Metamorph software (Zeiss) after 1, 5, 10 and 15 min.

### 3.8.5 DC spreading on with polysialic acid (polySia)-coated surfaces

5 cm cell culture dishes (Falcon) were coated overnight at 4°C with 10  $\mu\text{g/ml}$  polySia (Sigma-Aldrich) in PBS. After two washing steps with PBS the dishes were blocked for 30 min at 37°C with Tris-sucrose-magnesium (TSM) buffer containing 1% BSA. After rinsing

## Material and Methods

with PBS the dishes were let dry before a drop of either 22.5 µg/ml CCL21 or 22.5 µg/ml CCL19 in PBS containing 0.1% BSA mixed with 10 µg/ml ICAM-1 was applied. For controls, spots of 0.1 % BSA in PBS mixed with 10 µg/ml ICAM-1 were applied. The contours of the drops were marked and the dishes incubated for 30 min at 37°C. After washing the chemokine/ICAM-1 coated area was covered with  $1 \times 10^6$  DCs/ml. The surface area of the cells was determined microscopically after 1, 5, 10 and 15 min.

*TSM buffer*                      20 mM Tris-HCl (Merck), 150 mM NaCl (Merck), 1 mM CaCl<sub>2</sub> (Merck),  
1 mM MgCl<sub>2</sub> (Merck)

### 3.8.6 DC adherence on CCL21-coated fibroblasts

$5 \times 10^4$  *p19<sup>ARF-/-</sup>* LN-fibroblasts in 500 µl R10 medium were filled into a dish with a diameter of 2 cm. After two days the cells were washed two times with R10 medium followed by incubation with 200 µl of 1.25 µg/ml CCL21 in R10 medium. After 30 min at 37°C, 5% CO<sub>2</sub> the fibroblasts were rinsed twice with R10 medium and subsequently covered with 200 µl of  $1 \times 10^6$  DCs/ml resuspended in R10 medium for 5 min. Afterwards the dishes were washed three times with medium and the remaining, adherent cells counted.

### 3.8.7 Under-agarose migration assay (UAA)

UAAs allow the separation of migrating cells from diverse chemotactic sources and to determine the chemotactic potential of different chemoattractants (adapted from: Heit & Kubes, 2003). In a solid agarose/medium layer three holes were punched. The hole in the middle, the “responder hole”, was filled with DCs, the neighboring attractor holes with chemokines, inhibitors and/or DCs. The “attractor holes” allow the establishment of a concentration gradient and potential chemoattraction of the DCs. The DCs can react and migrate between the agarose layer and the underlying bottom of the cell culture dish towards the “attractor holes” (Figure 16).

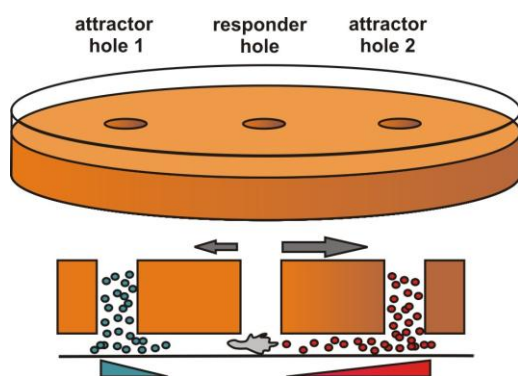


**Figure 14: Scheme of an under-agarose assay (UAA).** In a solid agarose/medium layer three holes were punched. In the responder hole in the middle DCs were filled. In the attractor holes to the left and the right potential chemoattractants were applied. When a chemotactic concentration gradient is formed the cells in the middle can react and migrate towards the chemotactic source.



10 ml of 4% Agarose (UltraPure™, Invitrogen) resuspended in ddH<sub>2</sub>O were heated up until the agarose was solved. The agarose solution was then mixed with an on 55°C preheated mixture of 10 ml 2x Hank's buffered salt solution (HBSS) with 20 ml R20 medium. 2 ml of the final solution was filled into a dish with a diameter of 3 cm. After the agarose solidified three holes with a diameter of 3 mm were punched into the agarose. The holes were arranged in on line with a distance of 6 mm in-between. After the assay equilibrated for 30 min at 37°C, 5% CO<sub>2</sub> the holes (volume approximately 7μl) were filled with 6x10<sup>4</sup> DCs and/or 625 ng/ml CCL19, CCL21 or truncated CCL21 expressed in *E.coli* B834(DE3)pLysS (3.5.2, p.57). Pertussis toxin (List Biochemicals) was applied at 20 μg/ml and aprotinin (Calbiochem) at 150 μM. After 15 hr at 37°C, 5% CO<sub>2</sub> cells, which migrated out of the “responder” hole in the middle towards the “attractor holes” to the left and the right, were imaged using a Zeiss Axiovert 40 CFL microscope (20x objective) operated via custom-made software (Firewire recorder, SVS Vistek). Cells migrated out of the responder hole were counted in a defined area.

<i>HBSS (2x)</i>	<i>0,975 g/l Hanks' balanced salts (Sigma-Aldrich), 7 mM Na<sub>2</sub>CO<sub>3</sub> (Merck), pH 7.2</i>
<i>R20 medium</i>	<i>RPMI (Gibco) with 20% FCS (Gibco), 5% penicillin/streptomycin (PAA), 5% glutamine (PAA)</i>

### 3.8.8 Modified UAA for TIRF microscopy

To analyze the actin cytoskeleton and the localization pattern of different GFP-tagged proteins during DC migration a modified variant of the described UAA was used in combination with total internal reflexion fluorescence (TIRF) microscopy. TIRF microscopy uses an evanescent wave to selectively illuminate and excite fluorophores in a restricted 200 nm thick region adjacent to the cell membrane. The basic principal of TIRF microscopy is the excitation at a critical angle that generates an evanescent field when light passes from a medium of high refractive index (e.g. glass) to one of low refractive index (e.g. the cell). The field of excitation decays rapidly with distance from the coverslip, thereby limiting the depth of excitation to a small distance.

For all TIRF-UAA's custom made glass bottom dishes were used. The glass slides were untreated, coated with CCL21 and ICAM-1 after plasma-treatment or coated with polyethylene glycol (PEG). For chemokine coating the glass bottom dishes were plasma-treated for 1 min in a plasma cleaner (Harrick) and afterwards covered with 22.5 μg/ml CCL21 and 10 μg/ml ICAM-1 in PBS. After 30 min at 37°C the slides were rinsed three times with PBS. PEG coated slides were kindly provided by Julien Polleux. Shortly, glass coverslips were immersed in a 1 mmol solution of a linear PEG, CH<sub>3</sub>-(O-CH<sub>2</sub>-CH<sub>2</sub>)<sub>43</sub>-NH-CO-NH-CH<sub>2</sub>-CH<sub>2</sub>-

$\text{CH}_2\text{-Si(OEt)}_3$  dissolved in dry toluene under nitrogen atmosphere for 20 hr. Finally, the substrates were rinsed intensively with ethyl acetate, methanol and ddH<sub>2</sub>O, and dried with nitrogen.

For this variant of UAA, 5 ml of 5% Agarose (UltraPure™, Invitrogen) dissolved in ddH<sub>2</sub>O was heated up until the agarose was completely solubilized. The agarose solution was subsequently mixed with 55°C warm solution of 5 ml 2xHBSS and 10 ml R20 medium. 400 µl of the final solution was filled into a custom made gas bottom dish with a diameter of 2 cm and equilibrated at 37°C for 30 min. A hole was stamped into the agarose layer and filled with 600 ng/ml CCL19. Within a distance of approximately 5 mm 10.000 DCs were injected between the glass coverslip and the agarose layer. Lifeact-GFP macrophages or Lifeact-GFP 3T3 fibroblasts were directly injected under the agarose layer without additional chemoattraction. TIRF microscopy was performed with an Axiovert 200 (Zeiss) microscope, a TIRF 488 nm laser system (Visitron systems) and a Cool-Snap-HQ camera (Roper scientific) triggered by Metamorph software (Molecular Devices).

### 3.8.9 Carbon fiber migration assay

To simulate the DC migration in the LN along fibroblastic reticular cells *in vitro* a modified variant of a 3D collagen migration assay (Lämmermann et al., 2008) with incorporated protein coated carbon fibers providing a haptokinetic scaffold was performed. At the same time the cells can sense an applied chemotactic concentration gradient (Figure 17).

For the collagen gels 750 µl PureCol (stock: 3 mg/ml, bovine Collagen I, Nutacon) were carefully mixed with 100 µl 10xMEM (Sigma-Aldrich) and 50 µl NaHCO<sub>3</sub>-solution (Sigma-Aldrich, 7.5%) to avoid bubbles. 600 µl of the collagen mix was subsequently added to 300 µl of  $3 \times 10^6$  DC/ml cell suspension in R10 medium and again mixed gently resulting in a final collagen concentration of 1.6 mg/ml. The final cell concentration in the gel was  $1 \times 10^6$  DC/ml. The gels were casted into a custom-made chamber (thickness 2 mm) with protein-coated carbon fibers (BALTIC, BP 2308) with a diameter of 5 µm. For coating, carbon fibers were incubated with 5 µg/ml ICAM-1 and either 0.1% BSA or 5 µg/ml CCL21/CCL19 for 30 min. Polymerized gels were covered with R10-medium or R10-medium containing 0.17 µg/ml CCL19 or 0.54 µg/ml truncated CCL21, respectively, and observed via time-lapse video microscopy. Manual cell tracking was carried out using the software ImageJ with the 'Manual Tracking Plugin' (<http://rsbweb.nih.gov/ij/>).

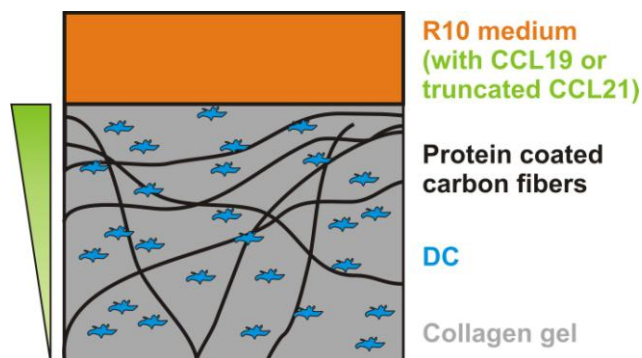


Figure 15: Scheme of the carbon fiber migration assay. A DC-collagen mixture was casted into a custom made chamber. Into the collagen gel chemokine-coated carbon fibers were incorporated. On top of the gel medium with chemoattractant was filled to establish a chemotactic concentration gradient, as depicted in green.

### 3.9 Statistical analysis

Student's t-tests and analysis of variance (ANOVA) were performed after data were confirmed to fulfil the criteria of normal distribution and equal variance. Student's t-test is used to compare the means of two samples and ANOVA to compare the means of three or more groups. Kruskal-Wallis tests or Mann-Whitney U-test were applied for data which does not fulfill the criteria of t-test and ANOVA (normal distribution and equal variance). The Mann-Whitney U test is a non-parametric statistical hypothesis test for assessing whether two independent samples of observations have equally large values. The Kruskal-Wallis one-way analysis of variance by ranks is an extension of the Mann-Whitney U test to three or more groups. For posthoc test of Kruskal-Wallis tests data were pairwise compared with Dunn's method. Dunn's method is used when the number of comparisons is small compared to the number of possible comparisons. All analyses were performed with Sigma Stat 2.03.

## 4 Results

### 4.1 Chemotactically biased haptokinesis

Most of the here presented data are published in Schumann et al., 2010 Immunity. 2010 May 28;32(5):703-13.

#### 4.1.1 A reductionist *in vitro* system to study chemokine-driven DC migration

Two-photon microscopy allows intravital observation of migrating leukocytes *in vivo*, but living tissues are notoriously complex and the multitude of cellular cross-talks makes it difficult to investigate molecular mechanisms that are non cell-autonomous. Thus, I chose a reductionist *in vitro* setup to analyze the chemokine-driven migration of DCs within LNs. CCL21 and CCL19 are both expressed by fibroblastic reticular cells (FRCs) in the T cell area of LNs. As mature DCs carry the CCL21-receptor CCR7 on their surface, I tested whether DCs could be used as environmental sensors of the chemokine distribution on LN cryosections. I layered mature bone-marrow derived DCs on unfixed, native cryosections of peripheral mouse LNs that were immobilized on a glass slide. Hence, the cells of the tissue substrate were not alive anymore, but proteins were unfixed and mainly in their natural conformation. The cell behavior was analyzed via time-lapse video microscopy over a period of 18 hr.

When mature DCs were applied to these assays, cells that directly settled on the tissue, showed a random migration pattern. After 20 min also cells that were not in direct contact but in proximity to the tissue showed directed migration towards the cryosection. This resulted in a highly synchronized wave of directed migration from the periphery towards the inner part of the LN section (Figure 16 A-C; Movie S1). 12-18 hr after the onset of migration, DCs accumulated in the centre of the LN, the T cell area. After 18 hr almost no DCs could be detected on the glass control area [C] and only 20% of the overall cell density were locate at the rim of the section which represents the SCS. Migration was only observed when mature DCs were employed and not immature DCs (Figure 16 B; Movie S2) or other cell types, like macrophages, mast cells, B or T cells (personal communication M. Sixt). Mature DCs are the only cells that show directional migration towards LN cryosections.

Surprisingly, DCs entered cryosections via special entry routes, suggesting migration along preformed tracks (Figure 16 A, red arrows). To investigate whether this reflects the physiological process, *in vivo* and *in vitro* migration assays were combined. Mice were injected subcutaneously with CFSE, a green fluorescent dye, labelled mature DCs into the foot pads and the draining popliteal LNs were excised after 10 hr. Histological analysis revealed immigrating CFSE positive cells in the interfollicular areas as shown by laminin co-staining of the stromal infrastructure. Consecutive sections were then used as substrates for

## Results

the described *in vitro* migration assay (Figure 16 D, right panel). The applied DCs showed directed motility in regions that also contained the CFSE-labelled DCs that had migrated *in vivo*. DCs localised on the B cell areas showed almost no motility. These results demonstrate that DC migration on tissue cryosections resembles the *in vivo* process as the cells still stick to their interfollicular entry routes migrating around B cell follicles and accumulate in the T cell area (Figure 16 D, right panel) as also described by Lämmermann et al. (2008).

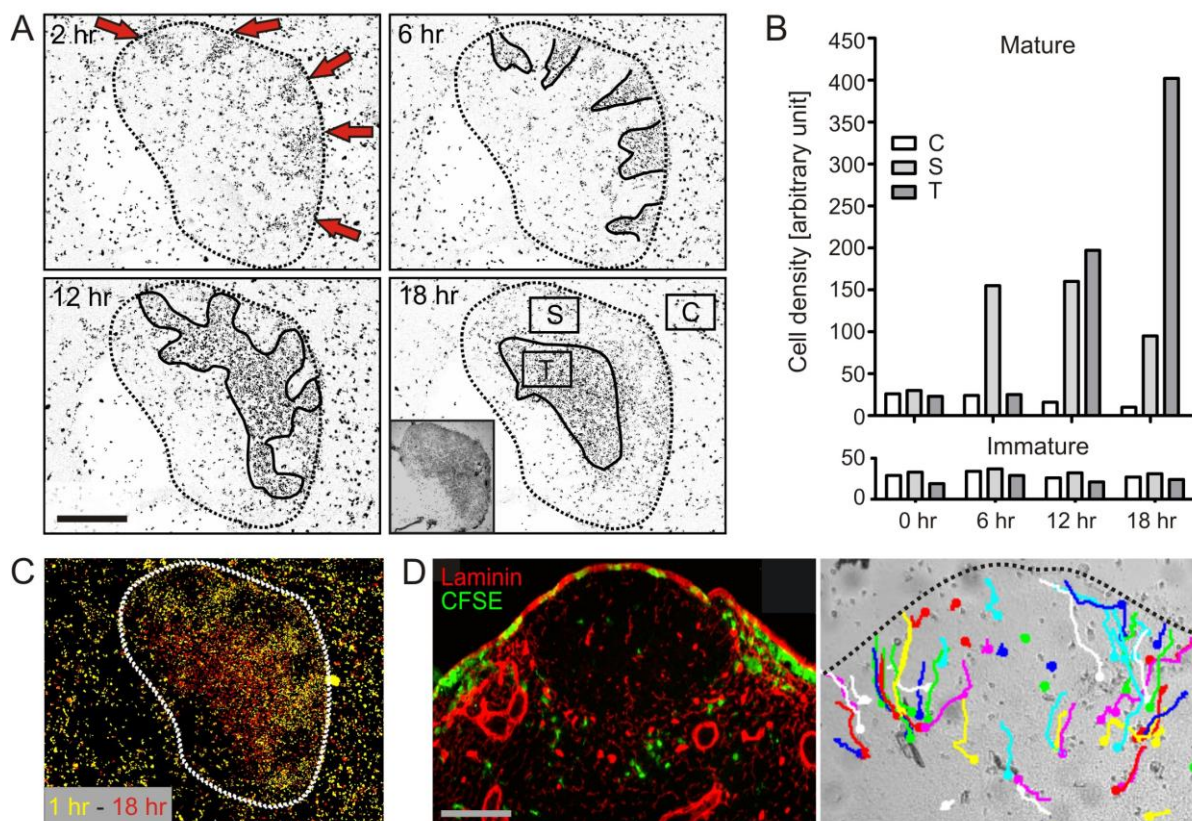


**Figure 16: Organized DC migration on LN cryosections. (A)** Contrast enhanced serial images of mature DCs on a section. Margins of the section are highlighted by the dotted line. Areas of high DC density are outlined (black line). Red arrows indicate entry sites of DCs. Small insert: brightfield image of the LN cryosection. Black boxes mark T cell area (T), sinus area (S), control area (C) used for quantification in (B). Scale bar represents 200  $\mu\text{m}$ . **(B)** DCs were quantified in the areas C, S and T by automated density measurement. The upper diagram represents mature, the lower immature DCs. Data represent one out of >30 independent experiments. **(C)** Composite picture of serial images of (A). Different time points were colored in graded wavelengths from yellow (1 hr) to red (18 hr) to show migratory fractions of DCs on the section. Dotted line: Outline of the section. **(D)** Left panel: section of a LN showing fluorescently labelled DCs (green) entering the LN via interfollicular areas 10 hr after subcutaneous injection. Laminin staining (red) highlights the reticular fibers surrounding the B cell follicle. Right panel: single cell tracking of DCs migrating on a consecutive section of the one shown left. Each track represents the pathway of a single cell. Dotted line: outline of the section. Scale bar represents 50  $\mu\text{m}$  (taken from: Schumann et al., 2010).

Next, I wanted to define the guidance cues which establish these preformed migration pathways. As already mentioned, the predominant chemokines in the T cell area are the CCR7 ligands, CCL21 and CCL19. To test if the observed migration patterns on LN cryosection are CCR7-dependent, too, I applied mature *Ccr7*<sup>-/-</sup> DCs to the cryosection assays. *Ccr7*<sup>-/-</sup> DCs showed no directional migration toward the center of the LN cryosections (Figure 17 A). The same result was achieved by employing wild-type (WT) DCs to LN sections obtained from *plt/plt* mice, which lack the expression of both CCR7 ligands in the LN (Nakano et al., 1998). However, *plt/plt* DCs accumulated on WT LN cryosections (Figure 17 A). These findings suggest that the observed DC migration patterns depend on the chemokine receptor CCR7 expressed on DCs and CCR7-ligands present on the LN cryosections.

### 4.1.2 Soluble chemotactic gradient guides DCs on cryosection

I could clearly observe directional DC migration on LN cryosections. Thus, an either immobilized or soluble gradient must persist in the *in vitro* LN migration assays and direct the cells. I immunostained LN cryosections for CCL21 and CCL19 in order to visualize a potential graded chemokine distribution. In conformity with previous studies (Luther et al., 2000) CCL19 was not detectable on LN cryosection by this histological technique; probably because of the lower expression level of CCL19 and the marginal binding efficiency of CCL19 towards GAGs (Luther et al., 2001; Link et al., 2007; de Paz et al., 2007). By contrast the CCL21 signal highlighted the FRC network in the T cell area and left B cell follicles unstained (Luther et al., 2000; Woolf et al., 2007 and Figure 17 B). As previously described by Okada et al. (2005) the overall LN staining pattern was suggestive of a higher CCL21 concentration in the centre of the LN and a CCL21 gradient extending into the B cell follicles (Figure 17 B).

To challenge the possibility of DC migration along an immobilized CCL21 gradient, a peripheral part of a LN cryosection was removed, inverted by 180° and repositioned next to the remaining tissue section (Figure 17 C, left panel). Also in this setup DCs showed a wave of directed migration, but the migration on the inverted small tissue segment was still directed towards the centre of the larger segment (Figure 17 C, right panel; Movie S3). The DCs migrating towards the big LN segment stopped at the margin of the inverted section, because DCs migrate poorly on glass surfaces and prefer to stay in contact with the tissue. Because the direction of migration had changed relatively to the tissue, the reason for directional DC migration cannot be an immobilized chemokine gradient. The DCs migrated towards a soluble chemotactic gradient emanating from the T cell area. Also the fact that DCs which are dislodged from the tissue show directed migration toward the cryosection support the idea of a soluble gradient (Figure 16 A, Figure 17 C).



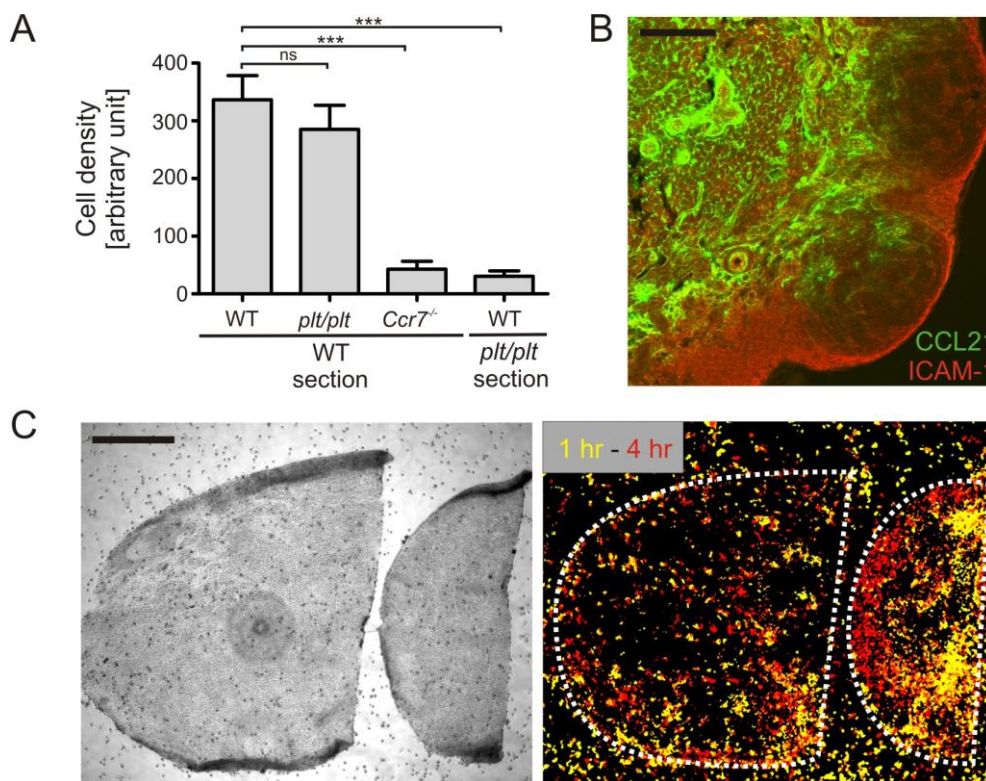


**Figure 17: DCs are directed by soluble gradients. (A)** Accumulation of wild type (WT), *Ccr7<sup>-/-</sup>* and *plt/plt* DCs on either WT or *plt/plt* LN sections. Bars represent mean  $\pm$  SEM, n = 3. **(B)** Fluorescent staining of a LN section for CCL21 (green) and ICAM-1 (red). Scale bar represents 200  $\mu$ m. **(C)** A peripheral part of a LN section was dissected, inverted by 180° and repositioned in close proximity to the remaining part of the section. Left panel: Bright-field image of the manipulated section. Right panel: Migratory course of mature DCs on this section. Different time points were colorized in graded wavelengths from yellow (1 hr) to red (4 hr) to show migrating fractions of DCs. Dotted line: outline of the section. Scale bar. Data represent one out of four independent experiments. Scale bar represents 250  $\mu$ m. \*\*\*P<0.001, ns: not significant (taken from: Schumann et al., 2010).

### 4.1.3 Response patterns to CCL21

In order to investigate how the soluble chemotactic gradient is generated, I further simplified the migration assay. The experiments with *Ccr7<sup>-/-</sup>* and *plt/plt* DCs on cryosections indicated a central role of CCL21 (Figure 17 A), thus I assayed DC migration in the exclusive presence of recombinant CCL21.

CCL21 was dropped onto the bottom of a polystyrene cell culture dish within a circular area of about 1 mm diameter and incubated at 37°C to enhance chemokine binding to the surface. Non-immobilized CCL21 was thoroughly washed away with PBS. Mature DCs were added and the coated area and its surrounding observed by time laps video microscopy (Figure 18 A). DCs directly settling onto the coated area showed rapid spreading, followed by increased random migration. In addition, 10 minutes after the onset of migration, DCs outside but adjacent to the coated area began a co-ordinate migration towards the coated area. During the following 15 hr, DCs continuously migrated in a directed manner towards

## Results

the CCL21 spot from regions of up to 1 mm away from the margins of the coated area, resulting in a dense aggregation of DCs on the coated area (Figure 18 C; Movie S4). When the cells reached the CCL21 spot, they also showed an increased random migration. *Ccr7*<sup>-/-</sup> DC showed no response to immobilized CCL21 (Figure 18 B). Previous work in the Sixt lab has shown that CCL19 spotted onto cell culture dishes induces some random motility in mature DCs, which are in direct contact with the chemokine, but no directional migration from the periphery to the chemokine spot (M. Sixt).

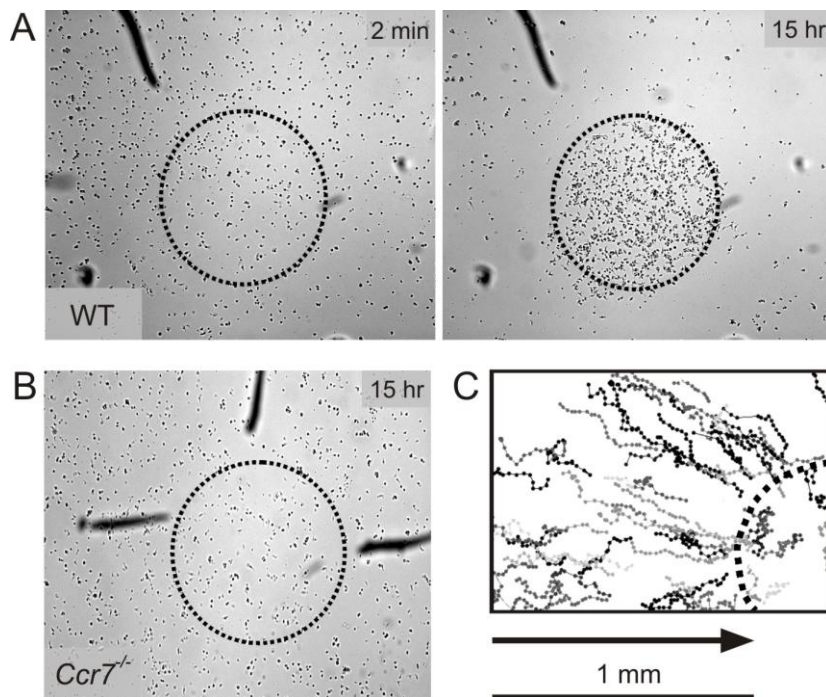


**Figure 18: Migration of DCs towards immobilized CCL21.** CCL21 was plated on cell culture plastic (coated area marked by dotted circle). (A) Distribution of DCs on CCL21 coated area after 2 min (left panel) and 15 hr (right panel). Data show one representative out of >30 independent experiments. (B) *Ccr7*<sup>-/-</sup> DC distribution after 15 hr. (C) Single cell tracking of migrating WT DCs. Each track represents the pathway of a single cell over 30 min. Migration is directed towards the CCL21 coated area (arrow) and is observed in uncoated areas up to 1 mm from the coated area (taken from: Schumann et al., 2010).

These observations suggest that immobilized CCL21 has three different effects on mature DCs that appear in a distinct order:

- 1) rapid spreading
- 2) random migration
- 3) release of a soluble chemoattractant that leads to a positive feedback event attracting more DCs.

I continued to dissect these individual responses with reductionist *in vitro* approaches.



### 4.1.4 DCs turn immobilized CCL21 into soluble CCL21 that resembles CCL19

To further analyze the nature of the soluble attractant, I performed under-agarose migration assays, which allow the spatial separation of migrating DCs from the place where the chemotactic factor is released. Three holes were punched into an agarose/medium-layer. In the hole in the middle, the so-called “responder hole”, DCs were filled, the neighboring “attractor holes” contained different mixtures of chemokines, DCs and inhibitors. The “attractor holes” allow the establishment of a concentration gradient and potential chemoattraction of the cells that can migrate between the agarose and the underlying bottom of the culture dish (Figure 17 A). After 15 hr “responder” DCs, which migrated towards one of the “attractor holes”, were counted to determine the chemotactic capacity of the mixtures administered to the “attractor holes” (Figure 19 B).

CCL21 triggered only minimal chemotactic response in under-agarose assays. The second CCR7 ligand, CCL19, on the other hand induced a vigorous, directed migration in responder DCs. These results indicated that CCL19, but not CCL21, is able to establish chemotactic concentration gradients. Responder DCs also migrated in a directed manner towards a mixture of DCs with CCL21 comparable to the migration towards CCL19. DCs alone did not attract other DCs. These results proved the induction of a soluble chemotactic gradient once DCs get into contact with CCL21. I observed the same effect when DCs were pre-incubated with CCL21 and only the cell supernatant was applied as an attractant.

To elucidate the nature of the chemoattractant, responder DCs were incubated with pertussis toxin (ptx) which resulted in a complete blockade of migration. The outcome indicates G-protein coupled receptor (GPCR) dependent migration. The next step was to analyze if the soluble gradient is still sensed by the GPCR CCR7. *Ccr7*<sup>-/-</sup> DC were unable to respond to CCL21 alone as well as to a mixture of CCL21 and DCs. Therefore, the cells still sense the tactic signal via CCR7, suggesting that either an unknown CCR7 ligand, CCL19 or a modified variant of CCL21 is released upon contact of DCs with CCL21.

To test if the release of the chemotactic substance requires a CCR7 dependent signal I directly compared *Ccr7*<sup>-/-</sup> DCs as well as WT DCs co-incubated with CCL21 and found contrastable migration towards both attractor holes. Thus, the emerging soluble chemoattractant is constitutively produced upon direct contact between CCL21 and DCs; previous binding of CCL21 to the receptor CCR7 is not necessary to induce the chemoattractant. Besides FRCs also some hematopoietic cell subsets like mature DCs secrete CCL19 (Luther et al., 2000). To exclude CCL19-dependent chemoattraction *plt/plt* DCs, which cannot produce CCL19 (Vassileva et al., 1999; Mori et al., 2001; Nakano & Gunn 2001), and WT DCs were incubated with CCL21 and the chemotactic response of the WT responder DCs were directly compared. In both cases comparable chemotaxis was observed (Figure 19 B). To rule out the third option, the release of an unknown chemoattractant by DCs after contact with CCL21, DCs were incubated with CCL21 in the absence or presence of

## Results

brefeldinA. BrefeldinA inhibits Golgi export and thereby protein secretion (Low et al., 1992). Application of BrefeldinA did not change the chemotactic potential of CCL21 incubated with DCs (personal communication M. Sixt). DCs do not release an unknown chemotactic factor after contact with CCL21. Together these results argue for a modified variant of CCL21 itself that is produced upon direct contact between DCs and CCL21. Modified CCL21 is able to establish chemotactic concentration gradients and induces CCR7-dependent chemotaxis.

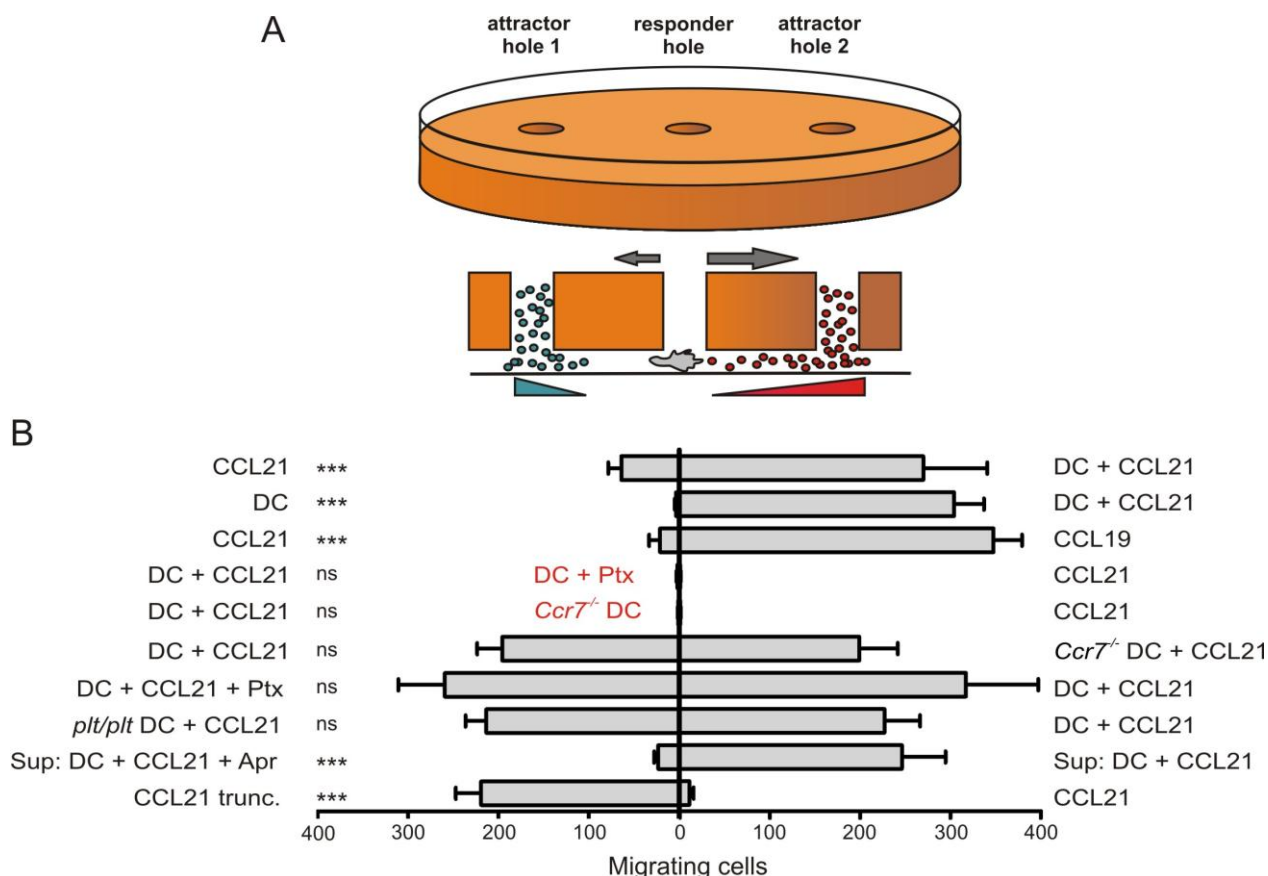


**Figure 19: DCs modify CCL21.** (A) Scheme of the under-agarose assay. The “responder hole” in the middle was filled with DCs, the “attractor holes” outside were filled with DCs and/or chemokine or inhibitor, allowing the establishment of a concentration gradient. When the cells sense a chemotactic gradient, they migrate out of the “responder hole”. (B) Number of cells that migrated out of the “responder hole” after 15 hr. Ptx: Pertussis toxin. Apr: Aprotinin. Sup: Cell supernatant. CCL21 trunc.: CCL21 with truncated C-terminus. If not indicated in red, WT DCs were applied as “responder cells”. Error bars represent mean  $\pm$  SEM,  $n = 4-8$ , \*\*\* $P < 0.001$ , ns: not significant. (B) taken from: Schumann et al., 2010.

To test for modifications after contact of CCL21 with DCs I performed Western blot analysis of CCL21 before and after incubation with DCs (Figure 20 A). With increasing incubation times a CCL21 fragment of reduced size (approximately 8 to 9 kDa) appeared, implicating proteolytic processing. In approximately 20% of the experiment two CCL21 fragments slightly differing in size appeared (Figure 20 A; red arrows). With 150  $\mu$ M Aprotinin, a serine

protease inhibitor, the cleavage reaction could be blocked completely. Additionally Aprotinin was applied to the described under-agarose assay. DCs did not migrate towards cell supernatants of DCs pre-incubated with CCL21 and Aprotinin. Thus, the enzyme catalyzing the cleavage reaction belongs to the family of serine proteases. Besides that, I also examined if other cell population of the LN can process CCL21 (Figure 20 B). Incubation with T cells and B cells, respectively, lead to low, inefficient cleavage. The low amounts of CCL21 fragments also differ in size in comparison to the CCL21 fragment generated by DCs. Mouse embryonic fibroblasts, as an example of stromal cells, did not cleavage CCL21 (Figure 20 C).

Next, I wanted to test if the *in vitro* CCL21 cleavage recapitulates a physiological process. Therefore, peripheral LNs of WT mice were isolated, lysed and a CCL21 “pull-down” performed. With this technique full-length CCL21 as well as a CCL21 fragment of similar size as observed *in vitro* could be detected. Therefore, CCL21 cleavage clearly reflects an *in vivo* process. To test if the *in vivo* CCL21 cleavage reaction is influenced by LN inflammation, for example by the increasing number of mature DCs in the LN, pull-downs out of inflamed LNs were performed. In inflamed LNs the amount of mature DCs is higher in the tissue. 36 h before harvesting the popliteal draining LNs DCs were injected into the foot pads of mice. The isolated popliteal LNs were clearly enlarged – a sign for inflammation. However, in the pull-down only a faint band of the CCL21 fragment could be detected (Figure 20 D). Under inflammatory conditions the amount of cleaved CCL21 is reduced in LNs.

The main difference between CCL21 and CCL19 is the C-terminal extension of CCL21 that is highly charged and binds to anionic surfaces as for example heparan sulfate residues (Hirose et al., 2001; Hirose et al., 2002; Ueno et al., 2002; Uchimura et al., 2006). To map the cleavage site I expressed recombinant CCL21 carrying an N-terminal Flag and a C-terminal His tag in the yeast *Pichia pastoris* and detected on Western-blot the chemokine as well as the two tags after exposure to DCs (Figure 20 E, F). Mature DCs were able to process the recombinant, tagged CCL21 protein. In the  $\alpha$ CCL21 and the  $\alpha$ Flag-tag Western-blot full-length chemokine as well as CCL21 fragment were clearly detectable. But by detecting the His-tag only the unprocessed CCL21 could be observed (Figure 20 E, F). This result together with the difference in size between processed and full-length CCL21 proved the complete loss of the immobilizing C-terminus. This result is emphasized by the comparison of CCL19 and CCL21 in under agarose assays, where CCL19 in contrast to CCL21 induces directional migration that cannot be enhanced by co-incubation with DCs (Figure 19 B). Moreover, a truncated version of CCL21 without heparan sulfate binding C-terminus triggered vigorous directional DC migration without incubation with DCs (Figure 19 B). These findings demonstrate that upon contact with mature DCs CCL21 is proteolytically processed into a variant that lacks the heparan sulfate binding C-terminus. The CCL21 fragment diffuses and acts as a chemoattractant which functionally resembles unprocessed CCL19.

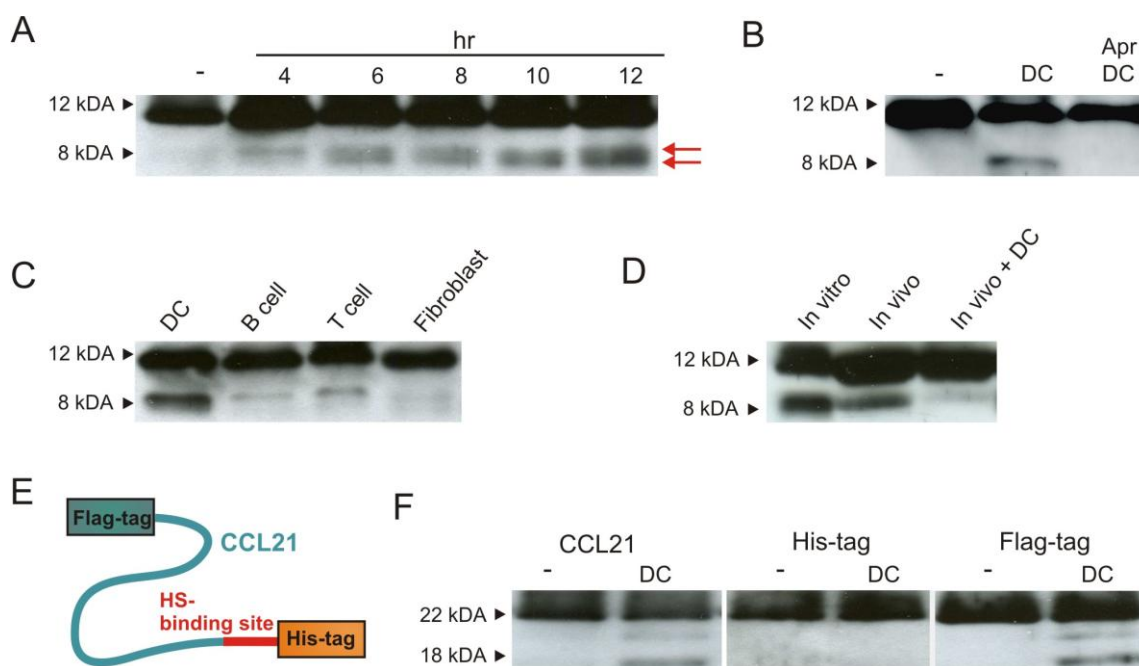


**Figure 20: DCs turn immobilized CCL21 into soluble CCL21:** (A) CCL21 was incubated with DCs for up to 12 hr. Processing of CCL21 was determined by western-blot analysis. Control (-): CCL21 incubated in medium without DCs. Red arrows indicate CCL21 fragments slightly differing in size. (B) CCL21 was incubated with DCs or with DCs and aprotinin for 15 hr. Control (-): CCL21 incubated in medium without DCs. (C) DCs, B cells, T cells and mouse embryonic fibroblasts were co-incubated with CCL21 for 12 hr before western-blot analysis of the supernatant. (D) *In vitro*: CCL21 cleavage after 12 hr co-incubation with DCs. *In vivo*: Pull-down of *in vivo* cleaved CCL21 out of LN-lysate. To test for CCL21 cleavage under inflammatory conditions 36 hr before isolation of popliteal LNs DCs were injected into the foot pads of the mice (*in vivo* + DCs). (E) Scheme of the *Pichia pastoris* CCL21 construct with N-terminal Strep-tag and C-terminal His-tag. (F) Western-blot analysis of tagged CCL21 (detection of CCL21, His- and Flag-tag) after 15 hr incubation with DCs (+). Control (-): CCL21-incubation in R10 medium without DCs. (A), (B), (C), (D) and (F) taken from: Schumann et al., 2010.

#### 4.1.5 Plasmin cleavage of CCL21

A seminal question arising from the previous findings is which protease cleaves CCL21. Using pharmacological inhibitors it could be shown that the sought-after protease belongs to the family of serine proteases (Figure 20 B). CCL21 processing is induced upon direct contact between chemokine and the DC cell surface. The CCL21 cleaving protease could either be produced by DCs themselves and transported to the cell membrane or be recruited from the surrounding FCS to the cell surfaces. To test the second hypothesis DCs were incubated with CCL21 without FCS or in the presence of FCS that was completely heat-inactivated at 95°C for 5 min. In both cases no CCL21 processing could be observed (Figure 21 A). These results were not due to a lack of nutrients in the absence of FCS or nutrient degradation in complete heat inactivated FCS; the DCs applied to these cleavage assays

## Results

showed a normal morphology and no increased apoptosis during the experiments. Hence, the conclusion was that the cleavage reaction is not a DC autonomous, but a FCS-dependent process. DCs recruit a serine protease or a co-factor from the applied serum to their surface to activate the enzyme, which then cleaves CCL21.

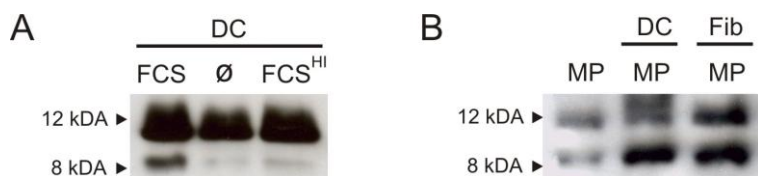


**Figure 21: CCL21 cleavage in the presence of serum or plasma, respectively, after 15 hr incubation. (A) DC-dependent processing of CCL21 with/without (Ø) FCS or completely at 95°C heat-inactivated FCS (FCS<sup>HI</sup>). (B) CCL21 processing by non-heat-inactivated mouse plasma (MP) or the combination of MP with DCs or *p19<sup>ARF-/-</sup>* LN-fibroblasts after 15 hr.**

Next, I replaced FCS with not-heat inactivated mouse plasma (MP), a more physiological supplement. Astonishingly CCL21 cleavage can take place in not-heat inactivated MP also without additional co-incubation with DCs. But the cleavage could be enhanced by the addition of DCs and surprisingly also by the addition of LN-derived *p19<sup>ARF-/-</sup>* fibroblasts (provided by S. Luther). MP comprehends a serine protease that cleaves CCL21. The efficiency of the cleavage reaction is higher in the presence of cells, which probably recruit the enzyme to their surface which leads to a fully activated serine protease. This result is contrary to previous results derived from co-incubation of mouse embryonic fibroblasts with the chemokine in the presence of FCS. In this case no CCL21 cleavage could be detected (Figure 20 C). Moreover, in the MP-supplemented CCL21 cleavage assays was the over-all amount of CCL21, the processed and unprocessed one, increased upon co-incubation with cells, either DCs or *p19<sup>ARF-/-</sup>* LN-derived fibroblasts compared to the incubation only with plasma, although the same amount of recombinant chemokine was employed to each of the cleavage assays (Figure 21 B). Cell surfaces seem to protect full-length as well as cleaved CCL21 from further degradation.

## Results

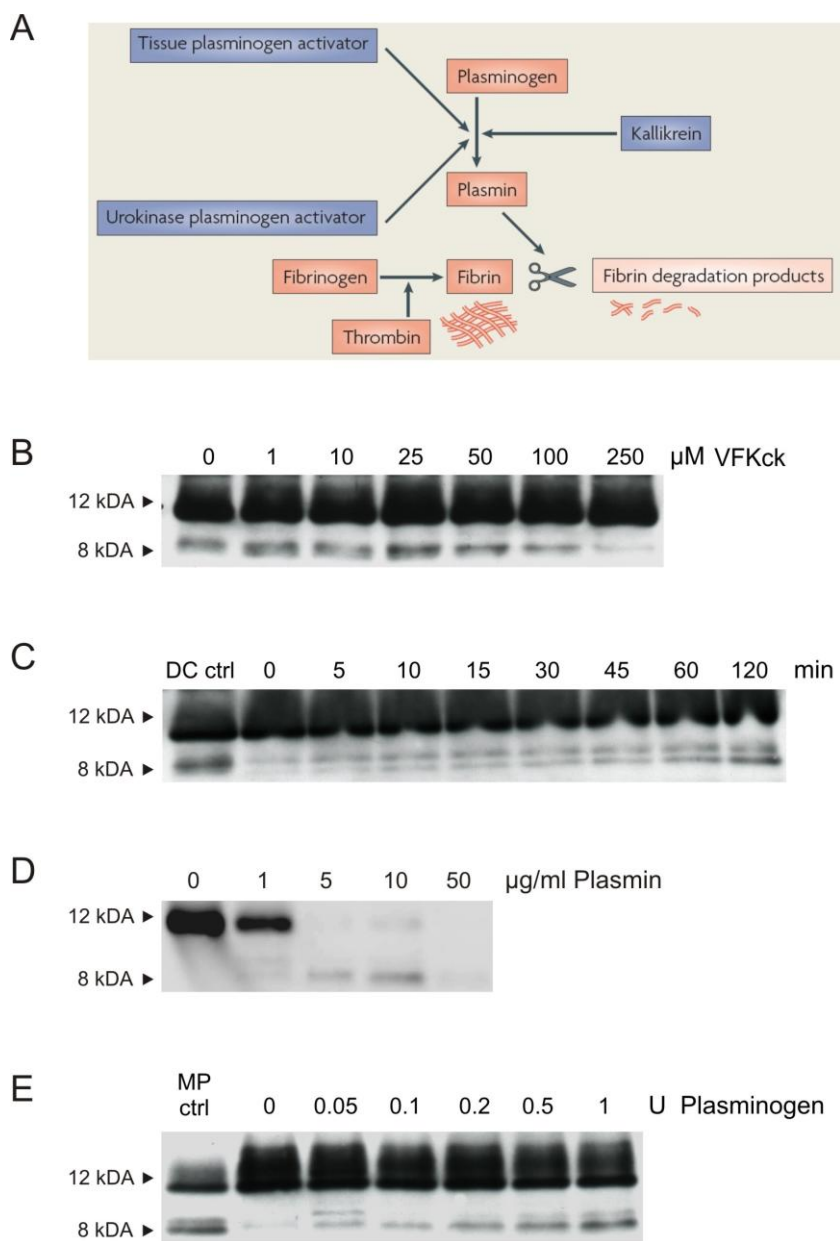


**Figure 22: Plasmin cleavage of CCL21.** (A) Scheme of the production and degradation of fibrin (taken from Schäfer & Werner, 2008). (B) Incubation of DCs and CCL21 with different amounts of the plasmin-inhibitor VFKck in R10 medium. (C) CCL21 was incubated with 50 nM human plasmin in PBS with 0.1% Tween-20. The reaction was stopped by heat-inactivation after different time points. DC control (DC ctrl): DC dependent CCL21 cleavage in R10 medium. (D) Different amounts of plasmin were incubated with CCL21 in PBS for 1 hr. (E) DC dependent CCL21 cleavage in R10 supplemented with different amounts of plasminogen instead of blood serum or plasma, respectively. Mouse plasma control (MP ctrl): CCL21 incubated with DCs in RPMI supplemented with not heat-inactivated MP. All samples were incubated for 15 hr.

Several reaction cascades depending on serine proteases, which bind to cell surfaces upon activation, are known, as for example the complement system, the blood coagulation cascade and fibrinolysis. Fibrinolysis is the process of disintegrating fibrin clots, the products of blood coagulation, by the enzyme plasmin. Plasmin cuts the fibrin network into small

fragments that can be transported by the blood circulation and finally be degraded by other proteases in kidney and liver. The liver releases the zymogen plasminogen into the blood circulation. Plasminogen is converted into the active enzyme by proteolytic processing of tissue plasminogen activator, urokinase plasminogen activator or serine proteases of the kallikrein family (Figure 22 A). Plasmin has also several non-fibrolytic functions like ECM degradation, matrix metalloproteinase- and growth factor activation (Plow & Hoover-Plow, 2004). It is known that plasmin cleaves several chemokines like CCL1, CCL2 and CXCL8 (Vakili et al., 2001; Sheehan et al., 2007; Proost et al., 2008). Plasminogen knockout (*Plg*<sup>-/-</sup>) mice are retarded in growth, have severe defects in mammary gland involution and female fertility, monocyte recruitment to inflamed tissue and exhibit fibrin depositions and thrombotic lesion in many tissues (Green et al., 2006; Ploplis et al., 1998). These defects result in an early mortality. Besides that, plasminogen can also be detected in lymphatic tissues (Yamakawa et al., 1991). Because of these reasons plasmin appeared to be a promising candidate.

First, I added the highly selective plasmin inhibitor D-Val-Phe-Lys chlormethyl ketone (VFKck, IC<sub>50</sub> = 100 pM to human plasmin [Merck]) to the cleavage assay composed of mature DCs and CCL21 in R10 medium. When the inhibitor was applied in extremely high concentrations of 250 µM only a very faint band of cleaved CCL21 remained (Figure 22 B). Moreover, when recombinant CCL21 was incubated with human plasmin two chemokine fragments appeared. The fragments exhibit a similar size as the CCL21 cleaved by DCs in the presence of FCS (Figure 22 C; DC ctrl). After 2 hr the second, shorter variant of CCL21 dominates (Figure 22 C). But it was not possible to accumulate cleaved CCL21 in this *in vitro* assay to further characterize the fragments, for example determine the exact cleavage site by mass spectrometry. Plasmin degraded the CCL21 fragments (Figure 22 D).

Plasmin is secreted into the blood circulation as an inactive zymogen, plasminogen. Next, I tested if DCs only recruit active plasmin to their surface or if they are also able to recruit plasminogen and activate the proenzyme by proteolytic processing. Therefore, DCs were incubated in RPMI medium supplemented with mouse plasminogen to replace FCS. Also in this experiment two CCL21 fragments could be detected, whereas the shorter CCL21 fragment accumulated with increasing amounts of added proenzyme. Hence, DCs can turn the zymogen plasminogen into its active form, plasmin, which then generates two CCL21 fragments.

Because the CCL21 processing can only inhibited in presence of very high concentrations of VFKck, blood plasma collected from *Plg*<sup>-/-</sup> mice was applied to the cleavage assay and compared to WT plasma to further confirm the results. Firstly, CCL21 was incubated with RPMI supplemented with either WT or *Plg*<sup>-/-</sup> MP. In both cases cleaved CCL21 could be detected. However, in the cleavage assay supplemented with WT plasma a higher amount of cleaved CCL21 could be detected. Moreover, the CCL21 fragments slightly differed in size between the WT and the *Plg*<sup>-/-</sup> cleavage assay. In addition to that, the band of cleaved CCL21 detected in the WT plasma was thicker and blurred. This band consisted of two CCL21 fragments which differed marginally in size. When these cleavage assays were

## Results

repeated in the presence of DCs, the amount of fragmented CCL21 was in both cleavage assays higher as described before. However, the overall result was the same as observed in the absence of DCs: In the cleavage assay with DCs and WT plasma to CCL21 fragments appeared only slightly differing in size, whereas in the assay with *Plg*<sup>-/-</sup> plasma only the smaller band could be detected. When the *Plg*<sup>-/-</sup> plasma cleavage assay was rescued with purified mouse plasminogen, almost all CCL21 was cleaved and only the second, smaller CCL21 fragment could be detected (Figure 23 A). The experiments with *Plg*<sup>-/-</sup> plasma reveal that plasmin is only one of two or even more serine proteases that can cleave CCL21: Two CCL21 fragments could be verified in WT MP and only the second smaller fragment is generated by plasmin. When recombinant plasminogen is added the second plasmin-dependent fragment accumulates over time.

To confirm these results in a more physiological setting CCL21 was pulled-down from LN-lysates of WT, *Plg*<sup>+/-</sup> and *Plg*<sup>-/-</sup> mice. In all three cases processed CCL21 could be isolated. In this experiment no difference between WT and *Plg*<sup>-/-</sup> could be detected either in the amount or the size of the CCL21 fragment. The amount of processed CCL21 was slightly increased in the heterozygous LNs (Figure 23 B). Thus, it is unclear if the plasmin cleavage of CCL21 is relevant *in vivo*. I want to mention that the results from these LN pull-down are only preliminary and should be repeated.

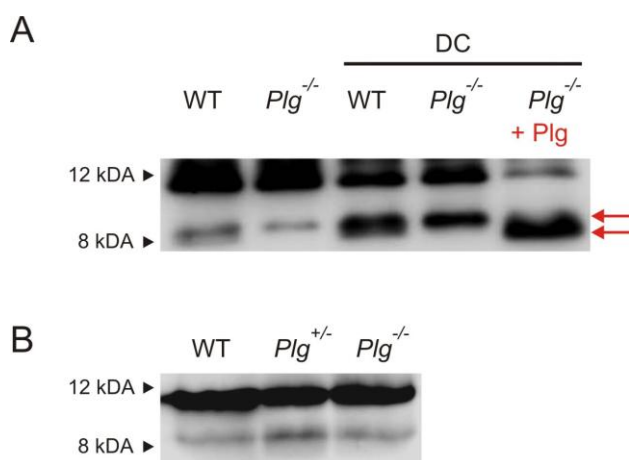


**Figure 23: Analysis of CCL21 processing in *Plg*<sup>-/-</sup> plasma and LN lysates. (A)** Incubation of R10 medium supplemented with WT and *Plg*<sup>-/-</sup> MP without/with DCs for 12 hr. Rescue with recombinant mouse plasminogen is marked in red. Red arrows indicate the size of the two CCL21 fragments. **(B)** CCL21-pulldown out of LN-lysates of WT, *Plg*<sup>+/-</sup> and *Plg*<sup>-/-</sup> mice.

### 4.1.6 Immobilized but not soluble chemokine triggers integrin activation on DCs

The morphology of migratory DCs on LN cryosection and on immobilized CCL21 point towards a central role of adhesion during migration on these substrates. Migratory DCs had



## Results

a polarized, elongated shape, whereas non-migratory DCs which settled on B cell follicles stayed roundish with small dendrites scanning the environment (Figure 24 A; Movie S5). Therefore, a possible crosstalk between CCL21 and integrins on DCs was assumed. Different integrins knockout DCs were applied to cryosection migration assays, but only  $\beta 2$  integrin knockout (*Itgb2*<sup>-/-</sup>) recapitulated the non-migratory phenotype: *Itgb2*<sup>-/-</sup> DCs showed significantly less migration on LN cryosections, also in the T cell area. The cells stayed roundish and unpolarized. Mature DCs normally carry inactive integrins on their surface (Figure 24 B; Movie S6). Hence, only  $\beta 2$  integrin can be activated on LN cryosections.

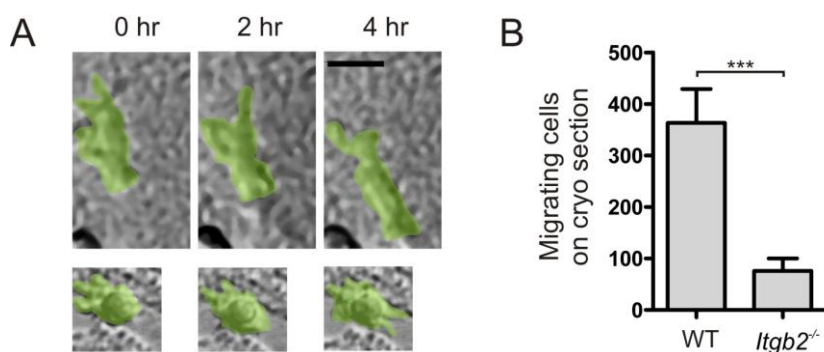


**Figure 24: DC migration on LN cryosections is  $\beta 2$  integrin dependent. (A) Morphology of a DC applied to a LN section after 0, 2 and 4 hr. Upper panels: Elongated, non-dendritic “amoeboid” shape of a DC migrating on a sinus area. Lower panels: Rounded, dendritic-like morphology of a non-migrating DC on a B cell follicle. The cell surfaces are highlighted in green. Scale bar represents 10  $\mu\text{m}$ . (B) Accumulation of WT and *Itgb2*<sup>-/-</sup> DCs on a LN sections. Error bars represent mean  $\pm$  SEM, n = 3. \*\*\*P<0.001. Adapted from: Schumann et al., 2010.**

I decided to analyze the chemokine dependent activation of  $\beta 2$  integrin to compare the capacity of CCL19 and CCL21 to induce cell spreading. The most important  $\beta 2$  integrin ligand in LNs is ICAM-1. Therefore, WT DCs were allowed to settle onto glass cover slips coated with a mixture of recombinant ICAM-1 with CCL21, CCL19 or BSA as a negative control, respectively. Changes in the 2D cell surface were measured over time.

DCs showed rapid spreading within minutes after contact with CCL21 plus ICAM-1 (Figure 25 A). The spreading response was transient and almost immediately followed by random polarization and initiation of migration (Figure 25 C). Coated ICAM-1 and BSA did not trigger spreading, indicating again a quiescent state of the ICAM-1 binding  $\beta 2$  integrins in mature DCs. When DCs were placed on co-coated CCL19 and ICAM-1, almost no spreading response could be observed (Figure 25 A). One possible explanation is that CCL19 failed to induce spreading because the chemokine is not presented in an appropriate way to the DCs due to the missing flexible C-terminus. Possibly CCL19 binding to an ECM molecule induces DC spreading. Bax et al. (2009) demonstrated that polysialic acid (PolySia) is a physiological platform for the immobilization of CCL21. Cell culture dishes were first coated with a

## Results

PolySia-solution. Afterwards the PolySia pre-treated dishes were coated with a mixture of recombinant ICAM-1 with CCL21, CCL19 or BSA, as described before. Mature DCs applied to these different coated surfaces showed the same behaviour as described for glass: Rapid spreading on CCL21 and no spreading response to CCL19 or BSA (Figure 25 B).

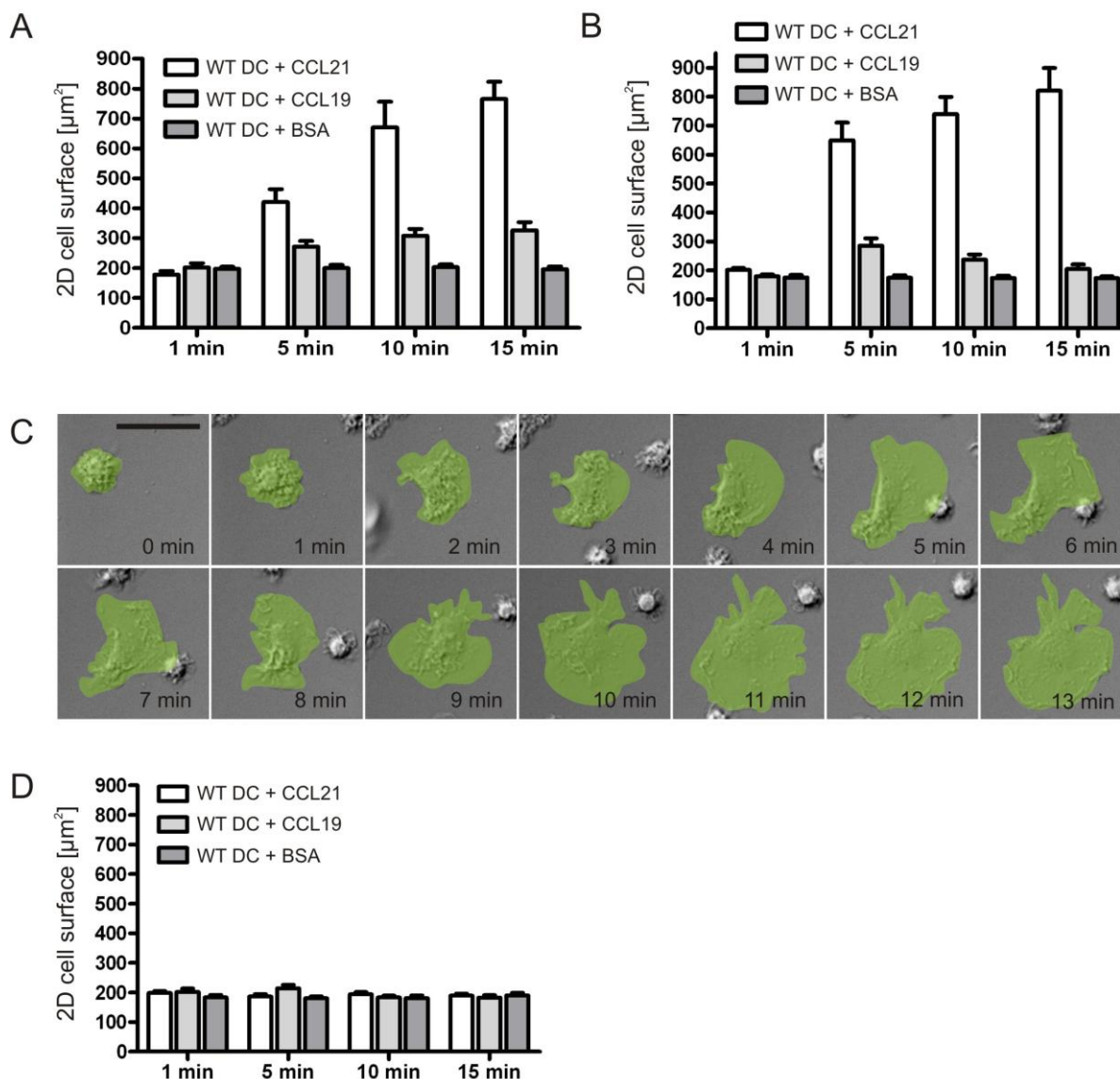


**Figure 25: DC spread on immobilized CCL21.** (A) Quantification of the 2D projected cell surface after contact with either CCL21/ICAM-1, CCL19/ICAM-1 or BSA/ICAM-1 coated glass surfaces after 1, 5, 10 and 15 min. Error bars show mean  $\pm$  SEM,  $n = 25$ . (B) 2D projected cell surface of DCs plated on with polysialic acid coated glass slides before application of either CCL21/ICAM-1, CCL19/ICAM-1 or BSA/ICAM-1 after 1, 5, 10 and 15 min. Error bars show mean  $\pm$  SEM,  $n = 25$ . (C) Outline of a DC polarizing on a CCL21/ICAM-1-spot over 13 min. The surface of the DC is highlighted in green. (D) 2D projected surface of DCs on ICAM-1 coated glass surfaces after 1, 5, 10 and 15 min incubation with CCL21, CCL19 or BSA applied to the medium. Scale bar represents 25  $\mu\text{m}$ . Error bars represent mean  $\pm$  SEM,  $n = 25$ . Adapted from: Schumann et al., 2010.

The lack of spreading response on plated CCL19 compared to CCL21 could either be due to differential signaling properties or to a lack of surface immobilisation due to the absent charged C-terminus. When CCL21 or CCL19 were directly applied to the cell supernatant in concentrations that largely overmatch the amounts needed to trigger chemotactic migration no spreading response could be observed. Soluble CCL21 or soluble CCL19 cannot activate  $\beta 2$  integrins (Figure 25 D). To revise the hypothesis that only the presenting mode of the two CCR7 ligands induces the different cell responses CCL19 was artificially immobilized. Therefore, glass surfaces were plasma-treated. During plasma treatment the glass surface gets electrically charged to enhance the protein loading capacity. The protein loading before and after plasma treatment was analyzed by fluorescent measurements (Figure 26 A). CCL19 immobilizes on the charged surface to the same amount as CCL21 on untreated glass. Indeed, in this setup also CCL19 induced cell spreading similar to CCL21, although more transiently and with only 80% of the efficiency of CCL21. When I employed *Itgb2*<sup>-/-</sup> and *Ccr7*<sup>-/-</sup> DCs on CCL21 ICAM-1 co-coated surfaces, no spreading was observed (Figure 26 B, Movie S7). These findings indicate that the interaction between CCR7 and immobilized CCL21 or artificially immobilized CCL19, but not soluble CCR7 ligands, induces inside-out-activation of  $\beta 2$  integrins resulting in cell spreading.

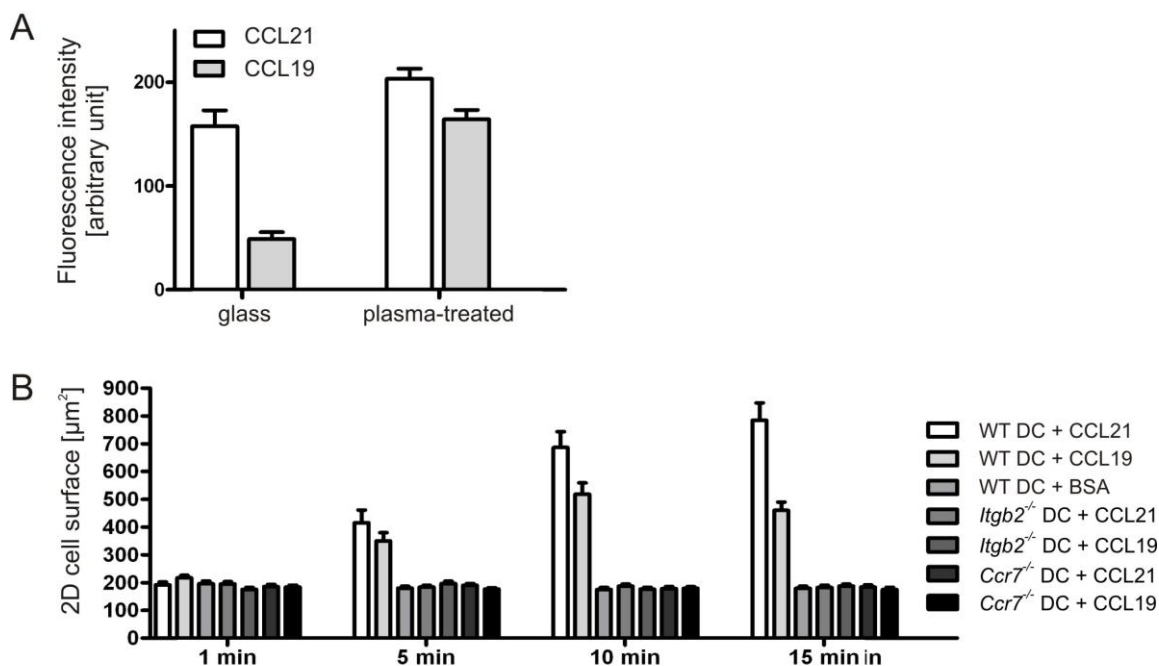


Figure 26: DCs can also spread on artificially immobilized CCL19. (A) Quantification of immobilized CCL21 or CCL19 on glass or plasma-treated glass by fluorescence staining. Error bars represent mean  $\pm$  SEM, n = 10. (B) 2D projected surface of WT, *Ccr7*<sup>-/-</sup> and *Itgb2*<sup>-/-</sup> DCs after contact with a plasma-treated and subsequently CCL21/ICAM-1, CCL19/ICAM-1 or BSA/ICAM-1 coated glass surface after 1, 5, 10 and 15 min. Error bars represent mean  $\pm$  SEM, n = 25. Adapted from: Schumann et al., 2010.

### 4.1.7 Directional steering of haptokinetic movement

It could be shown that DCs respond to immobilized CCL21 with cell spreading and random migration, whereas CCL19 or truncated, soluble CCL21 can induce directed motility. Immobilized CCL21 can thereby define a chemokine field, a haptokinetic area with sharp boundaries as shown in the “spot-assay”, or also a chemotactic track. Soluble CCR7 ligands are able to form chemotactic concentration gradients. These results raise fundamental questions. Are DCs able to sense immobilized and soluble CCR7 ligand at the same time? Can the cells integrate the different signals and respond to them together?

To test these considerations in a controlled experimental setup I established a 3D collagen gel chemotaxis assays with incorporated protein coated carbon fibers to simulate a haptokinetic scaffold. The carbon fibers with a diameter of 5  $\mu\text{m}$  were coated with ICAM-1 and CCL21, CCL19 or BSA. It was shown by Lämmermann et al. (2008) that DCs can respond to chemotactic gradients applied to collagen gels and squeeze themselves through the collagen meshwork to migrate towards the chemotactic source. In the 3D collagen gel fiber assay DCs are exposed to a chemotactic gradient and a haptokinetic migration scaffold at the same time.

First, I characterized this migration assay without an applied chemotactic gradient. DCs incorporated in collagen gels with BSA plus ICAM-1 coated carbon fibers show a random migration pattern ignoring the fibers (Figure 27 A, Movie S8). But when DCs get into contact with CCL21/ICAM-1 co-coated carbon fibers, the cells adhered to fibers and migrated up and down, frequently switching directionality (Figure 27 B, Movie S9). DIC microscopy showed adhesion and spreading on the fibers (Figure 27 C). When *p19<sup>ARF</sup>*<sup>-/-</sup> LN-fibroblasts isolated out of peripheral LNs, where they form the FRC network, were pre-incubated with CCL21 significantly more DCs adhered to the cells than without chemokine treatment (Figure 27 D). Hence, chemokine coated carbon fibers can mimic CCL21 decorated FRCs to a certain level. These results prove that CCL21 plus ICAM-1 co-coated carbon fibers provide a haptokinetic scaffold.

In the spreading assays described before surface-bound CCL21 induced inside-out activation of  $\beta 2$  integrins (Figure 26 B), which results in haptokinetic cell motility. Next I wanted to determine if the haptokinetic migration pattern on CCL21 coated carbon fibers also relies on  $\beta 2$  integrin activation. WT and *Itgb2*<sup>-/-</sup> DCs were incubated in collagen gels with incorporated CCL21/ICAM-1 co-coated carbon fibers. After 5 hr of incubation the numbers of cells attached to the fibers were determined. The result was that three times more WT than *Itgb2*<sup>-/-</sup> DCs were attached to the fibers (Figure 27 E). Thus, the haptokinetic migration on carbon fibers is again  $\beta 2$  integrin-dependent.

## Results

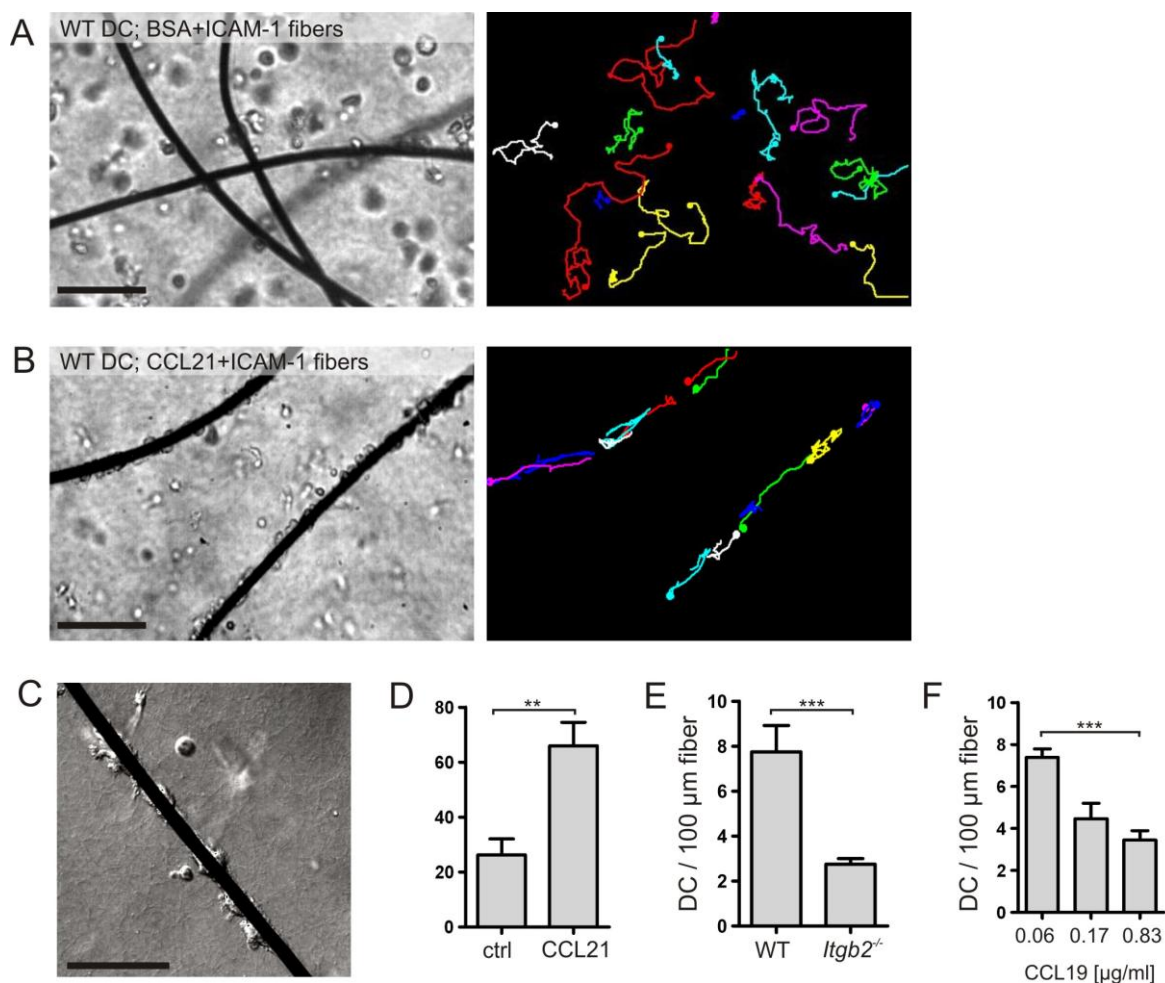


**Figure 27: CCL21 plus ICAM-1 co-coated carbon fibers act as haptokinetic scaffold. Three-dimensional collagen gel assays with incorporated protein-coated carbon microfibers. (A), (B):** Left panels: Bright-field image of the collagen gel with coated fibers. Right panels: Single cell tracking of DCs. Here, each colored track represents the pathway of a single cell. Scale bar represents 100  $\mu$ m. (A) WT DCs in the presence of BSA plus ICAM-1-coated carbon fibers. (B) WT DCs in the presence of CCL21 plus ICAM-1-coated carbon fibers. (C) Differential interference contrast image of DCs spreading on a CCL21 plus ICAM-1-coated fiber. Scale bar represents 100  $\mu$ m. (D) DC spreading on *p19<sup>ARF</sup>*-LN-fibroblasts without (ctrl) or with CCL21 pre-coating. (E) Quantification of WT and *Itgb2*<sup>-/-</sup> DCs associated with CCL21 plus ICAM-1-coated fibers after 5 hr incubation. Bars represent mean  $\pm$  SEM, n = 5. (F) Quantification of WT DCs associated with CCL21 plus ICAM-1-coated fibers after 5 hr incubation in a collagen gel with different CCL19-gradients applied. Error bars represent mean  $\pm$  SEM, n = 4. \*\*P<0.01, \*\*\*P<0.001. (A), (B), (C), (E) and (F) taken from: Schumann et al., 2010.

Next, I followed DC migration by time laps video microscopy, while the cells were exposed to CCL21 /ICAM-1 co-coated fibers and a chemotactic gradient at the same time. A soluble gradient of either CCL19 or truncated CCL21 were applied to the collagen gels containing CCL21/ICAM-1 co-coated carbon fibers. Strikingly, chemotactic gradients can steer DCs attached to the fibers. Furthermore, once cells contacted a fiber, they preferred to follow its surface even if they were distracted from the direct path. Not attached cells move freely through the gel towards the gradient (Figure 28 A, B; Movie S10, Movie S11).



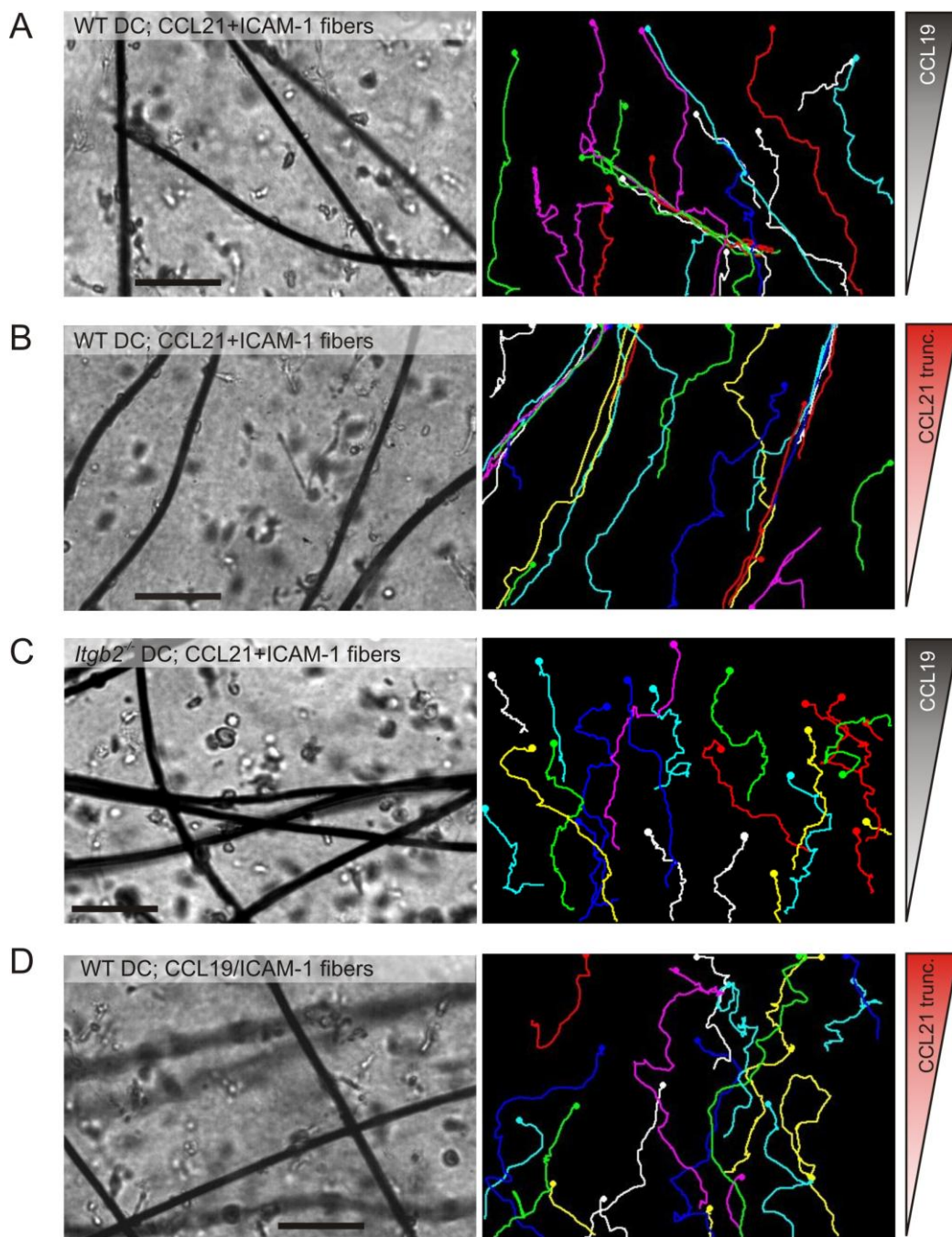


**Figure 28: Soluble chemokine steers haptokinetic migration.** Three-dimensional collagen gel assays with incorporated protein-coated carbon microfibers. (A), (B), (C), (D): Left panels: Bright-field image of the collagen gel with coated fibers. Right panels: Single cell tracking of DCs. Here, each colored track represents the pathway of a single cell. Scale bars represent 100  $\mu\text{m}$ . (A) Directionally biased DCs migration on CCL21 plus ICAM-1-coated fibers within a CCL19 gradient. DCs remote from coated fibers migrate through the collagen gel towards the CCL19 gradient. (B) WT DCs migrating with a directional bias in a collagen gel with CCL21 plus ICAM-1-coated fibers towards a gradient of truncated CCL21. (C) *Itgb2*<sup>-/-</sup> DCs migrating in a collagen gel with CCL21 plus ICAM-1-coated fibers and applied CCL19-gradient. (D) WT DCs migrating with a directional bias in a collagen gel with CCL19 plus ICAM-1-coated fibers towards a gradient of truncated CCL21. Adapted from: Schumann et al., 2010.

Occasionally DCs detached from the fibers and followed exclusively the soluble gradient. To further analyze if strong chemotactic gradients can counteract the haptokinetic scaffold CCL19 gradients of different steepness were applied to the described fiber assay and after 5 hr the number of cells attached to the chemokine coated fibers determined. With increasing amounts of CCL19, fewer WT DCs remained attached to the fibers (Figure 27 F). Soluble CCL19 gradients can counteract the haptokinetic CCL21 interface. These results suggest that the adhesive and the chemotactic signals compete with each other. *Itgb2*<sup>-/-</sup> DCs applied to the same assay showed in accordance with previous results no interaction with the fibers but moved with unimpaired speed and directionality within the gels (Figure 28 C; Movie S12). As a further control carbon fibers were coated with CCL19 plus ICAM-1 and combined with a gradient of truncated CCL21. In this case DCs followed strictly the soluble gradient of truncated CCL21 ignoring the fibers (Figure 28 D; Movie S13). The fiber-bound CCL21 induces inside-out activation of  $\beta$ 2 integrin which induces cell adherence to the fibers. CCL19 cannot provide a haptokinetic scaffold. These results showed that DCs can respond to a CCL21 field haptokinetically via CCR7 while simultaneously using another fraction of CCR7 to sense a soluble gradient that then introduces a directional bias.

## 4.2 Adaptive force transmission in amoeboid cell migration

The project “Adaptive force transmission in amoeboid cell migration” was carried out in cooperation with a master student in the lab, Jörg Renkawitz (Renkawitz et al., 2009). The aim of the project was to analyze how DCs can migrate in three-dimensional interstitium without transmitting traction forces by integrin transmembrane receptors to the environment (Lämmermann et al., 2008). This analysis can potentially also explain how DCs can overcome *chemotactically biased haptokinesis* and follow exclusively a chemotactic gradient.

For this purpose the under-agarose assay (UAA) was combined with TIRF microscopy, which allows the visualization of a 200nm thick layer close to the surface. The UAA generates a pseudo three-dimensional setting: The cells are squeezed between the bottom of a cell culture dish and an agarose-layer without altering the integrin-independency of migration. The cells were filmed while they chemotaxed towards a CCL19 gradient (Figure 29). The cortical actin-cytoskeleton was visualized with the probe Lifeact-GFP. Lifeact-GFP is a 17 amino acid peptide, which stains filamentous, assembled actin structures in living cells without interfering with actin treadmilling (Riedl et al., 2008; Riedl et al., 2009).

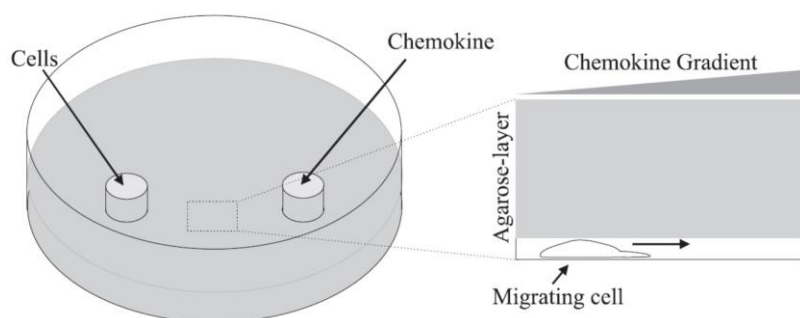


**Figure 29: Scheme of the under-agarose assay to analyze the actin cortex. Cells were squeezed between the bottom of a cell culture dish and an agarose-medium layer generating a confined pseudo three-dimensional environment. Cells were filled into a hole punched into the agarose layer or in the majority of the cases directly injected under the agarose. The chemokine CCL19 was filled into a second hole to establish a chemotactic concentration gradient (taken from: Renkawitz et al., 2009).**

### 4.2.1 Retrograde actin flow in WT and *Itg*<sup>-/-</sup> DCs

First, the described set-up was tested with WT DCs. The cells squeezed under the agarose formed a broad lamellipodium with diffusely distributed actin. In the trailing edge thicker actin bundles were detected (Figure 30 A; Movie S14). The central axis of the chemotaxing DCs was kymographic analyzed. The Kymograph demonstrated that the actin cortex mostly remained stationary. At the trailing edge actin started to move forward in relation to the substrate (Figure 30 A). In 50% of the examined WT DCs retrograde actin flow from the



lamellipodium into the cell center was measured. The retrograde actin flow was limited to the first 2 to 4  $\mu\text{m}$  of the lamellipodium. The maximum retrograde flow velocity in the 33 analyzed WT DCs was 4.7  $\mu\text{m}/\text{min}$ ; the mean retrograde flow velocity amount to 1.23  $\mu\text{m}/\text{min}$  ( $\pm 1.48$  standard derivation (STDV); Figure 30 C). The fact that almost no retrograde flow in WT DCs can be observed indicates force coupling to the substrate (median: 0  $\mu\text{m}/\text{min}$ ; Figure 30 C).

To test if force coupling is facilitated via integrin transmembrane receptors complete integrin knockout (*Itg*<sup>-/-</sup>) DCs were applied to this assay. In these cells all possible leukocyte integrin heterodimers are deleted by the knockout of the  $\beta 1$ ,  $\beta 2$ ,  $\beta 7$  and  $\alpha v$  subunits. In *Itg*<sup>-/-</sup> DCs the molecular clutch is genetically uncoupled. Surprisingly, no shape changes could be observed in *Itg*<sup>-/-</sup> DCs migrating under the agarose layer (Figure 30 B; Movie S15). Besides that, the cell reached the same migration speed compared to WT DCs while migrating towards CCL19 (Figure 30 D; Renkawitz et al., 2009). These results are consistent with previous results that in confined three-dimensional environments integrin-mediated force coupling is dispensable for cell movement (Lämmermann et al., 2008). Unimpaired protrusion speed and loss of adhesions seems to be contradictory. But the kymographic analysis of the actin cortex revealed a massive retrograde flow in *Itg*<sup>-/-</sup> DCs with an average actin flow velocity of 10.65  $\mu\text{m}/\text{min}$  ( $\pm 3.9$  STDV) and a maximum at 19.8  $\mu\text{m}/\text{min}$  (Figure 30 B, C). The uncoupling of the molecular clutch led to massive retrograde flow, which penetrated deeply into the cell center and stopped at in front of the trailing edge.

Normal cell shape, unaltered cell migration speed and increased retrograde actin flow indicated that the actin polymerization rate was enhanced in the absence of integrins. Indeed, the actin polymerization rate, the sum of protrusion and retrograde flow velocities, increased from a mean value of 9.1  $\mu\text{m}/\text{min}$  ( $\pm 0.7$  STDV) in WT DCs to 17.8  $\mu\text{m}/\text{min}$  ( $\pm 0.7$  STDV) in *Itg*<sup>-/-</sup> DCs (Figure 30 E). The myosin II dependent contractility in these cells was not altered, thus an increase in contractility was not the explanation for enhanced retrograde actin flow (Renkawitz et al., 2009). DCs seem to compensate the loss of adhesive interaction and of traction force transmission by higher actin dynamics in the leading edge. Hence, for DCs locomotion engagement of a molecular clutch is optional but not mandatory.

Both protrusion speed and retrograde actin flow differed widely among the analyzed WT or *Itg*<sup>-/-</sup> DCs, respectively (Figure 30 B). By looking at individual DCs it became obvious that fast protruding leading edges do not necessarily possess any retrograde actin flow. In growth cones and keratocytes the protrusions speed is inversely correlated to retrograde flow (Medeiros et al., 2006; Valloton et al., 2006). By plotting protrusion speeds against retrograde actin flow velocities of WT as well as *Itg*<sup>-/-</sup> DCs, no correlation between retrograde actin flow and protrusion speed could be detected (Figure 30 F).

## Results

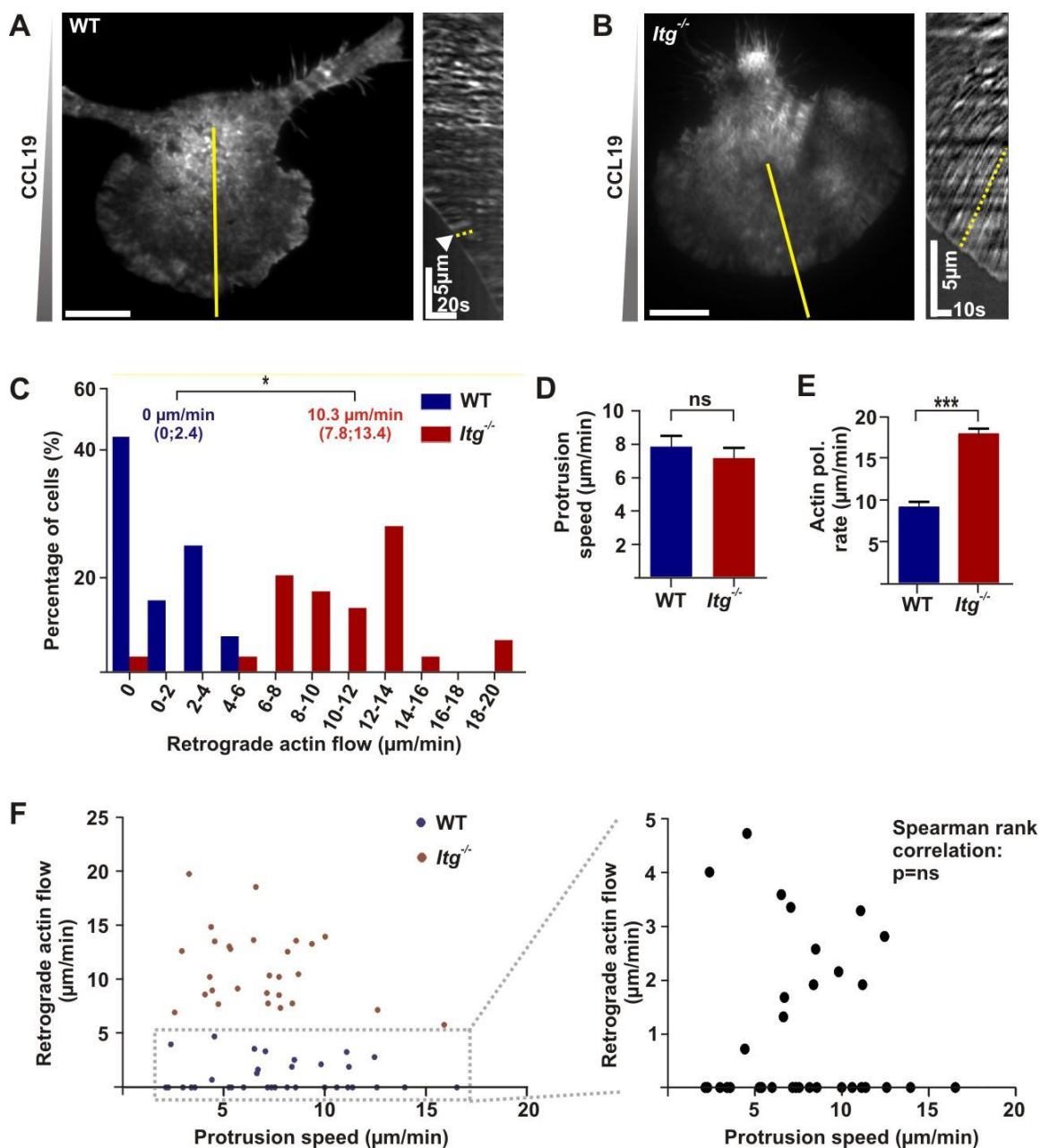


**Figure 30: Actin dynamics in WT and *Itg*<sup>-/-</sup> DCs migrating on a glass slide towards a CCL19 gradient. (A)** Left panel: TIRF image of a migrating Lifeact-GFP-transfected DC. Scale bar represents 10  $\mu\text{m}$ . Right panel: Kymograph of the yellow line in the left panel of A. The retrograde actin flow is highlighted with a dashed yellow line and an arrowhead. (B) Left panel: TIRF image of a migrating *Itg*<sup>-/-</sup> DC transfected with Lifeact-GFP. Scale bar: 10  $\mu\text{m}$ . Right panel: Kymographic analysis of the yellow line in (B) left panel. The retrograde flow is highlighted with a dashed yellow line. (C) Quantification of retrograde flow velocities in WT ( $n_{\text{WT}} = 33$ ) and *Itg*<sup>-/-</sup> DCs ( $n_{\text{Itg}^{-/-}} = 29$ ). Numbers represent median values with 25th and 75th percentiles in brackets. \* $P < 0.05$ . (D) Protrusion speed of WT ( $n_{\text{WT}} = 33$ ) and *Itg*<sup>-/-</sup> DCs ( $n_{\text{Itg}^{-/-}} = 29$ ). Error bars represent mean  $\pm$  SEM. ns, not significant. (E) Actin polymerization rates in WT ( $n_{\text{WT}} = 33$ ) and *Itg*<sup>-/-</sup> DCs ( $n_{\text{Itg}^{-/-}} = 29$ ). (F) Left: Retrograde actin flow in WT and *Itg*<sup>-/-</sup> DCs plotted against the protrusion speed. Right: Close-up of WT DCs from boxed region. Error bars represent mean  $\pm$  SEM. \*\*\* $P < 0.001$  (taken from: Renkawitz et al., 2009).

### 4.2.2 Flexible actin polymerization in the molecular clutch system

The previous results strongly implicate that disengagement of force coupling results in enhanced retrograde actin flow. But in principle the enhanced retrograde actin flow could be the result of altered biochemical properties in *Itg*<sup>-/-</sup> DCs like an enhanced actin nucleation for example, instead of the disconnection of the molecular clutch by the loss of integrins. To exclude this possibility the molecular clutch system was disengaged at the extracellular side. The integrin-ligand interaction was inhibited by cell migration on glass passivated with polyethylenglycol (PEG), an inert substrate.

On PEG migrating WT DCs displayed the same shape and protrusion velocities as on glass, but the retrograde actin flow was increased (Figure 31 A; Movie S16). The mean retrograde flow velocity increased from 1.23  $\mu\text{m}/\text{min}$  ( $\pm 1.48$  STDV) to 4.45  $\mu\text{m}/\text{min}$  ( $\pm 2.56$  STDV). Also here, the actin cortex slid back up till it stopped in front of the trailing edge (Figure 31 A, B). Even though the molecular clutch was blocked in another position the cells still exhibited enhanced retrograde flow. When *Itg*<sup>-/-</sup> DCs were placed on PEG, retrograde actin flow velocities were comparable to *Itg*<sup>-/-</sup> DCs migrating on uncoated glass (Figure 31 C). The retrograde actin flow velocities could not be further enhanced by placing *Itg*<sup>-/-</sup> DCs on inert PEG-substrate. This result indicated that no other force-coupling receptors had an effect in the used experimental setup. The comparison of WT and *Itg*<sup>-/-</sup> DCs demonstrated that the retrograde actin flow was less pronounced in WT DCs migrating on PEG, than in *Itg*<sup>-/-</sup> DCs chemotaxing on glass or the inert substrate.

These results showed that the molecular clutch system is of central importance for the cortical actin dynamics in migrating DCs. After disconnecting the molecular clutch at different positions and thereby enhancing retrograde flow, I tried to heighten the efficiency of the molecular clutch to see if the retrograde actin flow decreases under these conditions. In the first part of my thesis I showed that immobilized CCL21 leads to inside-out-activation of  $\beta 2$  integrins, which results in DC spreading followed by rapid, random cell migration (Figure 25 C). Thus, I analyzed the retrograde actin flow velocities in WT and *Itg*<sup>-/-</sup> DCs migrating on CCL21/ICAM-1 co-coated glass slides towards a CCL19 gradient. Surprisingly, retrograde actin flow velocities in WT DCs migrating on CCL21/ICAM-1 were enhanced in comparison to migration of WT DCs on uncoated glass (Figure 31 B). Whereas in *Itg*<sup>-/-</sup> DCs migrating on CCL21/ICAM-1 the retrograde actin flow velocities were significantly reduced compared to *Itg*<sup>-/-</sup> DCs migrating on glass (Figure 31 C).

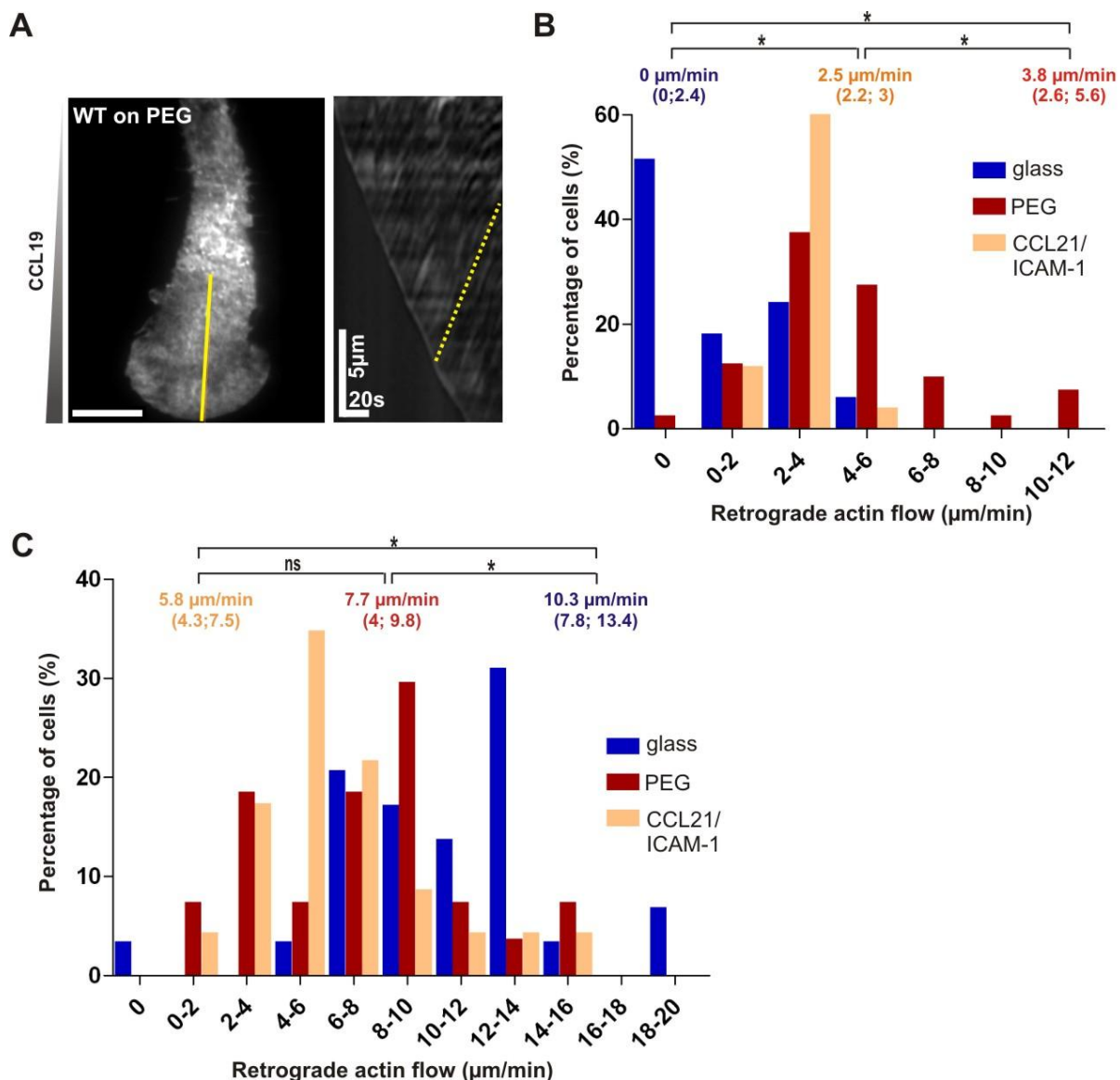


Figure 31: Variable actin polymerization rate in the molecular clutch system. (A) Left panel: TIRF image of a with Lifeact-GFP- transfected WT DC migrating on polyethylene glycol (PEG). Scale bar represents 10 µm. Right panel: Kymograph of the yellow line in the left panel of A. The retrograde actin flow is highlighted with a dashed yellow line. (B), (C) Quantitative analysis of WT DCs (B;  $n_{\text{glass}} = 33$ ,  $n_{\text{PEG}} = 40$ ,  $n_{\text{CCL21}} = 25$ ) or *Itg*<sup>-/-</sup> DCs (C;  $n_{\text{glass}} = 29$ ,  $n_{\text{PEG}} = 27$ ,  $n_{\text{CCL21}} = 23$ ) migrating on glass, PEG and with CCL21 and ICAM-1 co-coated glass, respectively. Numbers represent median values with 25th and 75th percentiles in brackets. Ns: not significant. \* $P < 0.05$  ((A) taken from; (B), (C) partly adapted from: Renkawitz et al., 2009).

#### 4.2.3 Adhesive interaction with CCL21/ICAM-1

Because of the surprising alterations in retrograde flow velocities in DCs performing chemotactically biased haptokinesis on CCL21/ICAM-1 co-coated glass slides, I decided to analyze more closely adhesive interactions of chemotaxing DCs with different migration substrates. To this end WT DCs were transfected with vinculin-GFP, which accumulates in

## Results

adhesion sites (Brown et al., 2006), and applied to the already described under-agarose migration assays.

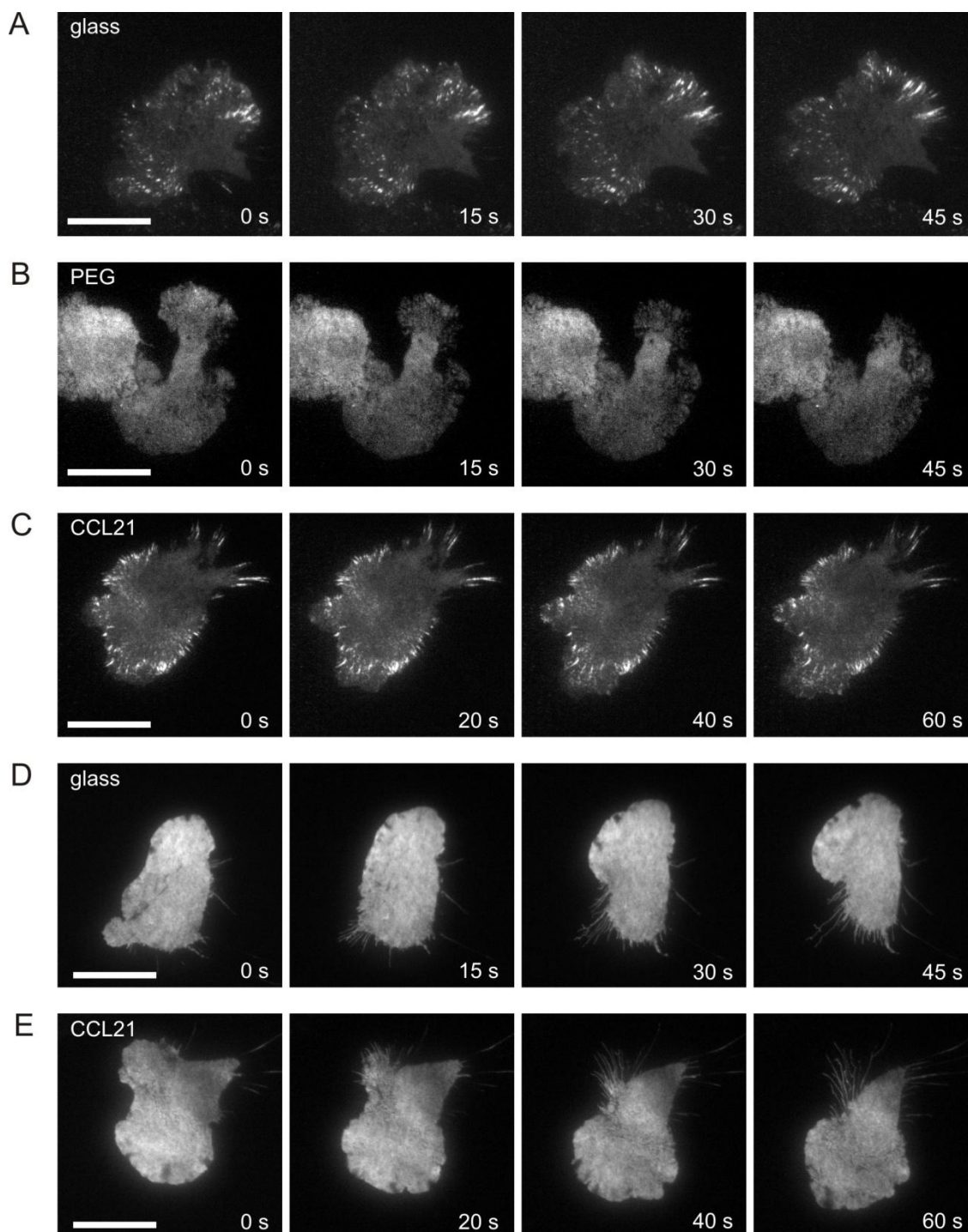


**Figure 32: DCs migrating on uncoated, CCL21/ ICAM-1 co-coated or PEG-passivated glass slides toward a CCL19 gradient. Scale bars represent 10  $\mu$ M. (A), (B), (C): DC transfected with vinculin-GFP migrating on glass, PEG or CCL21/ICAM-1 co-coated glass slides. In DCs migrating on glass and CCL21-coated glass vinculin-GFP accumulates in little spots in the leading edge and in longer stripes in the trailing edge. In DCs migrating on inert PEG vinculin-GFP shows a homogenous distribution. (D), (E):**

## Results

---

**Distribution of CCR7-GFP in DCs migrating on glass or CCL21. In both cases the chemokine receptor is homogeneously distributed over the whole cell body.**

In with vinculin-GFP transfected DCs migrating on glass little GFP-spots in the leading edge and longer stripes in areas of retraction could be observed (Figure 32 A). The spots were located approximately 2  $\mu\text{m}$  behind the front of the lamellipodium. This result further proved active force coupling in migrating DCs. As a negative control the migration of vinculin-GFP<sup>+</sup> DCs on PEG was analyzed. As expected no vinculin-GFP accumulations, only a diffuse staining of the whole cell could be detected (Figure 32 B). The vinculin spots are therefore no artificial protein accumulations; they indeed represent adhesion sites. In DCs migrating on CCL21/ICAM-1 co-coated glass no alterations in the localization, form or velocity of with vinculin-GFP marked adhesion sites in comparison to migration on uncoated glass could be observed (Figure 32 C).

Possibly also 'non classical' adhesive interactions exist in DCs migrating on immobilized chemokines. In this case the chemokine receptor CCR7 interacts with surface-bound CCL21 which can also be interpreted as a weak adhesive interaction. I examined the distribution of the chemokine receptor CCR7 in towards a CCL19 gradient chemotaxing DCs on untreated or on CCL21/ICAM-1 co-coated glass. In contrast to previous observations in T cells (Nieto et al., 1997; Gérard et al. 2007; Morley et al., 2010) in DCs migrating under agarose towards a CCL19 gradient no CCR7 accumulation in the lamellipodium could be observed. Instead small, fast flickering CCR7 spots were homogeneously distributed over the whole cell cortex (Figure 32 D). On CCL21/ICAM-1 co-coated glass no alterations in the CCR7 distribution could be observed in comparison to migration on uncoated glass (Figure 32 E).

### 4.2.4 Macrophages also adapt their actin polymerization rate

To test if only DCs can adapt their actin polymerization rate or if other cell types have similar capacities, I employed macrophages to the described under-agarose assays. Macrophages are amoeboid, haematopoietic cells, which can migrate, but most of the times remain stationary. Here, non-migratory cells, which were not exposed to a chemotactic gradient, were analyzed.

On glass as well on PEG the macrophages showed the same morphology: The cells were roundish with short protrusions. Also the diameter of the macrophages on the inert substrate was not altered. Kymographic analysis of the small protrusions in the two conditions displayed a similar behaviour as in DCs. Macrophages placed on glass exhibited no or only very low retrograde flow velocity (average retrograde flow velocity: 0.24  $\mu\text{m}/\text{min}$  ( $\pm$  0.42 STDV; median retrograde flow velocity: 0  $\mu\text{m}/\text{min}$ ; Figure 33 A, B). Macrophages on inert PEG substrate had an average retrograde flow velocity of 1.09  $\mu\text{m}/\text{min}$  ( $\pm$  0.45 STDV) and a significantly higher actin polymerization rate (Figure 33 C, D). The adaption of actin



## Results

dynamics to the adhesiveness of the surrounding is therefore not DC-specific, but of broader relevance.

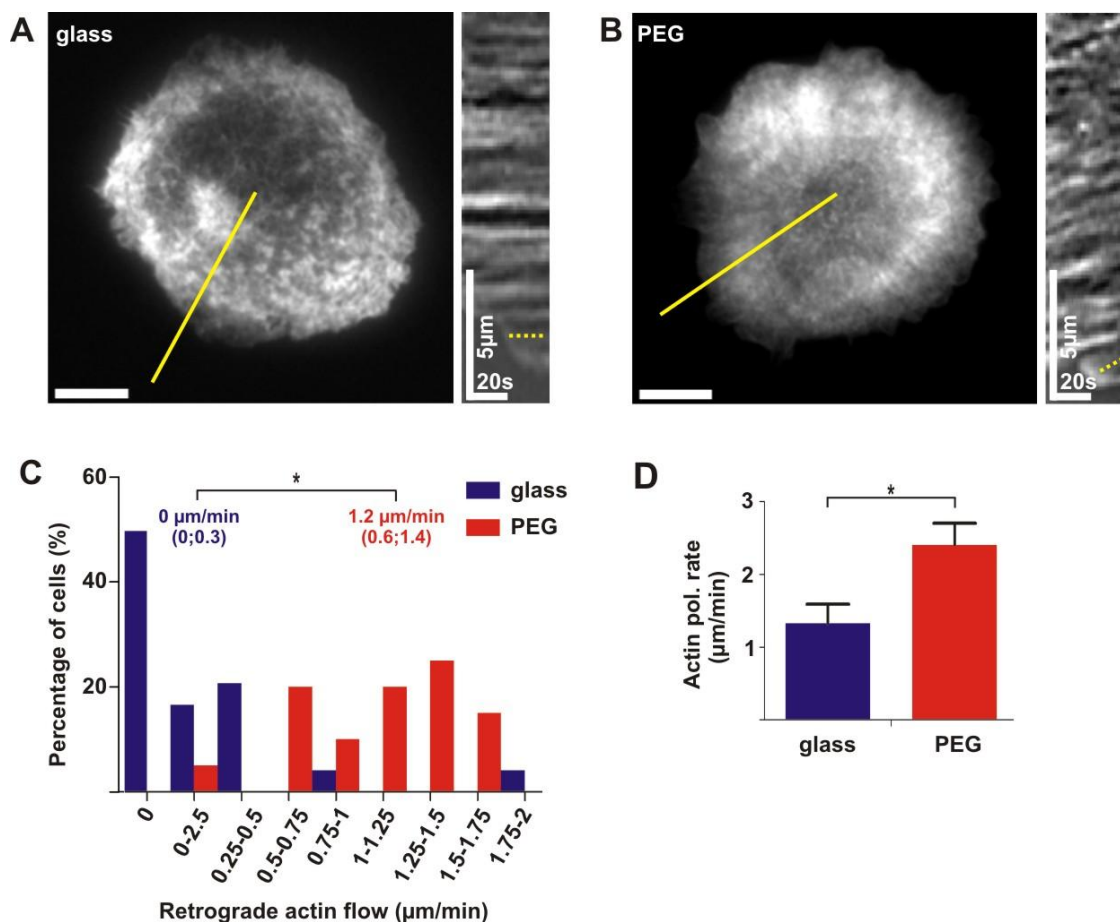


**Figure 33: Actin polymerization rates in macrophages on uncoated or PEG-coated glass surfaces.** Lifeact-GFP macrophages were applied to under-agarose assays. (A) Left panel: Lifeact-GFP macrophage on serum-coated glass surface. Scale bar: 5  $\mu\text{m}$ . Right panel: Kymographic analysis of the yellow line in (A), left panel. The actin flow is marked with a yellow dashed line. (B) Left panel: Lifeact-GFP macrophage on PEG-coated glass slide. Scale bar: 5  $\mu\text{m}$ . Right panel: Kymographic analysis of the yellow line in (B), left panel. The retrograde actin flow is highlighted with a yellow dashed line. (C) Quantification of actin flow velocities in macrophages on glass ( $n_{\text{glass}} = 23$ ) and on PEG ( $n_{\text{PEG}} = 19$ ). Numbers in brackets represent median, 25% and 75% percentile. (D) Actin polymerization rates of macrophages on serum or PEG slides. Error bars represent mean  $\pm$  SEM. \* $P < 0.05$  (taken from: Renkawitz et al., 2009).

### 4.2.5 Substrate-independent chemotactic DC migration

The previous results indicate a rapid adaption of the actin cytoskeleton to the adhesive properties of the environment in DCs. To test this assumption patterned surfaces were used where inert PEG areas alternated with adhesive glass tracks, which were coated with FCS

## Results

and red fluorescent BSA. When DCs were exposed to these surfaces, they migrated towards the CCL19 source without preferences for one of these surfaces (Figure 34 A). While DCs crossed an adhesive stripe no change in velocity or cell morphology could be observed (Figure 34 B; Renkawitz et al. 2009). Only transient retraction fibers formed at the trailing edge while leaving adhesive zones (Figure 34 B). While DCs crossed adhesive stripes the retrograde actin flow velocities adapted to the changed adhesive properties of the surfaces. Within one cell the retrograde flow was enhanced in the parts of the cell which were in contact with the PEG surface in contrast to protrusions expanding on serum-coated glass (Figure 34 C). The leading edge protrudes regardless if the molecular clutch is active or not.

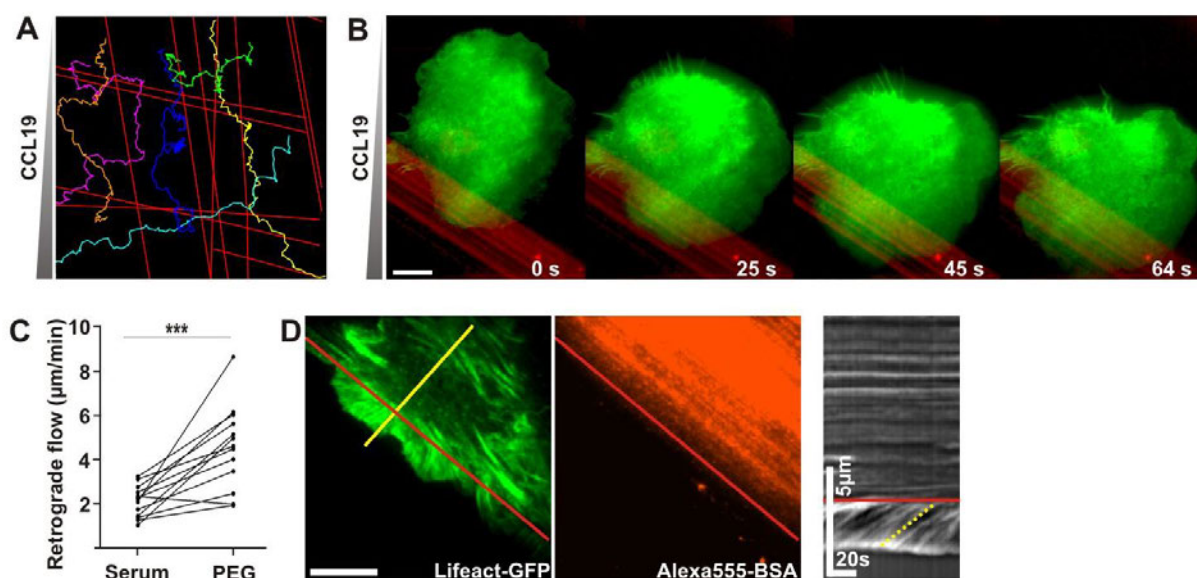


**Figure 34: Chemotactic movement of DCs is substrate-independent.** (A) Single cell tracking of DCs migrating in an under-agarose assay towards CCL19 on inert PEG-substrate (black) and adhesive tracks highlighted with fluorescent BSA (Alexa-555 BSA, red). (B) Lifact-GFP DC migrating over an adhesive track in the assay described in (A). Scale bar: 10 μm. (C) Retrograde actin flow velocities in Lifact-GFP DCs simultaneously migrating on Alexa-555 BSA/serum and PEG-coated glass surface. \*\*\*P<0.001 (D) Left panel: Lifact-GFP 3T3 fibroblast applied to the assay described in (A). Scale bar: 5 μm. Red lines mark the boarder of the Alexa-555 BSA/serum-coated track as shown in the panel in the middle. Right panel: Kymographic analysis of the yellow line in the left panel. The retrograde actin flow is marked with a dashed yellow line (taken from: Renkawitz et al., 2009).

As shown before macrophages have the same intrinsic property to adjust their actin cytoskeleton to the substrate adhesiveness. But is this a special feature of hematopoietic cells or is it a universal mechanism of the cytoskeleton and can for example also be applied to mesenchymal cells? Therefore, Lifact-GFP expressing fibroblasts were exerted to the described patterned surfaces. Fibroblasts strictly adapted their shape to the adhesive, BSA-coated stripes. On the border between inert and adhesive substrate the fibroblast generated small, 2-3 μm long protrusions on the PEG (Figure 34 D; Movie S17). Kymographs revealed



## Results

---

massive retrograde flow in these protrusions. The retrograde actin flow exactly stopped at the border to the adhesive track (Figure 34 D). The ability to locally adapt is therefore a general intrinsic property of the cytoskeleton. But only amoeboid cells like DCs can increase their actin polymerization rate to an amount that allows the compensation of the loss of adhesive interaction.

## 5 Discussion

### 5.1 Chemotactically biased haptokinesis

Chemokines can be bound to GAGs or distribute as soluble molecules; they can be homogeneously distributed or form a gradient. Depending on their presentation mode chemokines can cause random (kinetic), directed (tactic) or adhesive (haptic) cell migration. Here, I exemplified how the presenting mode of the chemokines CCL19 and CCL21 can influence DC migration. CCL19 and CCL21 are expressed in the T cell areas of SLOs and guide naive T cells and mature DCs, which both express the corresponding chemokine receptor CCR7 to draining LNs. As such CCR7 and its ligands are responsible for the establishment of T cell areas in lymphoid organs. The main difference between the two CCR7 ligands is that CCL21 can immobilize to anionic surfaces via its highly charged C-terminal extension, whereas CCL19 is lacking this C-terminal tail and remains soluble.

In mature DCs surface-bound CCL21 or artificially immobilized CCL19 induce both inside-out activation of  $\beta 2$  integrins and cytoskeletal polarization, which results in random, haptokinetic migration (Figure 35 C). Soluble CCL19 cannot activate integrins, but leads to cytoskeletal polarization. As a consequence CCL19 concentration gradients induce directional, chemotactic cell migration. By proteolytically truncating the heparan sulfate binding residue of CCL21 DCs generate a soluble variant of CCL21 that functionally resembles CCL19 (Figure 35 A). This proteolytic cleavage creates a positive feedback phenomenon which leads to the recruitment of further cells from the periphery to the place where the truncated CCL21 is released. The result is a self-perpetuating wave of collective migration. DCs can furthermore sense immobilized and soluble CCR7 ligands at the same time and integrate these different signals. Using the terminology introduced above I call the resulting phenomenon “haptokinesis directionally biased by a chemotactic gradient”: CCL21 defines a track and CCL19 or truncated CCL21 direct the cells on the track. (Figure 35 B). Adhesive random migration and directional steering could cooperate to produce dynamic but spatially restricted cell migration patterns which closely resemble cellular dynamics observed in SLOs by intravital microscopy.

For the analysis I used reductionistic *in vitro* approaches because only they allow a detailed, controlled dissection of the different cell behaviours. I will discuss here if the resulting model of ‘chemotactically biased haptokinesis’ can also be applied to *in vivo* motility patterns of leukocytes.

### 5.1.1 CCL19 and CCL21 are functionally not redundant

*CCR7*<sup>-/-</sup> and *plt/plt* mice, which lack the expression of CCL19 and CCL21 in SLOs, exhibit to a large extent the same phenotype: SLOs with rudimentary T cell areas which lack a clear border to the B cell follicles (Förster et al., 1999; Davalos-Miszlitz & Rot, 2008; Miszlitz et al., 2004; Nakano et al., 1997; Nakano et al., 1998). These results implicate that CCR7 has only two ligands, CCL19 and CCL21, and suggest that these two chemokines, which have both similar binding affinities towards CCR7 and similar expression patterns in the LN, act redundantly. However, in my thesis I provide evidences suggesting that CCL19 and CCL21 exhibit non-overlapping functions, and that these non-overlapping functions are mainly determined by their presenting mode.

For each chemokine a dynamic equilibrium between soluble and immobilized molecules exists. In the case of CCL21 the dominating form is the immobilized chemokine, because of its highly charged C-terminus which mediates linkage to GAGs. For CCL21 diverse immobilizing substrates are published like for example heparan sulfates or the proteoglycan podoplanin expressed on FRCs (Breiteneder-Geleff et al., 1999; Kriehuber et al., 2001; Pegu et al., 2007). The immobilization of CCL21 is the basic prerequisite that CCL21 can form homogenous chemokine fields with sharp boundaries. Moreover, immobilized CCL21 leads to  $\beta 2$  integrin inside-out activation and, therefore, to cell spreading and adhesion. Homogenous CCL21 fields lead furthermore to spontaneous cell polarization followed by rapid, random migration. CCL19 lacks a highly charged C-terminal tail and has therefore only a low affinity towards GAGs - CCL19 remains primarily soluble (Patel et al., 2001). Soluble CCL19 cannot activate integrins but is very efficient in concentration gradient formation and therefore in directing DCs. *In vitro* experiments proved that CCL19 is ten times more potent than CCL21 in inducing directional migration in DCs (Ricart et al., 2010). Additionally, Bao et al. (2010) showed that the binding capacity of CCL19 to lymphatic endothelial cells is about half of that of CCL21. The binding affinities of the two CCR7 ligands towards FRCs, the stromal network in the T cell area, are not determined yet. The fact that it is possible to immunostain CCL21 but not CCL19 on LN cryosections implies that the binding affinities towards FRCs resemble the one described for lymphatic endothelium. Besides that FRCs express GAGs which most likely mediate CCL21 binding, but do not, or to a smaller extent, influence CCL19 molecules (Breiteneder-Geleff et al., 1999; Kriehuber et al., 2001; Pegu et al., 2007; Patel et al., 2001).

By interfering with the presenting mode of CCL19 and CCL21 one chemokine can gain the functions of the other one. C-terminally truncated, solubilised CCL21 is able to generate concentration gradients in under-agarose as well as in carbon fiber migration assays. DCs are able to interpret these concentration gradients and respond with directional movement. Truncated CCL21 functionally resembles CCL19. Ueno et al. (2002) described a similar situation in *ex vivo* experiments: CCL21 is less efficient in organizing T cells egress from explanted thymus slices in comparison to CCL19. But when the C-terminus of CCL21 was removed, the chemokine gained the function of CCL19 and promoted T cell egress at the same rate.

## Discussion

CCL19 can be artificially surface-bound on plasma-treated, highly charged glass surfaces. In this experimental setup CCL19 immobilized approximately to the same level as CCL21 on untreated glass as shown by fluorescence measurements. Artificially immobilized CCL19 acted like full-length CCL21: It induced cells spreading facilitated via  $\beta 2$  integrin inside-out activation which is followed by rapid, random migration. But the spreading response was more transient in comparison to CCL21. One possible explanation for this observation could be that the mechanical anchorage of CCL19 is less stable and the cells still internalize a certain amount of chemokine. These results implicate that leukocyte behaviour is determined by the presenting mode of the two CCR7 ligands, not by special signaling sequences or differences in the tertiary structure of the molecules.

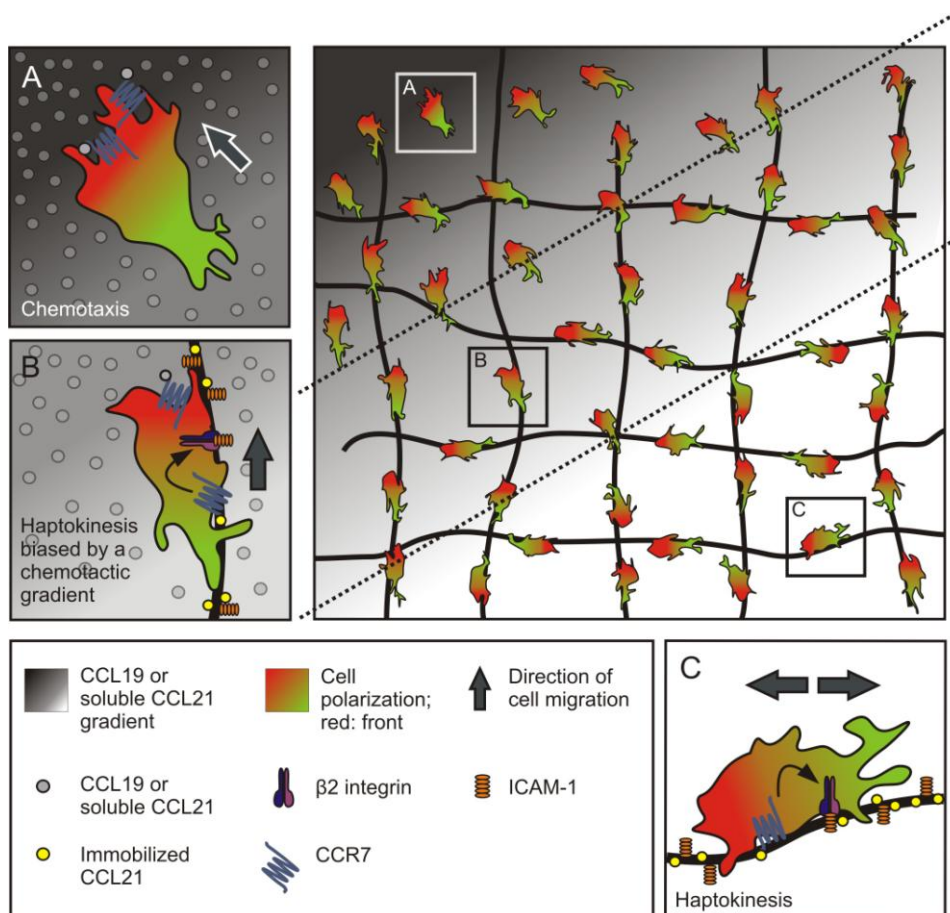


**Figure 35: Schematic representation of chemotactically biased haptokinesis.** The scaffold in the big panel represents the fibroblastic reticular cell network of secondary lymphoid organs. The scaffold is decorated with the integrin ligand ICAM-1 and immobilized CCL21. The soluble chemokine gradient (grey; either CCL19 or solubilized CCL21) establishes three principle motility patterns that are depicted in panels A-C. (A) Steep gradients of soluble CCR7 ligand lead to detachment of the DCs from the haptokinetic scaffold and integrin-independent migration along the gradient. (B) Shallow gradients induce directionally biased haptokinesis. Here, immobilized CCL21 induces inside-out activation of  $\beta 2$  integrins that confine the cells to the scaffold while soluble CCR7 ligand induces the directional bias. (C) In the absence of soluble CCR7 ligands, cells perform haptokinetic random migration that is strictly confined to the fiber scaffold (taken from: Schumann et al., 2010).

Until now it is unclear which signaling events induce the different cell behaviours after contact with soluble or surface bound chemokine, respectively. One promising hint is that in contrast to CCL21 CCL19 is very efficiently internalized by DCs. CCL19 internalization likely enables the cells to adapt to high CCL19 concentrations (Otero, Groettrup & Legler, 2006; Byers et al., 2008; Sierra et al., 2010). Possibly, the lack of CCL21 internalization is due to the mechanical anchorage to surfaces. These differences potentially lead to the different signaling properties of the CCR7 ligands: CCL21 is longer bound to the chemokine receptor and not internalized, whereas CCL19 is rapidly endocytosed and degraded (Otero, Groettrup & Legler, 2006; Byers et al., 2008), which leads to cell spreading or directed migration, respectively.

DCs can establish a positive feedback loop when they migrate on LN cryosections or immobilized recombinant CCL21: After several minutes DCs from the adjacent environment migrate in a highly synchronized way towards these migration substrates and accumulate there. The cells achieve this by actively manipulating the balance between soluble and bound CCL21. DCs proteolytically remove the heparan sulfate binding C-terminus of CCL21, transform CCL21 in an easily diffusible molecule and thereby establish a chemotactic concentration gradient. *In vitro*, two CCL21 fragments only slightly differing in size could be detected after incubation with DCs. Fragmented CCL21 could also be isolated out of LN lysates by pull-down experiments. I also analyzed the amount of cleaved CCL21 in inflamed LNs, which contained a high amount of mature DCs. Surprisingly, under inflammatory conditions the amount of solubilised CCL21 in LNs is lower, maybe because in reactive LNs the lymph flow is enhanced (von Andrian & Mempel, 2003) and fragmented CCL21 rapidly washed away.

How the processing of CCL21 influences DC migration *in vivo* is not analyzed yet. However, there are several *in vivo* observations described, which could potentially be explained by the chemokine cleavage. Martin-Fontecha et al. (2003) described a DC migration pattern under inflammatory conditions called 'LN conditioning': When a first cluster of DCs enters the LN, these cells "prime" the tissue for following DCs. These following cells arrive faster in the draining LN and in higher numbers. The reason for the collective movement could be the proteolytic shedding of CCL21 bound on FRCs by the first wave of DCs entering the LN. The DCs could thereby generate a stronger chemotactic gradient to recruit further cells, DCs and also naïve T cells, and accelerate adaptive immune response.

Another interesting study demonstrated that in inflamed LNs the borders between T and B cell areas become blurred (Okada et al., 2005). Potentially immigrating DCs cut off CCL21 bound to FRCs and reduce the amount of the homeostatic chemokine in the T cell area. The alterations in lymphatic organ architecture in *CCR7<sup>-/-</sup>* and *plt/plt* mice together with the fact that *CCL19<sup>-/-</sup>* mice have no obvious phenotype implicate that immobilized CCL21 is a prerequisite for the establishment for T cell areas with sharp boundaries in SLOs (Förster, Davalos-Misnitz & Rot, 2008; Britschgi et al., 2010). By reducing the amount of immobilized CCL21 the cells could optionally give rise to indistinct T cell area boundaries.

Furthermore, it was shown that stroma cells of reactive LNs down regulate the transcription of homeostatic chemokines, probably to regulate the overall cellularity in the organ (Mueller et al., 2007). Shedding of CCL21 might act in the same way and also limit the amount of leukocytes by reducing the amount of CCL21 bound to FRCs in the T cell area. Thereby the retention time of leukocytes in the LN could potentially be decreased. This mechanism could act before the transcriptional down-regulation of CCL21 is in effect. I detected truncated CCL21 in non-inflamed LNs, which could optionally explain why *CCL19*<sup>-/-</sup> mice have no gross abnormalities in DC maturation and migration (Link et al., 2007; Britschgi et al., 2010): Fragmented CCL21 resembles CCL19 and can therefore probably compensate the loss of CCL19 *in vivo*.

### 5.1.2 CCL21 is cleaved by serine proteases

To further characterize the CCL21 cleavage I conducted *in vitro* cleavage assays. The first important result was that the CCL21 cleavage can be blocked completely by the serine protease inhibitor Aprotinin. Moreover, DC mediated *in vitro* cleavage of CCL21 strictly depends on the presence of blood serum or plasma, whereas the cleavage was much more efficient in the presence of not heat-inactivated mouse plasma than in the presence of FCS. Blood plasma is the solvent, cell-free fraction of whole blood, whereas blood serum is plasma after blood clotting and removal of the fibrinogen. In the presence of mouse plasma CCL21 cleavage could be observed even in the absence of DCs, albeit the observed processing is less efficient. Additionally the overall amount of chemokine of processed as well as full-length CCL21 was reduced under DC-free conditions. From these results it can be concluded that the cleavage of CCL21 is not a cell-autonomous process. DCs potentially recruit one or several serine protease from the surrounding blood plasma or serum to their cell membranes thereby activating the enzymes and enhancing their cleavage efficiency. At the same time the cell surfaces seem to protect fragmented as well as full-length CCL21 variants from further proteolytical degradation.

I also tested other cell types found in LNs for their capability to cleave CCL21. B and T cell were able to process the chemokine, although only in very low amounts. These leukocytes seem to be less efficient in recruiting or activating serine proteases on their surfaces. These results support the idea of a regulated process: Potentially only special cell subsets possess the ability to promote cleavage. Furthermore, the CCL21 fragments generated by these two cell types differed slightly in size. Perhaps CCL21 processing is carried out by different proteases in diverse cell subsets or cell type specific secondary proteases further process the cleaved chemokine.

I also incubated mouse embryonic fibroblasts, as an example for a stromal cell type, in medium supplemented with heat-inactivated FCS. In this experimental setup I could not observe CCL21 cleavage. However, LN derived fibroblasts cultured in mouse plasma, a more physiological experimental setup, can efficiently truncate CCL21. The CCL21

fragments generated by DCs or LN fibroblasts possess the same size implicating that both cell types might recruit the same enzyme to their surfaces. LN fibroblasts could constitute a soluble CCL21 gradient also under homeostatic conditions acting parallel to CCL19 concentration gradients, which would further explain why *CCL19*<sup>-/-</sup> mice have only minor defects (Link et al., 2007; Britschgi et al., 2010).

### 5.1.3 Plasmin cleaves CCL21 *in vitro*

Next, I wanted to identify the CCL21 cleaving serine protease. Using *in vitro* cleavage assays plasmin could be identified as one protease truncating CCL21. Plasmin is a serine protease which disintegrates fibrin clots and can furthermore also cleave several chemokines (Schäfer & Werner, 2008; Vakili et al., 2001; Sheehan et al., 2007; Proost et al., 2008). The inactive circulating precursor of plasmin is plasminogen. *In vitro* cleavage assays revealed that plasmin generates two soluble CCL21 fragments. The protease database MEROPS (<http://merops.sanger.ac.uk/>) predicted two potential plasmin cleavage sites (APGK-QSPG and PGCR-KNRG) resulting in 8.4 kDa and 9 kDa CCL21 fragments in size, respectively. These fragments would match the western blot results which showed two distinct protein bands between 8 and 9 kDa. With increasing incubation times the smaller CCL21 fragment dominated. The same results were achieved by co-incubation of CCL21, DCs and the inactive proenzyme of plasmin, plasminogen, under serum-free conditions. Hence, DCs have the ability to cleave the corresponding zymogen plasminogen, thus generating proteolytically active plasmin. Hence, it is likely that DCs regulate the cleavage process. Cell-free *in vitro* assays, where recombinant plasmin and CCL21 were co-incubated, showed that plasmin can further disintegrate CCL21 fragments as observed before in cleavage assays containing plasma.

After characterizing the plasmin CCL21 cleavage *in vitro*, I tried to verify these results in a more physiological setting. However, by repeating the *in vitro* cleavage assays in the presence of *Plg*<sup>-/-</sup> plasma, I showed that CCL21 can also be cleaved in the absence of plasmin. Plasminogen or plasmin, respectively, is not essential for this process. Hence, at least one other protease can exert CCL21 cleavage. Moreover, CCL21 pull-downs of LN lysates from *Plg*<sup>-/-</sup> mice revealed no differences compared to WT LN lysates, either in size or amount of cleavage product. In conclusion it remains unclear if plasmin does contribute to CCL21 cleavage *in vivo*. Possibly the plasmin cleavage of CCL21 does take place *in vivo*, but can be fully compensated by other serine proteases in the LN. Another possibility is that the influence of plasmin on the amount of fragmented CCL21 only becomes noticeable under inflammatory conditions. Besides that, the *in vitro* cleavage assay has also limitations; CCL21 was incubated in the presence of not heat-inactivated mouse plasma that contains for example activated serine proteases of the coagulation cascade, the complement system and fibrinolysis. Hence, these *in vitro* cleavage assays did not resemble the *in vivo* situation

in lymphatic organs. Thus, it cannot be ruled out completely that CCL21 is cleaved artificially *in vitro* by non-physiological proteases and plasmin is one of them.

### 5.1.4 Haptokinetic migration scaffold

B as well as T cells show rapid swarming behavior in SLOs but the cells remain strictly confined to their respective compartments (Miller et al., 2002; Miller et al., 2003; Wei et al., 2005). Randomly migrating T cells for example turn around once they reach the boarder to the B cell follicle (Bajenoff et al., 2006). Besides that, the knockout of CXCL13 or the deletion of CCL21 and CCL19 in the SLOs of *plt/plt* mice are both correlated with massively disrupted lymphoid organ architecture: In the absence of these chemokines barriers between compartments cannot be established. Hence, immune cell subsets are not completely separated anymore (Davalos-Misslitz & Rot, 2008; Förster et al., 1996; Förster et al., 1999; Ansel et al., 2000). The fact that these homeostatic chemokines can be detected by immunostaining of cryosections of SLO supports the idea that these chemokine immobilize to the tissue – soluble proteins would be rapidly washed out during the staining procedure.

Both T cell areas and B cell follicles contain a three-dimensional network of non-hematopoietic stroma cells; this scaffold is constituted of FRCs in the T cell area and FDCs in the B cell area (Mueller & Germain, 2009). Bajenoff et al. (2006) observed by intravital microscopy naïve T cells and B cells migrating along “their” respective stromal network in a random way. Several research groups identified chemokines as the central factor which keeps the cells motile and induces the described migration pattern: Without CCR7 or by inhibition of chemokine signaling by pertussis toxin the cells decelerate massively (Asperti-Boursin et al., 2007; Okada and Cyster, 2007; Worbs et al., 2007). In *plt/plt* mice T cell migration speed is reduced by about 30%, but by intravenously application of CCL21 the migration velocity can be restored (Worbs et al., 2007). It was proposed by Bajenoff et al. (2006) that CCL21 which is immobilized on FRCs keeps T cells motile. The same basic principle is assumed for B cells migrating on CXCL13 coated FDCs (Rozenendaal et al., 2009).

The carbon fiber migration assay revealed that such a system can be constituted *in vitro*: DCs are able to move along CCL21 coated carbon fibers, which act as an artificial migration scaffold. Before leading to rapid migration immobilized CCL21 induces cell adherence by integrin  $\beta 2$  activation; a precondition that the cells “do not lose the track” while migrating along the fibers. DC adherence was also observed on *p19<sup>ARF</sup>*<sup>-/-</sup> LN-fibroblasts coated with CCL21, which resemble more closely the *in vivo* situation. When both T cells and DCs migrate along FRCs, this could lead to more frequent encounters between both cell types and therefore to a faster initiation of the adaptive immune response. Spreading of LN resident DCs on FRCs potentially also influences the antigen uptake of the DCs from the stromal cells or conduits, because of the enhanced interaction surface (Fletcher et al., 2010;



Sixt et al., 2005; Hayakawa, Kobayashi & Hoshino, 1988). Migration on the stromal backbone as well as on carbon fibers co-coated with CCL21 and ICAM-1 lacked directional bias, a phenomenon that was also described as “guided randomness” by Mempel et al. (2006). The scenario of a haptokinetic scaffold could potentially explain the swarming behavior of leukocytes under homeostatic conditions. Further potential benefits of haptokinetic scaffolds are stability against convection forces and mechanical perturbations *in vivo*.

### 5.1.5 Chemotactic bias

The limitations of an immobilized chemokine field become apparent in reactive lymphoid tissue: During adaptive immune response leukocytes change their position or accumulate within one chemokine field. Thus, leukocytes must sense directional guidance cues. Long range gradients of CCL19, CCL21, CXCL13 and CXCL12 could explain cell localization under homeostatic and inflammatory conditions in SLOs. These gradients could on one hand lead to tactic movement; on the other hand leukocytes could integrate the signals of at least two counteracting gradients, which guide the cells then to one defined area, where the two gradients are “balanced”. Ricart et al. (2010) demonstrated that such a system is operative *in vitro*. DCs can integrate two opposing concentration gradients and home to an area where the signals derived from the different gradients are balanced. When the cells reach this region, they show random motility. Thus, cell positioning of DCs, B and T cells in SLOs can potentially be correlated with their individual CXCR5, CCR7 and CXCR4 chemokine receptor expression levels.

Most data which support these hypotheses derive from static cryosections: Th1 and naïve T cells for example exclusively express CCR7 and localize therefore to the CCL21 expressing T cell area. Th2 cells on the other hand lack CCR7 and home in close proximity to the B cell follicles, potentially because they express very low levels of CXCR5 (Randolph et al., 1999; Morita et al., 2011). Dermis-derived migratory DCs expressing high amounts of CXCR5 localize up to 40% in the CXCL13 rich B cell follicles. Bone marrow derived mature DCs displaying 14 times less CXCR5 localize strictly to the T cell zone as well as epidermis-derived DCs that only express CCR7 (Saeki et al., 2000; Kissenpfennig et al., 2005; Saeki et al., 2000; Wu & Hwang, 2002). Anergic B cells have reduced levels of CXCR5 and are therefore excluded from CXCL13 expressing follicles (Ekland et al., 2004). To enter germinal centers B cells express five to twenty fold more CXCR4 than follicular B cells. At the same time they reduce their CCR7 expression levels (Allen et al., 2004).

In addition to that, data derived from two-photon microscopy experiments in tissue slices or living animals, respectively, further support the idea of longer range gradients in SLOs: To change their position leukocytes modify their chemokine receptor levels. For follicular homing activated T cells up-regulate CXCR5 and simultaneously down regulate CCR7, which provides a counteracting signal to retain activated T cells in the T cell area (Ansel et al., 1999; Hardtke et al., 2005). Simultaneously activated B cells start to up regulate CCR7

and as a consequence move directionally towards the boundary between T and B cell area to interact with T helper cells. The area of directed migration involves the region extended up to 140  $\mu\text{m}$  away from the boundary, which further supports the idea of longer range gradients (Okada et al., 2005). But directed movement was also demonstrated on the single cell level. DCs release after successful encounters with  $\text{CD4}^+$  T cells the chemokines CCL3 and CCL4 to recruit  $\text{CD8}^+$  T cells leading to a cell cluster in the T cell area (Castellino et al., 2006).

Theoretically immobilized, haptotactic or soluble, chemotactic gradients could guide cells within lymphoid organs. Okada et al. (2005) indeed observed on LN cryosections a CCL21 gradient extending from the T cell zone into the B cell follicles. I observed a similar CCL21 distribution on LN sections, but it was not correlated with directional DC migration in LN cryosection migration assays. DCs clearly follow soluble guidance cues. Until now it is unclear, if also a diffusible isoform of CXCL13 is generated. But I showed that chemotactic gradients of truncated CCL21 can be generated *in vitro*, CCL19 concentration gradients are well established and also CXCL12 gradients are described (Lämmermann et al., 2008; Lämmermann et al., 2009; Ricart et al., 2010). These considerations together with the *in vitro* findings that T cells, B cells and DCs are all capable to migrate towards spatial chemokine gradients strongly argue for the presence of soluble chemokine gradients within lymphatic organs (Lämmermann et al., 2008).

In contrast to that, R. Germain and colleagues assumed that locally produced, diffusing chemokines directly immobilize on FRCs and thereby generate an immobilized gradient (Bajenoff et al., 2007). However, till now no haptotactic gradients could be visualized in SLOs. Besides that, immobilized gradients theoretically exhibit several disadvantages: For example immobilized gradients are harder to regulate and especially to disintegrate. The decomposition of immobilized gradients would presume endocytosis followed by proteolytical degradation. These processes are more time consuming than the breakdown of soluble gradients by convection. But a rapid adaption of tactic guidance cues is essential for quick leukocyte encounters during adaptive immunity. Soluble gradients are of course more unstable, but also more flexible adjustable during immune response.

### 5.1.6 Competition between immobilized and soluble CCR7 ligands

Surface-bound CCL21 induces after binding to CCR7  $\beta 2$  integrin activation and cell adherence. In contrast to that, CCL19 or truncated CCL21 bound to CCR7 induce cell polarization and integrin-independent, directional movement. By integrating both signals the cells can perform directional migration on a track (Figure 35 B). These results implicate that soluble and bound CCR7 ligands bind to different subsets of the chemokine receptor. In a steep gradient of CCL19 or truncated CCL21 the chemokine receptor fraction occupied by the soluble ligands probably grows. At a certain level the cells can override the adhesive signal, disconnect from the fiber and move freely toward the concentration gradients. These

results potentially entail important physiological implications: Strong chemotactic guidance cues could induce directional cell migration without cell distraction by the extracellular infrastructure. This could result in a faster accumulation of effector cells on sites of infection or SLOs and could explain why leukocytes can infiltrate almost all tissues. Integrins are therefore not essential for interstitial or intranodal leukocyte migration (Lämmermann et al., 2008), but integrins probably enable DCs to follow pathways on FRCs to efficiently engage naïve T cells and mediate close surface contact on conduits. In summary intranodal positioning and also dwell times of cell populations within the LN could be influenced by steep soluble gradients or sparse CCL21 and integrin ligand or chemokine coating of the FRCs.

### 5.1.7 Cell biological implications

Kinesis is the result of self-polarization, which is an intrinsic, spontaneous event or can be triggered by external stimulation and results in random cell movement. Taxis and spontaneous cell polarization were traditionally viewed as contradictory, independent events. But Arriemerlou & Meyer (2005) proposed a model called 'local coupling model for eukaryotic chemotaxis' which connects these two phenomena. In this model the leading edge of a polarized cell consists of independent coupling units or cell extensions. Stochastically single cell extensions enlarge by spontaneous intrinsic activation of PI3 kinase, which results in spontaneous cell polarization and random migration. In cells migrating in a chemotactic gradient, the chemokine receptors of one or more coupling units within the lamellipodium engage their ligands. The chemokine receptor activation leads in turn to a transient, locally restricted activation of PI3 kinase in the respective coupling units and an enlargement of these units. These small lamellipodium extensions finally lead to a turn in direction towards the steepest increase in local concentration. This model explained conclusively for the first time the „directionally biased random walk“ as observed in many migrating cells (Figure 36).

*Chemotactically biased haptokinesis* can be considered as an extension of this model. Immobilized chemokines induce adhesion and furthermore boost random self-polarization, which results in very rapid, undirected migration. The coupling units seem to be more "activated". Soluble chemokine gradients can still induce on top a directional bias leading to directed migration.

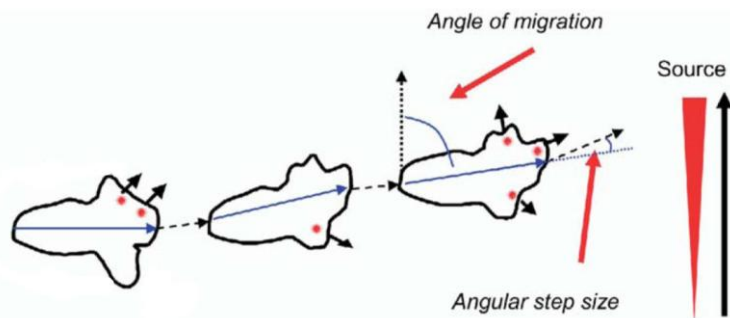


Figure 36: Local coupling model for eukaryotic chemotaxis. The leading edge of a cell consists of independent coupling units (red dots). By sensing a chemotactic gradient (red triangle) coupling units on one site of the cell expand leading to a turn in direction and finally in cell migration towards a gradient over time (adapted from: Arriemerlou & Meyer 2005).

### 5.1.8 Concluding remarks to chemotactically biased haptokinesis

With the carbon fiber migration assay I could show that mature DCs simultaneously sense haptokinetic, immobilized chemokine fields and chemotactic concentration gradients, which results in directed migration on a track. The described model chemotactically biased haptokinesis might explain the swarming behavior and directional migration of leukocytes in lymphoid organs. Moreover, it offers an explanation for the development of the two CCR7 ligands, CCL21 and CCL19.

Although the data presented here support the idea of soluble gradients guiding leukocytes in lymphoid organs, chemoattraction of leukocytes in peripheral tissues might work differently. An example for a haptotactic gradient was described by Massena et al. (2010), where a chemotactic gradient sequestered on endothelial heparan sulfates induces directional intraluminal crawling of neutrophils. McDonald et al. (2010) could even uncover an immobilized CXCL2 gradient in liver sinusoids ranging from 150 to 650  $\mu\text{m}$  of injured areas. It is the first time that an intrinsic immobilized gradient could be visualized. However, blood vessels provide a relatively plain, rather two-dimensional environment. To establish three-dimensional immobilized gradients in complex lymphoid organs, whose architecture changes rapidly upon inflammation, seems to be very challenging. Soluble gradients that only depend on a chemokine source and diffusion are probably easier to realize in SLOs.

It is unclear till now, if chemotactically biased haptokinesis can only be applied to the CCL19/CCL21 system or also to other “chemokine pairs”. There are several “chemokine pairs” described, which bind to one chemokine receptor, but differ in their individual affinities towards GAGs. The chemokine receptor CXCR8 has also two ligands with different abilities to bind to heparan sulfates CXCL1 and CXCL2. CXCL1 is thought to be mainly soluble, whereas CXCL2 binds to GAGs, which is indispensable for neutrophil extravasation to inflamed skin (Massena et al., 2010; Bao et al., 2010). For the chemokine CXCL12 expressed for example in germinal centers six different isoforms are published. CXCL12y

## Discussion

---

consists of a protein core shared by all CXCL12 isoforms, extended by a highly cationic C-terminal domain containing four heparan sulfate-binding motifs. Only CXCL12 $\gamma$  is the only isoform which is able to induce cell accumulations and angiogenesis CXCL12 $\alpha$  on the other hand has only a low GAG-binding capacity and is assumed to be soluble (Rueda et al., 2008; Lortat-Jacob, 2009). It will be interesting to see if the described model of chemotactically biased haptokinesis can also be applied to these chemokines and furthermore if this model derived from *in vitro* assays can be verified *in vivo* by two-photon microscopy. Besides that, it is still unclear which serine proteases cleave CCL21 *in vivo*, which is essential information to elucidate how this process is regulated.

Our model chemotactically biased haptokinesis can potentially explain leukocyte positioning as well as leukocyte migration patterns in SLOs. Up till now immunologists largely ignored the presenting mode of chemokines, but it massively influences cell behavior *in vitro* and in all probability also *in vivo*.

## **5.2 Adaptive force transmission in amoeboid cell migration**

Leukocytes are very rapidly migrating cells and can reach velocities two orders of magnitude higher than other cell types. Moreover, migrating leukocytes face diverse environments on their trafficking routes. In order to migrate cells have to transmit intracellular forces generated by the actomyosin system to their environment; these protrusive and contractile forces are transformed into 'traction', which is a prerequisite for forward movement (Renkawitz & Sixt, 2010). In the classical textbook model cellular traction is mediated via the integrin family of transmembrane receptors. This model can describe DCs migrating in a two-dimensional environment; here, DCs strictly depend on integrins in order to move. But against the textbook paradigm of force generation and transmission during cell migration, leukocytes are able to migrate in three-dimensional environments without using transmembrane receptors of the integrin family (Lämmermann et al., 2008). In three-dimensional interstitia leukocytes normally form rounded extensions, also called lobopodia, at their leading edge that can intercalate into pores and potentially allow the generation of traction force (Friedl et al., 2001).

To study how the actin cytoskeleton adapts under adhesion-independent conditions we established a migration assay in a clearly defined three-dimensional environment: The cells were squeezed between a layer of agarose and a cell culture dish while migrating towards a CCL19 gradient. The result is a pseudo three-dimensional setup, where the lobopodia are flattened to lamellipodia and the actin cortex can easily be analyzed by high-resolution TIRF microscopy and the actin probe Lifeact-GFP.

This study showed, that chemotactic DCs can switch between integrin-dependent and -independent locomotion and can thereby adapt to the adhesive properties of their environment. If actin-integrin clutches are active, actin polymerization is entirely converted into protrusion. Without a molecular clutch the actin cortex undergoes slippage and retrograde flow. But retrograde actin flow can be completely balanced by an enhanced actin polymerization rate keeping the migration velocity and the cell shape unaltered. Because of the adaption of actin polymerization amoeboid cells like DCs can follow soluble guidance cues without being distracted by adhesive interactions with tissue components. Mesenchymal cells on the other hand strictly depend on adhesive interaction and cannot invade areas which lack their respective adhesion ligands.

### **5.2.1 Amoeboid cells can adapt to different degrees of force coupling via actin polymerization**

Efficient cell migration relies on the transmission of the force generated by the actomyosin cytoskeleton to the extracellular substrate. Intracellularly this is achieved by the coupling of

## Discussion

actin filaments to integrin transmembrane receptors via a protein cluster including vinculin and talin (Brown et al., 2006; Hu et al., 2007). The coupling between actin cytoskeleton and adhesion receptor has been described as 'molecular clutch'. Without active force coupling via the molecular clutch polymerizing actin filaments are pushed backwards into the cell, because they experience a counter force by the cell membrane; the result is retrograde actin flow of the actin cell cortex (Hu et al., 2007; Giannone, Mège & Thoumine, 2007).

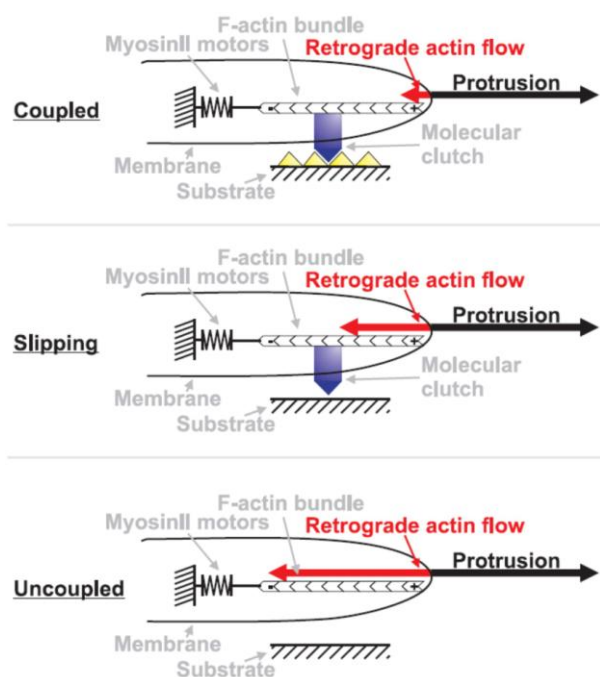


**Figure 37: Scheme of the adaption of protrusion and retrograde actin flow at different levels of force coupling in amoeboid cells. When the actin is coupled to the substrate, actin polymerization is directly converted into leading edge protrusion. When integrins cannot bind to a corresponding ligand, slipping, an intermediate state of force coupling occurs. By removal of the transmembrane receptors complete uncoupling proceeds. Because the protrusion rate always stays constant, during uncoupling the actin polymerization rate must be enhanced to compensate for the increased retrograde actin flow (taken from: Renkawitz et al., 2009).**

WT DCs show almost no retrograde actin flow while migrating in the described under-agarose assay on glass slides. In only 50% of the analyzed WT DCs retrograde flow could be observed in a small, 2-3  $\mu\text{m}$  wide region at the tip of the leading edge. Thus, the cells exhibit an active molecular clutch, which allows the optimal transfer of traction force and the conversion of actin polymerization into protrusion. WT DCs migrating on an inert substrate like polyethylene glycol (PEG), which eliminates integrin-ligand-interactions, show retrograde actin flow. The actin cortex slides backwards because integrins only streak the PEG substrate without ligand binding ('slipping'). This actin slippage can be further enhanced by applying *Itg*<sup>-/-</sup> DCs to glass or PEG slides. Here the coupling between substrate and actin filaments is completely abolished ('uncoupling'; Figure 37). But the DCs showed no alterations in their cell shape and the same migration and protrusion speed under all three

conditions. DCs adapt to the adhesiveness of their migration substrates by regulating their actin polymerization rate. Surprisingly, a correlation between protrusion speed and retrograde actin flow does not exist in our setup, which is contradictory to data derived from keratocytes and growth cones (Vallotton et al., 2006; Medeiros et al., 2006). Hence, it follows that the molecular clutch system in DCs does not only depend on expanding actin filaments and transmembrane receptors, but also on the actin polymerization rate, as a third component.

### 5.2.2 Surface anchoring cells cannot protrude into open space

Next, I tested if the adaption of actin polymerization is a unique feature of DCs or if it also occurs in other cell types. Macrophages, as an example for a resident haematopoietic cell, showed exactly the same behaviour as DCs: The cell shape does not change when they are placed on PEG or a serum coated glass surface. Macrophages on PEG exhibit an enhanced retrograde actin flow.

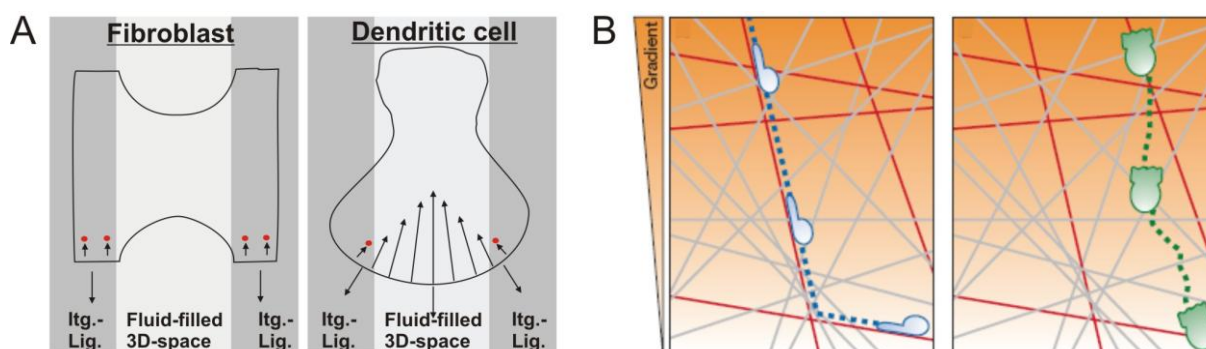


**Figure 38: Difference between surface anchoring cells like fibroblasts and the amoeboid cell type represented by DCs. (A) DCs can protrude into the open space and compensate the enhanced retrograde actin flow. Fibroblasts adapt their shape strictly to adhesive zones (depicted in grey). Red dots represent adhesion sites, downwards arrows protrusion direction and upwards arrows retrograde actin flow. Itg-Lig: integrin ligand (taken from: Renkawitz et al., 2009). (B) Migratory pathways of mesenchymal and amoeboid cells. Left panel: Mesenchymal cells depend on adhesive ligands matching to their integrin repertoire (marked in red). They strictly follow the track. Right panel: Amoeboid cells migrate towards a soluble gradient without being distracted by adhesive paths (adapted from: Renkawitz & Sixt, 2010).**

These results implicate that amoeboid cells can adapt very rapidly to changes in the adhesiveness of their environment. To prove this, Lifeact-GFP DCs migrating on a surface patterned with alternating inert PEG and adhesive serum coated stripes towards a CCL19 gradient were analyzed. The DCs strictly followed the gradient and migrated equally well on both stripes. Also cell shape and migration velocity were not altered while the DCs migrated over the different areas. Therefore, amoeboid cells can rapidly adapt to adhesive substrate properties, even within their lamellipodium. When fibroblasts (as a prototypic example for a



mesenchymal, surface anchoring cell) were applied to patterns of inert and adhesive areas, they strictly adapted their shape to the adhesive areas (Figure 38 A). Only very short protrusions touched the inert areas. These protrusions exhibited massively enhanced retrograde actin flow that stopped at the border to the adhesive region. Hence, the adaption of the actin polymerization to a varying engagement of the molecular clutch is a common mechanism in all cells. But only amoeboid cells can enhance actin polymerization to a level which allows them to be independent of adhesive interaction mediated by integrins. Therefore, rapid migrating leukocytes can leave adhesive tracks in a strong chemotactic gradient (Figure 35) or shuttle to other tissue compartments (Figure 38 B; Luster et al., 2005; Massberg et al., 2007). Mesenchymal cells like fibroblasts on the other hand depend on their integrin repertoire: They always migrate on adhesive tracks marked by the corresponding integrin ligands (Figure 38 B). Because of their strictly haptic movement they cannot invade external tissues with diverse ligands.

### 5.2.3 Immobilized chemokine influences adaptive force transmission

DCs migrating on glass slides possess no or almost no retrograde actin flow because of active force coupling. In the first part of my thesis I demonstrated that immobilized chemokine induces cell spreading and polarization in DCs. Surface-bound CCL21 massively affects the shape of the DCs, which is mainly defined by the cytoskeleton. Thus, I analyzed how the actin cytoskeleton is influenced by immobilized chemokine. Surprisingly, in DCs chemotaxing on glass co-coated with CCL21 and the  $\beta 2$  integrin ligand ICAM-1 towards CCL19 more retrograde actin flow could be measured. One explanation for this observation could be that CCR7 activates upon ligand binding the small GTPase Rac. Rac can in turn activate the actin elongating and nucleating protein complex Arp2/3. Thereby chemokine signaling can enhance the cellular actin polymerization rate (Rot & von Andrian, 2004; Thelen & Stein, 2008). Because of the already existing excellent force coupling in DCs migrating on uncoated glass, the cells can theoretically convert the additional CCL21-induced actin polymerization either into an increased migration velocity or into retrograde flow. Hence, DCs always move with the same speed irrespectively of the stickiness of their environment, they potentially transcribe chemokine-induced polymerization into retrograde actin flow.

To gain more detailed insights into adhesion sites in WT DCs migrating on either glass or CCL21 coated surfaces, DCs were transfected with vinculin-GFP. Vinculin acts as a marker for adhesive sites, because it is part of the molecular clutch which connects integrins with the actin cytoskeleton (Brown et al., 2006). In DCs migrating on glass vinculin-GFP formed spots in the leading edge and retraction fibers in the trailing edge, which further confirmed active force coupling in DCs. The same protein distribution was observed in DCs migrating on CCL21/ICAM-1 coated glass; also the dynamics and the size of the spots were not

altered. Immobilized CCL21 has no obvious effects on adhesion sites, but could modify signaling and composition of these spots.

In contrast to that, in *Itg<sup>-/-</sup>* DCs performing directional migration towards CCL19 on CCL21/ICAM-1 retrograde actin flow slows down in comparison to migration on uncoated glass. Optionally CCR7 could act as a surrogate molecular clutch: CCR7 engages surface-bound CCL21 and could thereby establish weak force coupling. To gain insights into the CCR7 dynamics DCs were transfected with CCR7-GFP and the distribution of fluorescent protein in the already described setup analyzed. In DCs migrating on glass over the whole cell surface small flickering CCR7 spots could be detected. The same was observed in DCs migrating on CCL21/ICAM-1 coated glass. CCR7 does not seem to be spatially connected to sites of adhesion. However, I cannot rule out weak force coupling distributed over the whole cell body. Strikingly, also no CCR7 accumulation on the leading edge was detectable in DCs migrating in a CCL19 gradient. This result is contradictory to observation in T cells performing directional migration (Nieto et al., 1997; Gérard et al. 2007; Morley et al., 2010).

### 5.2.4 Concluding remarks to ‘adaptive force transmission’

The finding that leukocytes can tune their actin polymerization rate depending on the extracellular migration substrate suggests a feedback mechanism between force coupling and actin polymerization rate. One purely mechanical explanation acts on the assumption that the membrane tension always stays constant because of a “force-actin velocity-relationship” between the plasma membrane and the barbed ends of the actin filaments pushing against the membrane. When actin filaments experience a counter force, for example by the stiffness of the plasma membrane, the actin polymerization rate slows down (Mitchison & Cramer, 1996). There are factors which can decrease membrane tension like a massive influx of H<sub>2</sub>O, which expands the lamellipodium, or a higher availability of plasma membrane due to exocytosis (Mitchison, Charras & Mahadevan, 2008; Doherty & McMahon, 2008). This decrease in tension leads to “more space” between membrane and actin filaments and therefore to an increased actin polymerization till the membrane tension is balanced again. An inactive molecular clutch could act in a similar way. Because the elongating actin filaments are not connected via integrins to extracellular molecules, they are less stabilized and can be easily pushed backwards by the plasma membrane. There is again a gap between filaments and membrane. However, GTP-actin monomers are available in overspill and can be incorporated on the actin filaments: The actin polymerization rate increases till the “force-actin velocity-relationship” is intact again.

This model would also explain why adaptive force transmission is a common cell biological phenomenon: All needed components are expressed in all known cell types. But this model has also limitations. It is still unclear why only amoeboid cells can increase their actin polymerization rate to such high levels. Probably these cells can regulate and initiate actin polymerization more efficiently. The next step to explain adaptive force transmission not only

## Discussion

---

mechanically, but also in a more detailed cell biological way is to identify actin initiatory and regulatory proteins, which boost actin polymerization in amoeboid cells. Till now it is also unclear how and why amoeboid cells adapt their migration velocities always to a somehow fixed value. There must be a limiting factor in the actin cytoskeleton. Another unanswered question is, which migration mode, an integrin-dependent or –independent one, dominates in physiological interstitium. In lymphoid organs with their high density of chemokine and integrin ligand coated surfaces most likely the integrin-dependent locomotion outranks.

In conclusion, we show that amoeboid protrusions unify two seemingly mutually exclusive migration models: they can autonomously extend into open space without requiring mechanical anchorage, but at the same time they can generate traction by transmitting the retrograde force of actin polymerization to a substrate. But how the cells generate traction without using integrins has not been analyzed so far and is a question of great interest to conclusively explain leukocyte migration in the interstitium.

## 6 References

- Ali S, Palmer AC, Banerjee B, Fritchley SJ, Kirby JA. Examination of the function of RANTES, MIP-1alpha, and MIP-1beta following interaction with heparin-like glycosaminoglycans. *J Biol Chem*. 2000 Apr 21;275(16):11721-7.
- Allen CD, Ansel KM, Low C, Lesley R, Tamamura H, Fujii N, Cyster JG. Germinal center dark and light zone organization is mediated by CXCR4 and CXCR5. *Nat Immunol*. 2004 Sep;5(9):943-52.
- Allen CD, Cyster JG. Follicular dendritic cell networks of primary follicles and germinal centers: phenotype and function. *Semin Immunol*. 2008 Feb;20(1):14-25.
- Allen CD, Okada T, Cyster JG. Germinal-center organization and cellular dynamics. *Immunity*. 2007 Aug;27(2):190-202.
- Alvarez D, Vollmann EH & von Andrian UH. Mechanisms and consequences of dendritic cell migration. *Immunity* 3, 325-42 (2008)
- Amara A, Lorthioir O, Valenzuela A, Magerus A, Thelen M, Montes M, Virelizier JL, Delepiepierre M, Baleux F, Lortat-Jacob H, Arenzana-Seisdedos F. Stromal cell-derived factor-1alpha associates with heparan sulfates through the first beta-strand of the chemokine. *J Biol Chem*. 1999 Aug 20;274(34):23916-25.
- Ansel KM, McHeyzer-Williams LJ, Ngo VN, McHeyzer-Williams MG, Cyster JG. In vivo-activated CD4 T cells up regulate CXC chemokine receptor 5 and reprogram their response to lymphoid chemokines. *J Exp Med*. 1999 Oct 18;190(8):1123-34.
- Ansel KM, Ngo VN, Hyman PL, Luther SA, Förster R, Sedgwick JD, Browning JL, Lipp M, Cyster JG. A chemokine-driven positive feedback loop organizes lymphoid follicles. *Nature*. 2000 Jul 20;406(6793):309-14.
- Arriemerlou C, Meyer T. A local coupling model and compass parameter for eukaryotic chemotaxis. *Dev Cell*. 2005 Feb;8(2):215-27.
- Asperti-Boursin F, Real E, Bismuth G, Trautmann A, Donnadieu E. CCR7 ligands control basal T cell motility within lymph node slices in a phosphoinositide 3-kinase-independent manner. *J Exp Med*. 2007 May 14;204(5):1167-79.

## References

---

- Bachmann MF, Kopf M, Marsland BJ. Chemokines: more than just road signs. *Nat Rev Immunol.* 2006 Feb;6(2):159-64.
- Bajénoff M, Egen JG, Koo LY, Laugier JP, Brau F, Glaichenhaus N, Germain RN. Stromal cell networks regulate lymphocyte entry, migration, and territoriality in lymph nodes. *Immunity.* 2006 Dec;25(6):989-1001.
- Bajénoff M, Egen JG, Qi H, Huang AY, Castellino F, Germain RN. Highways, byways and breadcrumbs: directing lymphocyte traffic in the lymph node. *Trends Immunol.* 2007 Aug;28(8):346-52.
- Bajénoff M, Glaichenhaus N, Germain RN. Fibroblastic reticular cells guide T lymphocyte entry into and migration within the splenic T cell zone. *J Immunol.* 2008 Sep 15;181(6):3947-54.
- Bajénoff M, Germain RN. B-cell follicle development remodels the conduit system and allows soluble antigen delivery to follicular dendritic cells. *Blood.* 2009 Dec 3;114(24):4989-97.
- Balogh P, Horváth G, Szakal AK. Immunoarchitecture of distinct reticular fibroblastic domains in the white pulp of mouse spleen. *J Histochem Cytochem.* 2004 Oct;52(10):1287-98.
- Banchereau J, Steinman RM. Dendritic cells and the control of immunity. *Nature.* 1998 Mar 19;392(6673):245-52.
- Baum J, Papenfuss AT, Baum B, Speed TP, Cowman AF. Regulation of apicomplexan actin-based motility. *Nat Rev Microbiol.* 2006 Aug;4(8):621-8.
- Bekiaris V, Withers D, Glanville SH, McConnell FM, Parnell SM, Kim MY, Gaspal FM, Jenkinson E, Sweet C, Anderson G, Lane PJ. Role of CD30 in B/T segregation in the spleen. *J Immunol.* 2007 Dec 1;179(11):7535-43.
- Birnbaumer L. Expansion of signal transduction by G proteins. The second 15 years or so: from 3 to 16 alpha subunits plus betagamma dimers. *Biochim Biophys Acta.* 2007 Apr;1768(4):772-93.
- Bleul CC, Fuhlbrigge RC, Casasnovas JM, Aiuti A, Springer TA. A highly efficacious lymphocyte chemoattractant, stromal cell-derived factor 1 (SDF-1). *J Exp Med.* 1996 Sep 1;184(3):1101-9.
- Böttcher RT, Lange A, Fässler R. How ILK and kindlins cooperate to orchestrate integrin signaling. *Curr Opin Cell Biol.* 2009 Oct;21(5):670-5.

## References

---

Breiteneder-Geleff S, Soleiman A, Kowalski H, Horvat R, Amann G, Kriehuber E, Diem K, Weninger W, Tschachler E, Alitalo K, Kerjaschki D. Angiosarcomas express mixed endothelial phenotypes of blood and lymphatic capillaries: podoplanin as a specific marker for lymphatic endothelium. *Am J Pathol.* 1999 Feb;154(2):385-94.

Britschgi MR, Favre S, Luther SA. CCL21 is sufficient to mediate DC migration, maturation and function in the absence of CCL19. *Eur J Immunol.* 2010 May;40(5):1266-71.

Bromley SK, Thomas SY, Luster AD. Chemokine receptor CCR7 guides T cell exit from peripheral tissues and entry into afferent lymphatics. *Nat Immunol.* 2005 Sep;6(9):895-901.

Brown CM, Hebert B, Kolin DL, Zareno J, Whitmore L, Horwitz AR, Wiseman PW. Probing the integrin-actin linkage using high-resolution protein velocity mapping. *J Cell Sci.* 2006 Dec 15;119(Pt 24):5204-14.

Byers MA, Calloway PA, Shannon L, Cunningham HD, Smith S, Li F, Fassold BC, Vines CM. Arrestin 3 mediates endocytosis of CCR7 following ligation of CCL19 but not CCL21. *J Immunol.* 2008 Oct 1;181(7):4723-32.

Carlsen HS, Haraldsen G, Brandtzaeg P, Baekkevold ES. Disparate lymphoid chemokine expression in mice and men: no evidence of CCL21 synthesis by human high endothelial venules. *Blood.* 2005 Jul 15;106(2):444-6.

Casamayor-Pallejà M, Mondière P, Amara A, Bella C, Dieu-Nosjean MC, Caux C, Defrance T. Expression of macrophage inflammatory protein-3 $\alpha$ , stromal cell-derived factor-1, and B-cell-attracting chemokine-1 identifies the tonsil crypt as an attractive site for B cells. *Blood.* 2001 Jun 15;97(12):3992-4.

Castellino F, Huang AY, Altan-Bonnet G, Stoll S, Scheinecker C, Germain RN. Chemokines enhance immunity by guiding naive CD8<sup>+</sup> T cells to sites of CD4<sup>+</sup> T cell-dendritic cell interaction. *Nature.* 2006 Apr 13;440(7086):890-5.

Castellino F, Germain RN. Chemokine-guided CD4<sup>+</sup> T cell help enhances generation of IL-6<sup>R</sup>highIL-7<sup>R</sup>high prememory CD8<sup>+</sup> T cells. *J Immunol.* 2007 Jan 15;178(2):778-87.

Charmoy M, Brunner-Agten S, Aebischer D, Auderset F, Launois P, Milon G, Proudfoot AE, Tacchini-Cottier F. Neutrophil-derived CCL3 is essential for the rapid recruitment of dendritic cells to the site of *Leishmania major* inoculation in resistant mice. *PLoS Pathog.* 2010 Feb 5;6(2):e1000755.

Chtanova T, Han SJ, Schaeffer M, van Dooren GG, Herzmark P, Striepen B, Robey EA. Dynamics of T cell, antigen-presenting cell, and pathogen interactions during recall responses in the lymph node. *Immunity.* 2009 Aug 21;31(2):342-55.

## References

---

Clark K, Langeslag M, Figdor CG, van Leeuwen FN. Myosin II and mechanotransduction: a balancing act. *Trends Cell Biol.* 2007 Apr;17(4):178-86.

Comerford I, Milasta S, Morrow V, Milligan G, Nibbs R. The chemokine receptor CCX-CKR mediates effective scavenging of CCL19 in vitro. *Eur J Immunol.* 2006 Jul;36(7):1904-16.

Cozine CL, Wolniak KL, Waldschmidt TJ. The primary germinal center response in mice. *Curr Opin Immunol.* 2005 Jun;17(3):298-302.

Cramer LP. Molecular mechanism of actin-dependent retrograde flow in lamellipodia of motile cells. *Front Biosci.* 1997 Jun 1;2:d260-70.

Cyster JG. Chemokines and cell migration in secondary lymphoid organs. *Science.* 1999 Dec 10;286(5447):2098-102.

Cyster JG. Lymphoid organ development and cell migration. *Immunol Rev.* 2003 Oct;195:5-14.

Cyster JG, Ansel KM, Reif K, Ekland EH, Hyman PL, Tang HL, Luther SA, Ngo VN. Follicular stromal cells and lymphocyte homing to follicles. *Immunol Rev.* 2000 Aug;176:181-93.

Debes GF, Arnold CN, Young AJ, Krautwald S, Lipp M, Hay JB, Butcher EC. Chemokine receptor CCR7 required for T lymphocyte exit from peripheral tissues. *Nat Immunol.* 2005 Sep;6(9):889-94.

de Paz JL, Moseman EA, Noti C, Polito L, von Andrian UH, Seeberger PH. Profiling heparin-chemokine interactions using synthetic tools. *ACS Chem Biol.* 2007 Nov 20;2(11):735-44.

Doherty GJ, McMahon HT. Mediation, modulation, and consequences of membrane-cytoskeleton interactions. *Annu Rev Biophys.* 2008;37:65-95.

Egawa T, Kawabata K, Kawamoto H, Amada K, Okamoto R, Fujii N, Kishimoto T, Katsura Y, Nagasawa T. The earliest stages of B cell development require a chemokine stromal cell-derived factor/pre-B cell growth-stimulating factor. *Immunity.* 2001 Aug;15(2):323-34.

Ehrlich LI, Oh DY, Weissman IL, Lewis RS. Differential contribution of chemotaxis and substrate restriction to segregation of immature and mature thymocytes. *Immunity.* 2009 Dec 18;31(6):986-98.

Ekland EH, Forster R, Lipp M, Cyster JG. Requirements for follicular exclusion and competitive elimination of autoantigen-binding B cells. *J Immunol.* 2004 Apr 15;172(8):4700-8.

## References

---

Fernandez EJ, Lolis E. Structure, function, and inhibition of chemokines. *Annu Rev Pharmacol Toxicol.* 2002;42:469-99.

Flanagan K, Glover RT, Hörig H, Yang W, Kaufman HL. Local delivery of recombinant vaccinia virus expressing secondary lymphoid chemokine (SLC) results in a CD4 T-cell dependent antitumor response. *Vaccine.* 2004 Jul 29;22(21-22):2894-903.

Fletcher AL, Lukacs-Kornek V, Reynoso ED, Pinner SE, Bellemare-Pelletier A, Curry MS, Collier AR, Boyd RL, Turley SJ. Lymph node fibroblastic reticular cells directly present peripheral tissue antigen under steady-state and inflammatory conditions. *J Exp Med.* 2010 Apr 12;207(4):689-97.

Förster R, Emrich T, Kremmer E, Lipp M. Expression of the G-protein-coupled receptor BLR1 defines mature, recirculating B cells and a subset of T-helper memory cells. *Blood.* 1994 Aug 1;84(3):830-40.

Förster R, Mattis AE, Kremmer E, Wolf E, Brem G, Lipp M. A putative chemokine receptor, BLR1, directs B cell migration to defined lymphoid organs and specific anatomic compartments of the spleen. *Cell.* 1996 Dec 13;87(6):1037-47.

Förster R, Davalos-Misslitz AC, Rot A. CCR7 and its ligands: balancing immunity and tolerance. *Nat Rev Immunol.* 2008 May;8(5):362-71.

Förster R, Schubel A, Breitfeld D, Kremmer E, Renner-Müller I, Wolf E, Lipp M. CCR7 coordinates the primary immune response by establishing functional microenvironments in secondary lymphoid organs. *Cell.* 1999 Oct 1;99(1):23-33.

Frederick MJ, Clayman GL. Chemokines in cancer. *Expert Rev Mol Med.* 2001 Jul 18;3(19):1-18.

Friedl P, Borgmann S, Bröcker EB. Amoeboid leukocyte crawling through extracellular matrix: lessons from the Dictyostelium paradigm of cell movement. *J Leukoc Biol.* 2001 Oct;70(4):491-509.

Friedl P, Weigelin B. Interstitial leukocyte migration and immune function. *Nat Immunol.* 2008 Sep;9(9):960-9.

Friedman RS, Jacobelli J, Krummel MF. Surface-bound chemokines capture and prime T cells for synapse formation. *Nat Immunol.* 2006 Oct;7(10):1101-8. Epub 2006 Sep 10. Erratum in: *Nat Immunol.* 2006 Nov;7(11):1234.

Gérard A, Mertens AE, van der Kammen RA, Collard JG. The Par polarity complex regulates Rap1- and chemokine-induced T cell polarization. *J Cell Biol.* 2007 Mar 12;176(6):863-75.



## References

---

Giannone G, Mège RM, Thoumine O. Multi-level molecular clutches in motile cell processes. *Trends Cell Biol.* 2009 Sep;19(9):475-86.

Gosling J, Dairaghi DJ, Wang Y, Hanley M, Talbot D, Miao Z, Schall TJ. Cutting edge: identification of a novel chemokine receptor that binds dendritic cell- and T cell-active chemokines including ELC, SLC, and TECK. *J Immunol.* 2000 Mar 15;164(6):2851-6.

Grabovsky V, Feigelson S, Chen C, Bleijs DA, Peled A, Cinamon G, Baleux F, Arenzana-Seisdedos F, Lapidot T, van Kooyk Y, Lobb RR, Alon R. Subsecond induction of alpha4 integrin clustering by immobilized chemokines stimulates leukocyte tethering and rolling on endothelial vascular cell adhesion molecule 1 under flow conditions. *J Exp Med.* 2000 Aug 21;192(4):495-506.

Gunn MD, Tangemann K, Tam C, Cyster JG, Rosen SD, Williams LT. A chemokine expressed in lymphoid high endothelial venules promotes the adhesion and chemotaxis of naive T lymphocytes. *Proc Natl Acad Sci U S A.* 1998 Jan 6;95(1):258-63.

Handel TM, Johnson Z, Crown SE, Lau EK, Proudfoot AE. Regulation of protein function by glycosaminoglycans--as exemplified by chemokines. *Annu Rev Biochem.* 2005;74:385-410

Hardtke S, Ohl L, Förster R. Balanced expression of CXCR5 and CCR7 on follicular T helper cells determines their transient positioning to lymph node follicles and is essential for efficient B-cell help. *Blood.* 2005 Sep 15;106(6):1924-31.

Hargreaves DC, Hyman PL, Lu TT, Ngo VN, Bidgol A, Suzuki G, Zou YR, Littman DR, Cyster JG. A coordinated change in chemokine responsiveness guides plasma cell movements. *J Exp Med.* 2001 Jul 2;194(1):45-56.

Hayakawa M, Kobayashi M, Hoshino T. Direct contact between reticular fibers and migratory cells in the paracortex of mouse lymph nodes: a morphological and quantitative study. *Arch Histol Cytol.* 1988 Jul;51(3):233-40.

Haynes NM, Allen CD, Lesley R, Ansel KM, Killeen N, Cyster JG. Role of CXCR5 and CCR7 in follicular Th cell positioning and appearance of a programmed cell death gene-1high germinal center-associated subpopulation. *J Immunol.* 2007 Oct 15;179(8):5099-108.

Heinzel K, Benz C, Bleul CC. A silent chemokine receptor regulates steady-state leukocyte homing in vivo. *Proc Natl Acad Sci U S A.* 2007 May 15;104(20):8421-6.

Heit B, Kubes P. Measuring chemotaxis and chemokinesis: the under-agarose cell migration assay. *Sci STKE.* 2003 Feb 18;2003(170):PL5.

Hirose J, Kawashima H, Swope Willis M, Springer TA, Hasegawa H, Yoshie O, Miyasaka M. Chondroitin sulfate B exerts its inhibitory effect on secondary lymphoid tissue chemokine

## References

---

(SLC) by binding to the C-terminus of SLC. *Biochim Biophys Acta*. 2002 Jul 3;1571(3):219-24.

Hirose J, Kawashima H, Yoshie O, Tashiro K, Miyasaka M. Versican interacts with chemokines and modulates cellular responses. *J Biol Chem*. 2001 Feb 16; 276(7):5228-34.

Hoogwerf AJ, Kuschert GS, Proudfoot AE, Borlat F, Clark-Lewis I, Power CA, Wells TN. Glycosaminoglycans mediate cell surface oligomerization of chemokines. *Biochemistry*. 1997 Nov 4;36(44):13570-8.

Hu K, Ji L, Applegate KT, Danuser G, Waterman-Storer CM. Differential transmission of actin motion within focal adhesions. *Science*. 2007 Jan 5;315(5808):111-5.

Hynes RO. Integrins: bidirectional, allosteric signaling machines. *Cell*. 2002 Sep 20;110(6):673-87.

Imai Y, Park EJ, Peer D, Peixoto A, Cheng G, von Andrian UH, Carman CV, Shimaoka M. Genetic perturbation of the putative cytoplasmic membrane-proximal salt bridge aberrantly activates alpha(4) integrins. *Blood*. 2008 Dec 15;112(13):5007-15.

Ito T, Wang YH, Liu YJ. Plasmacytoid dendritic cell precursors/type I interferon-producing cells sense viral infection by Toll-like receptor (TLR) 7 and TLR9. *Springer Semin Immunopathol*. 2005 Jan;26(3):221-9.

Junt T, Nakano H, Dumrese T, Kakiuchi T, Odermatt B, Zinkernagel RM, Hengartner H, Ludewig B. Antiviral immune responses in the absence of organized lymphoid T cell zones in plt/plt mice. *J Immunol*. 2002 Jun 15;168(12):6032-40.

Junt T, Scandella E, Ludewig B. Form follows function: lymphoid tissue microarchitecture in antimicrobial immune defence. *Nat Rev Immunol*. 2008 Oct;8(10):764-75.

Jurado C, Haserick JR, Lee J. Slipping or gripping? Fluorescent speckle microscopy in fish keratocytes reveals two different mechanisms for generating a retrograde flow of actin. *Mol Biol Cell*. 2005 Feb;16(2):507-18.

Kabashima K, Shiraishi N, Sugita K, Mori T, Onoue A, Kobayashi M, Sakabe J, Yoshiki R, Tamamura H, Fujii N, Inaba K, Tokura Y. CXCL12-CXCR4 engagement is required for migration of cutaneous dendritic cells. *Am J Pathol*. 2007 Oct; 171(4):1249-57.

Katakai T, Suto H, Sugai M, Gonda H, Togawa A, Suematsu S, Ebisuno Y, Katagiri K, Kinashi T, Shimizu A. Organizer-like reticular stromal cell layer common to adult secondary lymphoid organs. *J Immunol*. 2008 Nov 1;181(9):6189-200.

## References

---

Khandoga AG, Khandoga A, Reichel CA, Bihari P, Rehberg M, Krombach F. In vivo imaging and quantitative analysis of leukocyte directional migration and polarization in inflamed tissue. *PLoS One*. 2009;4(3):e4693.

Kinashi T. Intracellular signalling controlling integrin activation in lymphocytes. *Nat Rev Immunol*. 2005 Jul;5(7):546-59.

Kissenpfennig A, Henri S, Dubois B, Laplace-Builhé C, Perrin P, Romani N, Tripp CH, Douillard P, Leserman L, Kaiserlian D, Saeland S, Davoust J, Malissen B. Dynamics and function of Langerhans cells in vivo: dermal dendritic cells colonize lymph node areas distinct from slower migrating Langerhans cells. *Immunity*. 2005 May;22(5):643-54.

Kriehuber E, Breiteneder-Geleff S, Groeger M, Soleiman A, Schoppmann SF, Stingl G, Kerjaschki D, Maurer D. Isolation and characterization of dermal lymphatic and blood endothelial cells reveal stable and functionally specialized cell lineages. *J Exp Med*. 2001 Sep 17;194(6):797-808.

Kohrgruber N, Gröger M, Meraner P, Kriehuber E, Petzelbauer P, Brandt S, Stingl G, Rot A, Maurer D. Plasmacytoid dendritic cell recruitment by immobilized CXCR3 ligands. *J Immunol*. 2004 Dec 1;173(11):6592-602.

Kurobe H, Liu C, Ueno T, Saito F, Ohigashi I, Seach N, Arakaki R, Hayashi Y, Kitagawa T, Lipp M, Boyd RL, Takahama Y. CCR7-dependent cortex-to-medulla migration of positively selected thymocytes is essential for establishing central tolerance. *Immunity*. 2006 Feb;24(2):165-77.

Kuschert GS, Coulin F, Power CA, Proudfoot AE, Hubbard RE, Hoogewerf AJ, Wells TN. Glycosaminoglycans interact selectively with chemokines and modulate receptor binding and cellular responses. *Biochemistry*. 1999 Sep 28;38(39):12959-68.

Lämmermann T, Bader BL, Monkley SJ, Worbs T, Wedlich-Söldner R, Hirsch K, Keller M, Förster R, Crichtley DR, Fässler R, Sixt M. Rapid leukocyte migration by integrin-independent flowing and squeezing. *Nature*. 2008 May 1;453(7191):51-5.

Lämmermann T, Renkawitz J, Wu X, Hirsch K, Brakebusch C, Sixt M. Cdc42-dependent leading edge coordination is essential for interstitial dendritic cell migration. *Blood*. 2009 Jun 4;113(23):5703-10

Lämmermann T, Sixt M. Mechanical modes of 'amoeboid' cell migration. *Curr Opin Cell Biol*. 2009 Oct;21(5):636-44

Lämmermann T, Sixt M. The microanatomy of T-cell responses. *Immunol Rev*. 2008 Feb;221:26-43.

## References

---

Le Contel C, Temime N, Charron DJ, Parant MA. Modulation of lipopolysaccharide-induced cytokine gene expression in mouse bone marrow-derived macrophages by muramyl dipeptide. *J Immunol.* 1993 May 15;150(10):4541-9.

Ley K, Laudanna C, Cybulsky MI, Nourshargh S. Getting to the site of inflammation: the leukocyte adhesion cascade updated. *Nat Rev Immunol.* 2007 Sep;7(9):678-89.

Link A, Vogt TK, Favre S, Britschgi MR, Acha-Orbea H, Hinz B, Cyster JG, Luther SA. Fibroblastic reticular cells in lymph nodes regulate the homeostasis of naive T cells. *Nat Immunol.* 2007 Nov;8(11):1255-65.

Low SH, Tang BL, Wong SH, Hong W. Selective inhibition of protein targeting to the apical domain of MDCK cells by brefeldin A. *J Cell Biol.* 1992 Jul;118(1):51-62.

Luther SA, Bidgol A, Hargreaves DC, Schmidt A, Xu Y, Paniyadi J, Matloubian M, Cyster JG. Differing activities of homeostatic chemokines CCL19, CCL21, and CXCL12 in lymphocyte and dendritic cell recruitment and lymphoid neogenesis. *J Immunol.* 2002 Jul 1;169(1):424-33.

Luther SA, Tang HL, Hyman PL, Farr AG, Cyster JG. Coexpression of the chemokines ELC and SLC by T zone stromal cells and deletion of the ELC gene in the *plt/plt* mouse. *Proc Natl Acad Sci U S A.* 2000 Nov 7;97(23):12694-9.

Lutz MB, Kukutsch N, Ogilvie AL, Rössner S, Koch F, Romani N, Schuler G. An advanced culture method for generating large quantities of highly pure dendritic cells from mouse bone marrow. *J Immunol Methods.* 1999 Feb 1;223(1):77-92.

Ma J, Wang JH, Guo YJ, Sy MS, Bigby M. In vivo treatment with anti-ICAM-1 and anti-LFA-1 antibodies inhibits contact sensitization-induced migration of epidermal Langerhans cells to regional lymph nodes. *Cell Immunol.* 1994 Oct 15;158(2):389-99.

Mailloux AW, Young MR. NK-dependent increases in CCL22 secretion selectively recruits regulatory T cells to the tumor microenvironment. *J Immunol.* 2009 Mar 1;182(5):2753-65.

Mantovani A, Bonecchi R, Locati M. Tuning inflammation and immunity by chemokine sequestration: decoys and more. *Nat Rev Immunol.* 2006 Dec;6(12):907-18.

Marsland BJ, Bättig P, Bauer M, Ruedl C, Lässig U, Beerli RR, Dietmeier K, Ivanova L, Pfister T, Vogt L, Nakano H, Nembrini C, Saudan P, Kopf M, Bachmann MF. CCL19 and CCL21 induce a potent proinflammatory differentiation program in licensed dendritic cells. *Immunity.* 2005 Apr;22(4):493-505.

Martin-Fontecha A, Sebastiani S, Höpken UE, Ugucioni M, Lipp M, Lanzavecchia A, Sallusto F. Regulation of dendritic cell migration to the draining lymph node: impact on T lymphocyte traffic and priming. *J Exp Med.* 2003 Aug 18;198(4):615-21.

## References

---

Mebius RE, Kraal G. Structure and function of the spleen. *Nat Rev Immunol*. 2005 Aug;5(8):606-16.

Medeiros NA, Burnette DT, Forscher P. Myosin II functions in actin-bundle turnover in neuronal growth cones. *Nat Cell Biol*. 2006 Mar;8(3):215-26.

Mempel TR, Junt T, von Andrian UH. Rulers over randomness: stroma cells guide lymphocyte migration in lymph nodes. *Immunity*. 2006 Dec;25(6):867-9.

Middleton J, Neil S, Wintle J, Clark-Lewis I, Moore H, Lam C, Auer M, Hub E, Rot A. Transcytosis and surface presentation of IL-8 by venular endothelial cells. *Cell*. 1997 Oct 31;91(3):385-95.

Miller MJ, Wei SH, Cahalan MD, Parker I. Autonomous T cell trafficking examined in vivo with intravital two-photon microscopy. *Proc Natl Acad Sci U S A*. 2003 Mar 4;100(5):2604-9.

Miller MJ, Wei SH, Parker I, Cahalan MD. Two-photon imaging of lymphocyte motility and antigen response in intact lymph node. *Science*. 2002 Jun 7;296(5574):1869-73.

Misslitz A, Pabst O, Hintzen G, Ohl L, Kremmer E, Petrie HT, Förster R. Thymic T cell development and progenitor localization depend on CCR7. *J Exp Med*. 2004 Aug 16;200(4):481-91.

Mitchison TJ, Charras GT, Mahadevan L. Implications of a poroelastic cytoplasm for the dynamics of animal cell shape. *Semin Cell Dev Biol*. 2008 Jun;19(3):215-23.

Mitchison TJ, Cramer LP. Actin-based cell motility and cell locomotion. *Cell*. 1996 Feb 9;84(3):371-9.

Miyasaka M, Tanaka T. Lymphocyte trafficking across high endothelial venules: dogmas and enigmas. *Nat Rev Immunol*. 2004 May;4(5):360-70.

Moon JJ, Chu HH, Pepper M, McSorley SJ, Jameson SC, Kedl RM, Jenkins MK. Naive CD4(+) T cell frequency varies for different epitopes and predicts repertoire diversity and response magnitude. *Immunity*. 2007 Aug;27(2):203-13.

Mori S, Nakano H, Aritomi K, Wang CR, Gunn MD, Kakiuchi T. Mice lacking expression of the chemokines CCL21-ser and CCL19 (plt mice) demonstrate delayed but enhanced T cell immune responses. *J Exp Med*. 2001 Jan 15;193(2):207-18.

Morita R, Schmitt N, Bentebibel SE, Ranganathan R, Bourdery L, Zurawski G, Foucat E, Dullaers M, Oh S, Sabzghabaei N, Lavecchio EM, Punaro M, Pascual V, Banchereau J, Ueno H. Human blood CXCR5(+)CD4(+) T cells are counterparts of T follicular cells and contain specific subsets that differentially support antibody secretion. *Immunity*. 2011 Jan 28;34(1):108-21. Epub 2011 Jan 6. Erratum in: *Immunity*. 2011 Jan 28;34(1):135.

## References

---

Morley SC, Wang C, Lo WL, Lio CW, Zinselmeyer BH, Miller MJ, Brown EJ, Allen PM. The actin-bundling protein L-plastin dissociates CCR7 proximal signaling from CCR7-induced motility. *J Immunol.* 2010 Apr 1;184(7):3628-38.

Mueller SN, Germain RN. Stromal cell contributions to the homeostasis and functionality of the immune system. *Nat Rev Immunol.* 2009 Sep;9(9):618-29

Mueller SN, Hosiawa-Meagher KA, Konieczny BT, Sullivan BM, Bachmann MF, Locksley RM, Ahmed R, Matloubian M. Regulation of homeostatic chemokine expression and cell trafficking during immune responses. *Science.* 2007 Aug 3;317(5838):670-4.

Nakano H, Gunn MD. Gene duplications at the chemokine locus on mouse chromosome 4: multiple strain-specific haplotypes and the deletion of secondary lymphoid-organ chemokine and EBI-1 ligand chemokine genes in the plt mutation. *J Immunol.* 2001 Jan 1;166(1):361-9.

Nakano H, Mori S, Yonekawa H, Nariuchi H, Matsuzawa A, Kakiuchi T. A novel mutant gene involved in T-lymphocyte-specific homing into peripheral lymphoid organs on mouse chromosome 4. *Blood.* 1998 Apr 15;91(8):2886-95.

Nakano H, Tamura T, Yoshimoto T, Yagita H, Miyasaka M, Butcher EC, Nariuchi H, Kakiuchi T, Matsuzawa A. Genetic defect in T lymphocyte-specific homing into peripheral lymph nodes. *Eur J Immunol.* 1997 Jan;27(1):215-21.

Nagasawa T, Nakajima T, Tachibana K, Iizasa H, Bleul CC, Yoshie O, Matsushima K, Yoshida N, Springer TA, Kishimoto T. Molecular cloning and characterization of a murine pre-B-cell growth-stimulating factor/stromal cell-derived factor 1 receptor, a murine homolog of the human immunodeficiency virus 1 entry coreceptor fusin. *Proc Natl Acad Sci U S A.* 1996 Dec 10;93(25):14726-9.

Ngo VN, Tang HL, Cyster JG. Epstein-Barr virus-induced molecule 1 ligand chemokine is expressed by dendritic cells in lymphoid tissues and strongly attracts naive T cells and activated B cells. *J Exp Med.* 1998 Jul 6;188(1):181-91.

Nieto M, Frade JM, Sancho D, Mellado M, Martinez-A C, Sánchez-Madrid F. Polarization of chemokine receptors to the leading edge during lymphocyte chemotaxis. *J Exp Med.* 1997 Jul 7;186(1):153-8.

Nitta T, Nitta S, Lei Y, Lipp M, Takahama Y. CCR7-mediated migration of developing thymocytes to the medulla is essential for negative selection to tissue-restricted antigens. *Proc Natl Acad Sci U S A.* 2009 Oct 6;106(40):17129-33.

Nolte MA, Beliën JA, Schadee-Eestermans I, Jansen W, Unger WW, van Rooijen N, Kraal G, Mebius RE. A conduit system distributes chemokines and small blood-borne molecules through the splenic white pulp. *J Exp Med.* 2003 Aug 4;198(3):505-12.

## References

---

- Nomura T, Hasegawa H, Kohno M, Sasaki M, Fujita S. Enhancement of anti-tumor immunity by tumor cells transfected with the secondary lymphoid tissue chemokine EBI-1-ligand chemokine and stromal cell-derived factor-1alpha chemokine genes. *Int J Cancer*. 2001 Mar 1;91(5):597-606.
- Nourshargh S, Hordijk PL, Sixt M. Breaching multiple barriers: leukocyte motility through venular walls and the interstitium. *Nat Rev Mol Cell Biol*. 2010 May;11(5):366-78.
- Ohl L, Mohaupt M, Czeloth N, Hintzen G, Kiafard Z, Zwirner J, Blankenstein T, Henning G, Förster R. CCR7 governs skin dendritic cell migration under inflammatory and steady-state conditions. *Immunity*. 2004 Aug;21(2):279-88.
- Okada T, Ngo VN, Ekland EH, Förster R, Lipp M, Littman DR, Cyster JG. Chemokine requirements for B cell entry to lymph nodes and Peyer's patches. *J Exp Med*. 2002 Jul 1;196(1):65-75.
- Okada T, Miller MJ, Parker I, Krummel MF, Neighbors M, Hartley SB, O'Garra A, Cahalan MD, Cyster JG. Antigen-engaged B cells undergo chemotaxis toward the T zone and form motile conjugates with helper T cells. *PLoS Biol*. 2005 Jun;3(6):e150.
- Okada T, Cyster JG. B cell migration and interactions in the early phase of antibody responses. *Curr Opin Immunol*. 2006 Jun;18(3):278-85.
- Okada T, Cyster JG. CC chemokine receptor 7 contributes to Gi-dependent T cell motility in the lymph node. *J Immunol*. 2007 Mar 1;178(5):2973-8.
- O'Shea JJ, Paul WE. Mechanisms underlying lineage commitment and plasticity of helper CD4+ T cells. *Science*. 2010 Feb 26;327(5969):1098-102.
- Otero C, Groettrup M, Legler DF. Opposite fate of endocytosed CCR7 and its ligands: recycling versus degradation. *J Immunol*. 2006 Aug 15;177(4):2314-23.
- Paavola CD, Hemmerich S, Grunberger D, Polsky I, Bloom A, Freedman R, Mulkins M, Bhakta S, McCarley D, Wiesent L, Wong B, Jarnagin K, Handel TM. Monomeric monocyte chemoattractant protein-1 (MCP-1) binds and activates the MCP-1 receptor CCR2B. *J Biol Chem*. 1998 Dec 11;273(50):33157-65.
- Pape KA, Catron DM, Itano AA, Jenkins MK. The humoral immune response is initiated in lymph nodes by B cells that acquire soluble antigen directly in the follicles. *Immunity*. 2007 Apr;26(4):491-502. Epub 2007 Mar 22.
- Patel DD, Koopmann W, Imai T, Whichard LP, Yoshie O, Krangel MS. Chemokines have diverse abilities to form solid phase gradients. *Clin Immunol*. 2001 Apr;99(1):43-52.

## References

---

Paul WE, Zhu J. How are T(H)2-type immune responses initiated and amplified? *Nat Rev Immunol.* 2010 Apr;10(4):225-35.

Pegu A, Flynn JL, Reinhart TA. Afferent and efferent interfaces of lymph nodes are distinguished by expression of lymphatic endothelial markers and chemokines. *Lymphat Res Biol.* 2007;5(2):91-103.

Pelletier AJ, van der Laan LJ, Hildbrand P, Siani MA, Thompson DA, Dawson PE, Torbett BE, Salomon DR. Presentation of chemokine SDF-1 alpha by fibronectin mediates directed migration of T cells. *Blood.* 2000 Oct 15;96(8):2682-90.

Peters NC, Egen JG, Secundino N, Debrabant A, Kimblin N, Kamhawi S, Lawyer P, Fay MP, Germain RN, Sacks D. In vivo imaging reveals an essential role for neutrophils in leishmaniasis transmitted by sand flies. *Science.* 2008 Aug 15;321(5891):970-4.

Pflicke H, Sixt M. Preformed portals facilitate dendritic cell entry into afferent lymphatic vessels. *J Exp Med.* 2009 Dec 21;206(13):2925-35. Epub 2009 Dec 7.

Pilkington KR, Clark-Lewis I, McColl SR. Inhibition of generation of cytotoxic T lymphocyte activity by a CCL19/macrophage inflammatory protein (MIP)-3beta antagonist. *J Biol Chem.* 2004 Sep 24;279(39):40276-82.

Potocnik AJ, Brakebusch C, Fässler R. Fetal and adult hematopoietic stem cells require beta1 integrin function for colonizing fetal liver, spleen, and bone marrow. *Immunity.* 2000 Jun;12(6):653-63.

Plow EF, Hoover-Plow J. The functions of plasminogen in cardiovascular disease. *Trends Cardiovasc Med.* 2004 Jul;14(5):180-6.

Proudfoot AE, Handel TM, Johnson Z, Lau EK, LiWang P, Clark-Lewis I, Borlat F, Wells TN, Kosco-Vilbois MH. Glycosaminoglycan binding and oligomerization are essential for the in vivo activity of certain chemokines. *Proc Natl Acad Sci U S A.* 2003 Feb 18;100(4):1885-90. Epub 2003 Feb 5.

Randolph DA, Huang G, Carruthers CJ, Bromley LE, Chaplin DD. The role of CCR7 in TH1 and TH2 cell localization and delivery of B cell help in vivo. *Science.* 1999 Dec 10;286(5447):2159-62.

Randolph GJ, Angeli V, Swartz MA. Dendritic-cell trafficking to lymph nodes through lymphatic vessels. *Nat Rev Immunol.* 2005 Aug;5(8):617-28.

Reif K, Ekland EH, Ohl L, Nakano H, Lipp M, Förster R, Cyster JG. Balanced responsiveness to chemoattractants from adjacent zones determines B-cell position. *Nature.* 2002 Mar 7;416(6876):94-9.



## References

---

- Reis e Sousa C. Dendritic cells in a mature age. *Nat Rev Immunol.* 2006 Jun;6(6):476-83.
- Renkawitz J, Schumann K, Weber M, Lämmermann T, Pflücke H, Piel M, Polleux J, Spatz JP, Sixt M. Adaptive force transmission in amoeboid cell migration. *Nat Cell Biol.* 2009 Dec;11(12):1438-43.
- Renkawitz J, Sixt M. Mechanisms of force generation and force transmission during interstitial leukocyte migration. *EMBO Rep.* 2010 Oct;11(10):744-50.
- Ricart BG, John B, Lee D, Hunter CA, Hammer DA. Dendritic Cells Distinguish Individual Chemokine Signals through CCR7 and CXCR4. *J Immunol.* 2010 Nov 24.
- Riedl J, Crevenna AH, Kessenbrock K, Yu JH, Neukirchen D, Bista M, Bradke F, Jenne D, Holak TA, Werb Z, Sixt M, Wedlich-Soldner R. Lifeact: a versatile marker to visualize F-actin. *Nat Methods.* 2008 Jul;5(7):605-7.
- Riedl J, Flynn KC, Raducanu A, Gärtner F, Beck G, Bösl M, Bradke F, Massberg S, Aszodi A, Sixt M, Wedlich-Söldner R. Lifeact mice for studying F-actin dynamics. *Nat Methods.* 2010 Mar;7(3):168-9.
- Roosendaal R, Mempel TR, Pitcher LA, Gonzalez SF, Verschoor A, Mebius RE, von Andrian UH, Carroll MC. Conduits mediate transport of low-molecular-weight antigen to lymph node follicles. *Immunity.* 2009 Feb 20;30(2):264-76.
- Rot A. Neutrophil attractant/activation protein-1 (interleukin-8) induces in vitro neutrophil migration by haptotactic mechanism. *Eur J Immunol.* 1993 Jan;23(1):303-6.
- Rot A, von Andrian UH. Chemokines in innate and adaptive host defense: basic chemokine grammar for immune cells. *Annu Rev Immunol.* 2004;22:891-928.
- Rueda P, Balabanian K, Lagane B, Staropoli I, Chow K, Levoye A, Laguri C, Sadir R, Delaunay T, Izquierdo E, Pablos JL, Lendinez E, Caruz A, Franco D, Baleux F, Lortat-Jacob H, Arenzana-Seisdedos F. The CXCL12gamma chemokine displays unprecedented structural and functional properties that make it a paradigm of chemoattractant proteins. *PLoS One.* 2008 Jul 2;3(7):e2543.
- Saeki H, Wu MT, Olsz E, Hwang ST. A migratory population of skin-derived dendritic cells expresses CXCR5, responds to B lymphocyte chemoattractant in vitro, and co-localizes to B cell zones in lymph nodes in vivo. *Eur J Immunol.* 2000 Oct;30(10):2808-14.
- Sallusto F, Palermo B, Lenig D, Miettinen M, Matikainen S, Julkunen I, Forster R, Burgstahler R, Lipp M, Lanzavecchia A. Distinct patterns and kinetics of chemokine production regulate dendritic cell function. *Eur J Immunol.* 1999 May;29(5):1617-25.

## References

---

Sanger F, Nicklen S, Coulson AR. DNA sequencing with chain-terminating inhibitors. *Proc Natl Acad Sci U S A*. 1977 Dec;74(12):5463-7.

Santiago B, Baleux F, Palao G, Gutiérrez-Cañas I, Ramírez JC, Arenzana-Seisdedos F, Pablos JL. CXCL12 is displayed by rheumatoid endothelial cells through its basic amino-terminal motif on heparan sulfate proteoglycans. *Arthritis Res Ther*. 2006;8(2):R43. Epub 2006 Feb 3.

Schneider MA, Meingassner JG, Lipp M, Moore HD, Rot A. CCR7 is required for the in vivo function of CD4+ CD25+ regulatory T cells. *J Exp Med*. 2007 Apr 16;204(4):735-45.

Schumann K, Lämmermann T, Bruckner M, Legler DF, Polleux J, Spatz JP, Schuler G, Förster R, Lutz MB, Sorokin L, Sixt M. Immobilized chemokine fields and soluble chemokine gradients cooperatively shape migration patterns of dendritic cells. *Immunity*. 2010 May 28;32(5):703-13.

Sen D, Forrest L, Kepler TB, Parker I, Cahalan MD. Selective and site-specific mobilization of dermal dendritic cells and Langerhans cells by Th1- and Th2-polarizing adjuvants. *Proc Natl Acad Sci U S A*. 2010 May 4;107(18):8334-9.

Shamri R, Grabovsky V, Gauguet JM, Feigelson S, Manevich E, Kolanus W, Robinson MK, Staunton DE, von Andrian UH, Alon R. Lymphocyte arrest requires instantaneous induction of an extended LFA-1 conformation mediated by endothelium-bound chemokines. *Nat Immunol*. 2005 May;6(5):497-506.

Shields JD, Emmett MS, Dunn DB, Joory KD, Sage LM, Rigby H, Mortimer PS, Orlando A, Levick JR, Bates DO. Chemokine-mediated migration of melanoma cells towards lymphatics--a mechanism contributing to metastasis. *Oncogene*. 2007 May 10;26(21):2997-3005.

Shields JD, Fleury ME, Yong C, Tomei AA, Randolph GJ, Swartz MA. Autologous chemotaxis as a mechanism of tumor cell homing to lymphatics via interstitial flow and autocrine CCR7 signaling. *Cancer Cell*. 2007 Jun;11(6):526-38.

Shortman K, Naik SH. Steady-state and inflammatory dendritic-cell development. *Nat Rev Immunol*. 2007 Jan;7(1):19-30.

Singh UP, Venkataraman C, Singh R, Lillard JW Jr. CXCR3 axis: role in inflammatory bowel disease and its therapeutic implication. *Endocr Metab Immune Disord Drug Targets*. 2007 Jun;7(2):111-23.

Sixt M, Kanazawa N, Selg M, Samson T, Roos G, Reinhardt DP, Pabst R, Lutz MB, Sorokin L. The conduit system transports soluble antigens from the afferent lymph to resident dendritic cells in the T cell area of the lymph node. *Immunity*. 2005 Jan;22(1):19-29.

## References

---

Small JV, Isenberg G, Celis JE. Polarity of actin at the leading edge of cultured cells. *Nature*. 1978 Apr 13;272(5654):638-9.

Smrcka AV. G protein betagamma subunits: central mediators of G protein-coupled receptor signaling. *Cell Mol Life Sci*. 2008 Jul;65(14):2191-214.

Stanley P, Smith A, McDowall A, Nicol A, Zicha D, Hogg N. Intermediate-affinity LFA-1 binds alpha-actinin-1 to control migration at the leading edge of the T cell. *EMBO J*. 2008 Jan 9;27(1):62-75

Stein JV, Rot A, Luo Y, Narasimhaswamy M, Nakano H, Gunn MD, Matsuzawa A, Quack-enbush EJ, Dorf ME, von Andrian UH. The CC chemokine thymus-derived chemotactic agent 4 (TCA-4, secondary lymphoid tissue chemokine, 6Ckine, exodus-2) triggers lymphocyte function-associated antigen 1-mediated arrest of rolling T lymphocytes in peripheral lymph node high endothelial venules. *J Exp Med*. 2000 Jan 3;191(1):61-76.

Suzuki K, Grigorova I, Phan TG, Kelly LM, Cyster JG. Visualizing B cell capture of cognate antigen from follicular dendritic cells. *J Exp Med*. 2009 Jul 6;206(7):1485-93. Epub 2009 Jun 8.

Szanya V, Ermann J, Taylor C, Holness C, Fathman CG. The subpopulation of CD4+CD25+ splenocytes that delays adoptive transfer of diabetes expresses L-selectin and high levels of CCR7. *J Immunol*. 2002 Sep 1;169(5):2461-5.

Tang HL, Cyster JG. Chemokine Up-regulation and activated T cell attraction by maturing dendritic cells. *Science*. 1999 Apr 30;284(5415):819-22.

Thelen M, Stein JV. How chemokines invite leukocytes to dance. *Nat Immunol*. 2008 Sep;9(9):953-9.

Theriot JA, Mitchison TJ. Comparison of actin and cell surface dynamics in motile fibroblasts. *J Cell Biol*. 1992 Oct;119(2):367-77.

Tomei AA, Siegert S, Britschgi MR, Luther SA, Swartz MA. Fluid flow regulates stromal cell organization and CCL21 expression in a tissue-engineered lymph node microenvironment. *J Immunol*. 2009 Oct 1;183(7):4273-83.

Torres R, Ramirez JC. A chemokine targets the nucleus: Cxcl12-gamma isoform localizes to the nucleolus in adult mouse heart. *PLoS One*. 2009 Oct 27;4(10):e7570.

Turley SJ, Fletcher AL, Elpek KG. The stromal and haematopoietic antigen-presenting cells that reside in secondary lymphoid organs. *Nat Rev Immunol*. 2010 Dec;10(12):813-25.

Uchimura K, Morimoto-Tomita M, Bistrup A, Li J, Lyon M, Gallagher J, Werb Z, Rosen SD. HSulf-2, an extracellular endoglucosamine-6-sulfatase, selectively mobilizes heparin-bound

## References

---

growth factors and chemokines: effects on VEGF, FGF-1, and SDF-1. *BMC Biochem.* 2006 Jan 17;7:2.

Ueno T, Hara K, Willis MS, Malin MA, Höpken UE, Gray DH, Matsushima K, Lipp M, Springer TA, Boyd RL, Yoshie O, Takahama Y. Role for CCR7 ligands in the emigration of newly generated T lymphocytes from the neonatal thymus. *Immunity.* 2002 Feb;16(2):205-18.

Vallotton P, Danuser G, Bohnet S, Meister JJ, Verkhovsky AB. Tracking retrograde flow in keratocytes: news from the front. *Mol Biol Cell.* 2005 Mar;16(3):1223-31.

Vassileva G, Soto H, Zlotnik A, Nakano H, Kakiuchi T, Hedrick JA, Lira SA. The reduced expression of 6Ckine in the plt mouse results from the deletion of one of two 6Ckine genes. *J Exp Med.* 1999 Oct 18;190(8):1183-8.

Veerman KM, Williams MJ, Uchimura K, Singer MS, Merzaban JS, Naus S, Carlow DA, Owen P, Rivera-Nieves J, Rosen SD, Ziltener HJ. Interaction of the selectin ligand PSGL-1 with chemokines CCL21 and CCL19 facilitates efficient homing of T cells to secondary lymphoid organs. *Nat Immunol.* 2007 May;8(5):532-9.

Villadangos JA, Schnorrer P. Intrinsic and cooperative antigen-presenting functions of dendritic-cell subsets in vivo. *Nat Rev Immunol.* 2007 Jul;7(7):543-55.

von Andrian UH, Mempel TR. Homing and cellular traffic in lymph nodes. *Nat Rev Immunol.* 2003 Nov;3(11):867-78.

Wagner N, Löhler J, Kunkel EJ, Ley K, Leung E, Krissansen G, Rajewsky K, Müller W. Critical role for beta7 integrins in formation of the gut-associated lymphoid tissue. *Nature.* 1996 Jul 25;382(6589):366-70.

Wang L, Fuster M, Sriramarao P, Esko JD. Endothelial heparan sulfate deficiency impairs L-selectin- and chemokine-mediated neutrophil trafficking during inflammatory responses. *Nat Immunol.* 2005 Sep;6(9):902-10.

Wei SH, Parker I, Miller MJ, Cahalan MD. A stochastic view of lymphocyte motility and trafficking within the lymph node. *Immunol Rev.* 2003 Oct;195:136-59.

Wilson RW, Ballantyne CM, Smith CW, Montgomery C, Bradley A, O'Brien WE, Beaud et al., Gene targeting yields a CD18-mutant mouse for study of inflammation. *J Immunol.* 1993 Aug 1;151(3):1571-8.

Witt DP, Lander AD. Differential binding of chemokines to glycosaminoglycan subpopulations. *Curr Biol.* 1994 May 1;4(5):394-400.

## References

---

Witt CM, Raychaudhuri S, Schaefer B, Chakraborty AK, Robey EA. Directed migration of positively selected thymocytes visualized in real time. *PLoS Biol.* 2005 Jun;3(6):e160.

Woolf E, Grigorova I, Sagiv A, Grabovsky V, Feigelson SW, Shulman Z, Hartmann T, Sixt M, Cyster JG, Alon R. Lymph node chemokines promote sustained T lymphocyte motility without triggering stable integrin adhesiveness in the absence of shear forces. *Nat Immunol.* 2007 Oct;8(10):1076-85.

Worbs T, Mempel TR, Bölter J, von Andrian UH, Förster R. CCR7 ligands stimulate the intranodal motility of T lymphocytes in vivo. *J Exp Med.* 2007 Mar 19;204(3):489-95. Epub 2007 Feb 26.

Wu MT, Hwang ST. CXCR5-transduced bone marrow-derived dendritic cells traffic to B cell zones of lymph nodes and modify antigen-specific immune responses. *J Immunol.* 2002 May 15;168(10):5096-102.

Xu H, Guan H, Zu G, Bullard D, Hanson J, Slater M, Elmets CA. The role of ICAM-1 molecule in the migration of Langerhans cells in the skin and regional lymph node. *Eur J Immunol.* 2001 Oct;31(10):3085-93.

Yanagawa Y, Onoé K. CCR7 ligands induce rapid endocytosis in mature dendritic cells with concomitant up-regulation of Cdc42 and Rac activities. *Blood.* 2003 Jun 15;101(12):4923-9.

Yang BG, Tanaka T, Jang MH, Bai Z, Hayasaka H, Miyasaka M. Binding of lymphoid chemokines to collagen IV that accumulates in the basal lamina of high endothelial venules: its implications in lymphocyte trafficking. *J Immunol.* 2007 Oct 1;179(7):4376-82.

Yoshida R, Nagira M, Kitaura M, Imagawa N, Imai T, Yoshie O. Secondary lymphoid-tissue chemokine is a functional ligand for the CC chemokine receptor CCR7. *J Biol Chem.* 1998 Mar 20;273(12):7118-22.

Zhu J, Paul WE. Heterogeneity and plasticity of T helper cells. *Cell Res.* 2010 Jan;20(1):4-12.

## 7 Supplementary movie legends

### **Movie S1. Migration of mature DCs on a LN cryosection (AVI 3090 kb)**

An unfixed cryosection of a murine inguinal LN was fixed on the bottom of a cell culture dish and covered with mature DCs. The DCs show a highly synchronized wave of migration from the peripheral parts of the section and even from the surrounding of the section towards the center of the LN cryosection. The cells enter the LN section along defined segments, suggesting migration along preformed tracks. 12-18 hr after the start of migration the cells accumulate in the inner part of the LN section. Cell behavior was followed by time-lapse video microscopy over 18 hr (103 frames, 15 frames/s).

### **Movie S2. Migration of immature DCs on a LN cryosection (AVI 1100 kb)**

The experiment described in Movie S2 was repeated with immature DCs. No migration could be observed in this case. Cell migration was recorded by time-lapse video microscopy over 3 hr (29 frames, 15 frames/s).

### **Movie S3. Migration of mature DCs on a LN cryosection with a removed and inverted peripheral part of the section (AVI 1840 kb)**

A peripheral part of a LN cryosection was cut off and repositioned inverted by 180° in close proximity to the remaining section to challenge the possibility of DC migration on immobilized gradients. Applied mature DCs again showed a wave of directed migration, but the migration on the small segment was still directed towards the center of the big segment. This result implicates the induction of a soluble chemotactic gradient. The DCs were imaged over 4 hr (41 frames, 15 frames/s).

### **Movie S4. DC migration on immobilized CCL21 (AVI 4930 kb)**

In this reductionistic *in vitro* approach CCL21 was dropped on cell culture plastic and after 30 min at 37 °C non-immobilized chemokine was washed away with PBS. The coated area was then covered with mature DCs. The cells settling directly on the immobilized area showed random migration. 5 – 10 min after the onset of migration, DCs near to the coated area start directed migration to the center of the spot and accumulate there. DC migration was monitored over 15 hr (104 frames, 15 frames/s).

**Movie S5. DC spreading on different structural parts of a LN cryosection (AVI 295 kb)**

In this time-lapse movie a representative DC migrating on an interfollicular area and a DC sitting on a B cell follicle is shown. DC migration was monitored over 1 min (29 frames, 15 frames/s).

**Movie S6. Migration of WT and *Itgb2*<sup>-/-</sup> DCs on a LN cryosection (AVI 1360 kb)**

The time-lapse movie over 20 min shows WT (left) and *Itgb2*<sup>-/-</sup> (right) DCs crawling on a LN cryosection (41 frames, 15 frames/s).

**Movie S7. DC spreading on immobilized CCL21 and artificially immobilized CCL19 (AVI 5100 kb)**

A plasma-treated glass surface was either coated with CCL21/ICAM-1 (left) or CCL19/ICAM-1 (right). Mature DCs were applied onto the surface and the cell behavior was monitored with differential interference contrast microscopy time-lapse microscopy over 15 min (150 frames, 30 frames/s).

**Movie S8. WT DCs migrating in a 3D collagen gel with incorporated BSA/ICAM-1-coated carbon fibers (AVI 2350 kb)**

DCs migrate in a 3D collagen matrix where BSA/ICAM-1-coated fibers were embedded. DCs show unbiased random migration in the collagen matrix. The DCs were recorded over 4 hr (241 frames, 30 frames/s, without/with cells tracked).

**Movie S9. WT DCs migrating in a 3D collagen gel with incorporated CCL21/ICAM-1-coated carbon fibers (AVI 2310 kb)**

Time-lapse movie of DCs migrating in a 3D collagen gel with incorporated CCL21/ICAM-1-coated carbon fibers. When the cells get into contact with the coated fibers, they adhere, and move along the fiber with frequent directional changes. Cell behavior was monitored over 4 hr (241 frames, 30 frames/s, without/with cells tracked).

**Movie S10. WT DCs migrating in a 3D collagen gel with incorporated CCL21/ICAM-1-coated carbon fibers towards a CCL19 gradient (AVI 2320 kb)**

DCs migrate in a 3D matrix with embedded CCL21/ICAM-1-coated fibers. An additional external CCL19 gradient is applied (highest concentration on top). Once the cells get into contact with the fibers, they adhere and move along the fibers with a bias towards the CCL19 source. Occasionally, cells detach from the fibers and migrate freely through the gel.

This movie shows directional steering of haptokinetic movement. The cells were monitored over 4 hr (241 frames, 30 frames/s, without/with cells tracked).

**Movie S11. WT DCs migrating in a 3D collagen gel with incorporated CCL21/ICAM-1-coated carbon fibers towards a gradient of truncated CCL21 (AVI 2340 kb)**

The time-laps movie shows WT DCs crawling in a 3D collagen matrix towards a gradient of truncated CCL21 over 4 hr (241 frames, 30 frames/s, without/with cells tracked). The DCs show directed migration with a directional bias towards the full-length CCL21 on the fibers. The truncated CCL21 resembles the CCL19 gradient in Movie S10.

**Movie S12. *Itgb2*<sup>-/-</sup> DCs migrating in a 3D collagen gel with incorporated CCL21/ICAM-1-coated carbon fibers towards a CCL19 gradient (AVI 2370 kb)**

The time-laps movie shows *Itgb2*<sup>-/-</sup> DCs crawling in a 3D collagen matrix towards CCL19 over 4 hr (241 frames, 30 frames/s, without/with cells tracked). The DCs show directed migration, but do not interact with the included CCL21/ICAM-1-coated fibers.

**Movie S13: WT DCs migrating in a 3D collagen gel with incorporated CCL19/ICAM-1-coated carbon fibers towards a of truncated CCL21 (AVI 2350 kb)**

In this movie directed migration of WT DCs in a 3D matrix towards a source of truncated CCL21 over 4 hr is shown (241 frames, 30 frames/s, without/with cells tracked). Cellular interaction with the CCL19/ICAM-1-coated carbon fibers cannot be observed. Instead, DCs chemotaxing towards truncated CCL21 migrate through the collagen matrix.

**Movie S14: Lifeact-GFP DC migrating on glass under agarose towards a CCL19 gradient (AVI 310 kb)**

The DC forms a broad leading edge with a diffusely protruding actin cortex. Only in the trailing edge thicker actin bundles can be observed. Time-laps movie over 50 s (30 frame/s), TIRF microscopy. The scale bar represents 10  $\mu$ m.

**Movie S15: With Lifeact-GFP transfected *Itg*<sup>-/-</sup> DC migrating on glass under agarose towards a CCL19 gradient (AVI 392 kb)**

This time-laps movie (70 s; 30 frame/s) shows that the retrograde actin flow in *Itg*<sup>-/-</sup> DCs is substantially increased in comparison to WT DCs migrating on glass. TIRF microscopy. The scale bar represents 10  $\mu$ m.



**Movie S16: Lifeact-GFP DC migrating on PEG under agarose towards a CCL19 gradient (AVI 696 kb)**

The retrograde actin flow can be enhanced in WT DCs by uncoupling of the molecular clutch on polyethylene glycol, an inert substrate. Time-laps movie over 150 s (30 frame/s), TIRF microscopy. The scale bar represents 10  $\mu\text{m}$ .

**Movie S17: Lifeact-GFP 3T3 fibroblasts sitting on patterned surface composed of inert PEG substrate and with serum and Alexa555-BSA co-coated adhesive stripes (AVI 482 kb)**

Left panel: Lifeact-GFP dynamics in 3T3 fibroblasts sitting on the patterned surface. Right panel: Alexa555-BSA highlights the serum coated adhesive area. Fibroblasts strictly adapt to the adhesive areas. Only short protrusions extend onto the inert PEG substrate, which exhibit massive retrograde actin flow. The retrograde actin flow stops at the border to the adhesive substrate. Time-laps movie over 100 s (30 frame/s), TIRF microscopy. The scale bar represents 5  $\mu\text{m}$ .

## 8 Supplementary statistical analyses

**Table 5: Statistical analyses. Kruskal-Wallis tests or Mann-Whitney U-test were applied for data which does not fulfill the criteria of t-test and ANOVA.**

Figure	Test statistic	Sample size/ degrees of freedom	P-value	Posthoc test
30 C	Kruskal-Wallis; H=117.18	df=6	P<0.001	Dunns, all pairwise
30 D	t-test; t=0.774	df=60	P=0.442	
30 E	t-test; t=8.7	df=60	P<0.001	
30 F	Spearman Rank correlation; r=0.12	n=33	P=0.52	
31 B	Kruskal-Wallis; H=35.603	df=2	P<0.001	Dunns, all pairwise
31 C	Kruskal-Wallis; H=17.820	df=2	P<0.001	Dunns, all pairwise
33 C	Mann-Whitney; T=594.000	n(small)= 19 n(big)=23	P<0.001	
33 D	t-test; t=-2.732	df=15	P<0.05	
34 C	t-test; t=5	df=12	P<0.001	

**Table 6: Posthoc tests of Kruskal-Wallis tests in Table 5. The data were compared pairwise with Dunn's method.**

Comparison	P-value
WT on glass vs <i>Itg</i> <sup>-/-</sup> on glass	P<0.05
WT on PEG vs WT on glass	P<0.05
WT on PEG vs WT on CCL21/ICAM-1	P<0.05
WT on CCL21 vs WT on glass	P<0.05
<i>Itg</i> <sup>-/-</sup> on glass vs <i>Itg</i> <sup>-/-</sup> on CCL21/ICAM-1	P<0.05
<i>Itg</i> <sup>-/-</sup> on glass vs <i>Itg</i> <sup>-/-</sup> on PEG	P<0.05
<i>Itg</i> <sup>-/-</sup> on PEG vs <i>Itg</i> <sup>-/-</sup> on CCL21/ICAM-1	ns

## 9 Publications

Schumann K\*, Lämmermann T\*, Bruckner M, Legler DF, Polleux J, Spatz J, Schuler G, Förster R, Lutz MB, Sorokin L, Sixt M. **Immobilized chemokine fields and soluble chemokine gradients cooperatively shape migration patterns of dendritic cells.** *Immunity* (2010) 32(5): 703-13. \*equal contribution

Renkawitz J, Schumann K, Weber M, Lämmermann T, Pflücke H, Piel M, Polleux J, Spatz JP, Sixt M. **Adaptive force transmission in amoeboid cell migration.** *Nat Cell Biol* (2009) 11(12): 1438-43.

Schumann K, Weber M & Sixt M. **Chemotactic gradients in lymphoid organs.** Manuscript in preparation

## Curriculum vitae

### Kathrin Schumann

#### Adresse

Passauer Str. 35, 81369 München, Germany

#### Date and place of birth

23.12.1982, Heilbronn, Germany

#### Education and scientific experience

- |                                  |   |
|----------------------------------|---|
| Since March 2008                 | <b>PhD thesis</b><br>Leukocyte Migration Research Group (Head: Dr Michael Sixt)<br>Max Planck Institute for Biochemistry, Department of Molecular Medicine, Martinsried, Germany  |
| April 2007 –<br>January 2008     | <b>Diploma thesis</b><br>Leukocyte Migration Research Group (Head: Dr Michael Sixt)<br><i>Project: The role of C-terminally truncated CCL21 in dendritic cell migration</i> , Max Planck Institute for Biochemistry, Department of Molecular Medicine, Martinsried, Germany |
| October 2005 -<br>September 2006 | <b>Research internship</b><br>Max Planck Institutes for Biochemistry and Neurobiology<br>Martinsried, Germany   |
| October 2004 –<br>March 2007     | <b>Graduate studies in Biochemistry</b><br>Eberhard-Karls-Universität, Tübingen, Germany<br>Main subjects: cell biology, organic chemistry  |
| October 2002 –<br>September 2004 | <b>Undergraduate studies in Biochemistry</b><br>Eberhard-Karls-Universität, Tübingen, Germany   |
| September 1993 -<br>July 2002    | <b>High School [Gymnasium]</b><br>Elly-Heuss-Knapp-Gymnasium, Heilbronn, Germany  |
| September 1989 –<br>July 1993    | <b>Elementary School</b><br>Deutschorden-Grundschule, Heilbronn, Germany  |

# Acknowledgement

I would like to express my sincere gratitude to the following people who made with their continuous support and encouragement this thesis possible:

First, I want to thank Prof. Dr. Michael Sixt for his excellent supervision and mentoring, especially for the nice, relaxed working atmosphere, a lot of brilliant ideas and the freedom to work in my own way

Prof. Dr. Reinhard Fässler for his constant support of the Sixt lab and for providing excellent working conditions

Prof. Dr. Sanjiv Luther and Prof. Dr. Tobias Bollenbach for agreeing to be member of my thesis committee and to evaluate my work

Dr. Walther Göhring, Carmen Schmitz, the Recombinant Protein Production core facility and the animal care takers for providing the “infrastructure” for this thesis

Prof. Dr. Daniel Legler, Markus Bruckner and Dr. Julien Polleux for very fruitful collaborations and discussions

My labmates for their help, a lot of discussions and to make the Sixt lab to a convenient place to work: Karin Hirsch, Tim Lämmeramn, Holger Pflücke, Jörg Renkawitz, Michele Weber and Alexander Eichner

All members of the Department of Molecular Medicine for their help. Expecially I want to thank Sarah Schmidt, Karin Hirsch and Raphael Ruppert for their friendship, nice chats and their uncensored point of view.

I also want to thank my clique from Tübingen for their continuous friendship

In the end I would like to thank my parents, Hubertus und Wilma Schumann, for their support, encouragement and confidence.